STIMULI-RESPONSIVE POLYMERS

IN SOLUTION AND ON GRAFTED SURFACES

A Dissertation

by

HUI FU

Submitted to the Office of Graduate Studies of
Texas A&M University
in partial fulfillment of the requirements for the degree of

DOCTOR OF PHILOSOPHY

May 2010

Major Subject: Chemistry

STIMULI-RESPONSIVE POLYMERS

IN SOLUTION AND ON GRAFTED SURFACES

A Dissertation

by

HUI FU

Submitted to the Office of Graduate Studies of
Texas A&M University
in partial fulfillment of the requirements for the degree of

DOCTOR OF PHILOSOPHY

Approved by:

Chair of Committee,	David E. Bergbreiter
Committee Members,	Daniel A. Singleton
	James D. Batteas
	Melissa A. Grunlan
Head of Department,	David H. Russell

May 2010

Major Subject: Chemistry

ABSTRACT

Stimuli-responsive Polymers in Solution and on Grafted Surfaces. (May 2010)

Hui Fu, B.S., Sichuan University; M.S., Tsinghua University; M.S., University of Southern California

Chair of Advisory Committee: Dr. David E. Bergbreiter

Thermoresponsive polymers such as poly(*N*-isopropylacrylamide) (PNIPAM) have lower critical solution temperature (LCST) in aqueous solutions. Below the LCST, these polymers are hydrophilic with an extended coil conformation. Above the LCST, they undergo a sharp phase transition to form a collapsed hydrophobic conformation. The LCSTs are also affected by cosolutes and the effects of anions on LCSTs follow the Hofmeister series.

We successfully used a simple digital melting point apparatus to study the effects of heating rates, solvent compositions, cosolutes, and redox state, on the LCSTs of thermoresponsive polymers. Moreover, the temperature range of the apparatus allowed for analyses at much higher temperatures and provides a simple way to examine irregular clouding behavior in more complex systems.

Meanwhile, stimuli-responsive surfaces grafted with thermoresponsive polymers can switch from hydrophilic to hydrophobic thermally. As the LCST can be subsequently changed with the addition of salts, the salt effects on the wettability of these thermoresponsive surfaces will dramatically impact the surface performance. In

this dissertation, I prepared PNIPAM/SiO_2 nanocomposite surfaces by a covalent layer-by-layer assembly procedure and such surfaces were then used in studies of salts effects on surface wettability.

Both the effects of anions and cations on the changes of advancing angles ($\Delta\Theta_a$) of the PNIPAM/SiO_2 nanocomposite surfaces were significant ($\Delta\Theta_a$ up to 90°). The anion effects on the surface wettability followed the Hofmeister effect as expected. Parallel studies on solution showed that variation of cations had a large effect on the LCST of PNIPAM too. Moreover, analyses of the Θ_a and LCST data using activity instead of using concentration showed different orders for the cation effects which were readily grouped by the cation charge numbers. No difference was seen for the anion effects in similar studies. AFM studies showed that surface morphology changes were correlated with the $\Delta\Theta_a$.

DEDICATION

To my husband, Yiqin for his encouragement, his unconditional support, and for his strong belief in my capability. To my children, Farrah and Andrew for bringing happiness and hope into my daily life, and for their understanding and support.

ACKNOWLEDGEMENTS

I would like to thank Dr. David Bergbreiter for giving me the opportunity to work in his lab as a research associate when I moved in College Station in 2005. This work experience turned out to be a smooth transition for my return to graduate school to finish my Ph.D. I would also like to thank him for being a great mentor, for his guidance, and for his support, during my graduate study.

I would like to express my gratitude to the members of Bergbreiter's group for giving me suggestions in the preparation of my student seminar, my preliminary presentation, and my final defense. I am glad to have had the chance to know and to work with all the former and current group members, especially Jianhua, Shawn, Film, Su, Chris, and Jeff.

I would also like to thank Dr. James Batteas, Mr. Albert Wan and Dr. Xiaoting Hong, for their collaborations and discussions on most of my research projects. I would like to thank Dr. Singleton, Dr. Batteas, Dr. Grunlan, and Dr. Connell for serving as my committee members. My gratitude also goes to Jill for helping everyone in the lab dealing with trivial business issues.

Finally, I would like to thank all the undergraduates I had worked with - David Darmon and Danielle Policarpio, who were sponsored by National Science Foundation (NSF) Research Experiences for Undergraduates (REU) program, for letting me guide them on their research projects; Alex Mijalis, for letting me teach him about chemistry, and for teaching me English in return.

TABLE OF CONTENTS

Page

CHAPTER Page

CHAPTER Page

LIST OF SCHEMES

LIST OF FIGURES

FIGURE Page

FIGURE Page

FIGURE Page

FIGURE Page

LIST OF TABLES

CHAPTER I

INTRODUCTION

Stimuli-responsive Polymers

Since the first synthetic polymer – Bakelite was made a century ago, numerous synthetic polymers have been made and used as materials. Stimuli-responsive polymers are but a small subset of these materials. They have nonetheless attracted a vast amount of attention due to their special properties and the applications of these properties in various areas. Stimuli-responsive polymers are often called smart polymers or intelligent polymers. Such polymers respond to external stimuli such as temperature, pH, ionic strength and solvent composition by undergoing some sort of property changes. More recently, subtler changes including changes in ambient electrical[1] and magnetic fields,[2] photochemical changes,[3] changes in a polymer's redox state,[4,5] and changes due to mechanical stress[6,7] have also been be used as external stimuli to usefully affect a responsive polymer's properties.

Thermoresponsive polymers probably are the most studied stimuli-responsive polymers and their temperature responsiveness can be further fine tuned by varying polymer composition and polymer stereochemistry.[8] Common examples of thermoresponsive polymers are polymers that undergo fast, reversible phase transitions such that the unfavorable entropy of solvation of a polymer leads them to change from a hydrophilic state to a hydrophobic state. These changes are apparent at the macroscopic

---

This dissertation follows the style of the *Journal of the American Chemical Society*.

level by visual inspection as the polymer solution changes from clear to cloudy at the polymer's lower critical solution temperature (LCST), the temperature at which the solvation entropy and solvation enthalpy terms of the Gibbs equation become equal.

During the phase transition, the polymer molecules change from an extended coil conformation to a globular conformation. These conformational changes are directly analogous to protein cold denaturation. In prior work by the Bergbreiter and Cremer groups, this property of temperature responsive polymers has been used to model the processes that occur in protein cold denaturation. In these studies, poly(*N*-isopropylacrylamide) (PNIPAM) has proven to be an especially useful model macromolecule for studying protein conformational changes.[9,10]

PNIPAM is one of the most well known and intensively studied thermoresponsive polymers in aqueous solution because its LCST of ~32 °C is close to the physiological temperature. Thus, it has potential applications in drug delivery as well as being generally useful in studies of 'smart' stimuli-responsive solubility. Other *N*-alkyl poly(acrylamide)s such as poly(*N*,*N*-dimethylacrylamide) and poly(*N*-propylacrylamide) also exhibit LCST properties.[11] In general, it is believed that an appropriate proportion of hydrophobicity and hydrophilicity in the polymer molecular structure is necessary for the phase transition that underlies an LCST to occur.[12] In addition to poly(*N*-alkylacrylamide)s, poly(*N*-vinyl alkylamide)s,[13] poly(vinyl ether)s, poly(alkene oxide)s and cellulose ethers[14,15] also exhibit temperature-induced phase transitions. Some examples of those polymers are shown in Scheme 1.

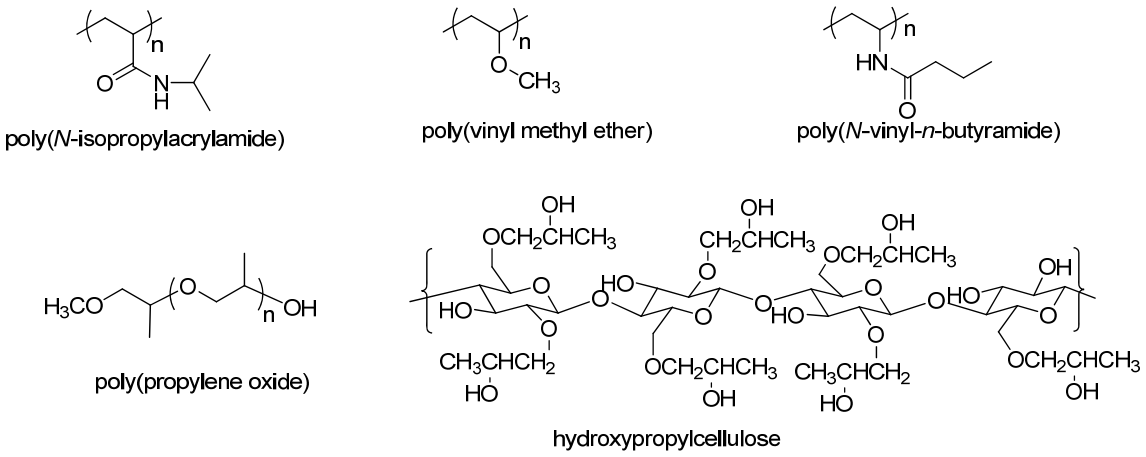

Scheme 1. Examples of temperature-responsive polymers.

Stimuli-responsive polymers have attracted great interest in bio-related applications such as drug delivery, bioseparations,[16] chromatography,[17-19] and cell culture. These polymers are used in those applications in three general ways. The first is to use a designed stimuli-responsive polymer in solution as a homopolymer, copolymer, or block polymer. For example, copolymers can be prepared such that they incorporate other functional groups into thermoresponsive polymers and the LCST can be altered depending on the nature of the added functional groups. An LCST study of the aqueous solutions of such copolymers is a useful method to test the effect of such substitutions and such LCST studies have also been used in attempts to understand macromolecule solvation. Block copolymers that consist of a thermoresponsive polymer segment and another functional polymer segment can self-assemble to form micelles in water. The resulting polymeric micelles can then encapsulate guest molecules under appropriate conditions. When a certain external stimulus is applied, the micelle structure can disassemble. This disassembly releases the guest molecules. Polymers that do not

contain thermoresponsive polymer segments can also be designed to respond to changes in pH, photochemical process,[3] electrical/magnetic fields, or mechanical stress. Such changes often lead to chemical changes of the polymer's functional groups, which in turn changes the physical properties of the polymer.

A second common way to use responsive polymers is to prepare cross-linked versions of these polymers in the form of gel that can swell or shrink in response to some external stimulus.[20-24] Stimuli-responsive hydrogels have been used in both drug loading and release formats. Such gels' release characteristics can be tailored to a range of target environments.

A final way to use stimuli-responsive polymers is to graft them onto a surface. If a polymer graft reversibly swells or collapses, the phase changes of the graft can change a surface from hydrophilic to hydrophobic or oleophilic to oleophobic[25] Stimuli-responsive polymer grafted surfaces can be used as separation media, tissue supports, in microfludic devices, and in biosensors.

My research is broadly focused on studying the behavior of stimuli-responsive polymers. As discussed below, it has included the development of new ways to study LCST events, ways to study and prepare new stimuli-responsive soluble polymers as well as studies where stimuli-responsive polymers are used to prepare nanocomposite grafts on organic and inorganic surfaces.

Analyses of Stimuli-responsive Behavior

Various instruments have been used to study LCST phenomena and the effects of external stimuli on the LCSTs. Different aspects of the phase transition process have

been probed by various instruments. Laser light scattering including dynamic and static laser light scattering spectrometers are used to detect the hydrodynamic radius changes of the thermoresponsive polymers that occur during the phase transition. A subtle radius change is often observed before and after the sample reaching its LCST. Wu observed the thermodynamically stable, collapsed single-chain globules of a linear PNIPAM sample for the first time by using a combination of static and dynamic laser light scattering.[26] In this study, a PNIPAM sample with high molar mass ($M_w > 10^7$ g/mol) and low dispersity ($M_w/M_n < 1.05$) was used and the phase transition behavior of individual polymer chains was carefully examined by measuring changes of the gyration (R_g) and hydrodynamic (R_h) radii. Before the phase transition happened, the ratio of R_g/R_h was a constant (~ 1.52) indicating a flexible coil in a good solvent. The ratio of R_g/R_h decreased with increasing of temperature during the phase transition and reached a plateau value of 0.63 suggesting that the globular form of this PNIPAM sample was a uniform sphere. At the collapsing limit, the single-chain globule still contained 80% of water in its hydrodynamic volume.

Laser light scattering is also a useful method in studying the responsiveness of stimuli-responsive micelles and vesicles. Zhang and coworkers studied the conformational changes of PNIPAM blocks in the corona of micelles and vesicles prepared from narrowly distributed polystyrene-*b*-poly(*N*-isopropylacrylamide) diblock copolymers in water by a combination of static and dynamic laser light scattering.[27] Their results revealed that brushes formed by PNIPAM chains in the corona of the micelles underwent a continuous collapse transition. PNIPAM brushes in the corona of

the vesicles exhibited a broad transition from 28 to 36 °C, shrinking in the range of 20 to 28 °C. The shrinking at a low temperature was attributed to interchain overlapping of the dense brushes on the concave surface of the vesicle.

As mentioned earlier, an aqueous solution of a thermoresponsive polymer turns cloudy at temperatures higher than its LCST, which leads to the light transmittance and light scattering changes in the sample. UV-Visible spectroscopy is a common tool used to study LCSTs by measuring the changes of amount of light that are transmitted by the sample. This method is often referred to as turbidimetry analysis. However, this method in general has low-throughput capabilities and requires relatively large amounts of polymer for analysis. Recently, other instrumental methods to study light scattering changes have been developed by using a digital camera equipped with a digital image processor to record the scattering intensity changes. For example, the Bergbreiter and Cremer groups used a dark-field microscope equipped with a DCC camera as a detector to measure the changes of light scattering intensity of PNIPAM samples undergoing phase separation. This detector setup was coupled with a temperature gradient device (Scheme 2) which applied a temperature gradient along the long axis of a capillary tube containing aqueous solution of a sample. The temperature of the sample inside the tube at different positions differed depending on the distance from a hot or cold thermal sink. This apparatus was especially useful as it provided high-throughput analytical procedure. Six samples can be analyzed simultaneously with each sample simultaneously experiencing a wide range of temperature. By using this apparatus, effects of end group polarity, effects of altered molecular weight, effects of polymer structure, and the effects

of changes in solution composition on the LCST of PNIPAM and other polymers were investigated. The results were published in several papers.[28-33]

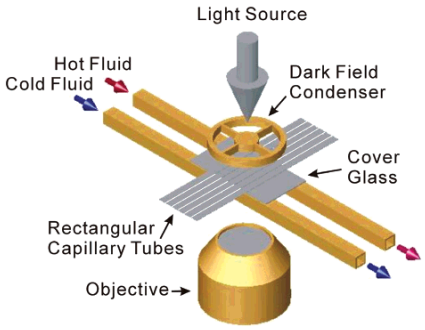

Scheme 2. Schematic drawing of a temperature gradient microfluidics device equipped with dark-field microscope.

Recently, we developed a second high-throughput cloud point assay. This procedure used a commercially available automatic melting point apparatus as the analytical instrument (Scheme 3). A melting point apparatus is usually used to measure the melting point of solid samples by detecting the light scattering changes that occur while the sample changes phase from being a strongly scattering solid to becoming a less scattering liquid. In this automatic melting point apparatus, a digital camera is used to record the scattering for up to three samples while the samples are being heated up under a precisely controlled heating ramp rate. A computerized digital image processor is then used to analyze the light scattering intensity changes on each image. This produces melting curves of scattering intensity *vs.* temperature for each sample. Since the changes of light scattering behavior of the aqueous solutions of a temperature responsive polymer are in a sense the reverse of melting, this same apparatus can be used to monitor the scattering intensity changes as an aqueous solution changes from a less scattering

solution to a more scattering cloudy mixture. Thus, a melting point apparatus is a simple tool for the studies of LCSTs. Details of this method are described in Chapter II below.

Scheme 3. A digital melting point apparatus that can be used to study LCSTs.

While my work has focused on using light scattering techniques to analyze LCSTs, other techniques too can be useful. Differential scanning calorimetry (DSC) is a method that measures the enthalpy changes during a phase transition process. It has been widely used in studies of LCSTs of stimuli-responsive polymers.[34] Other spectroscopic instruments including fluorescence spectroscopy,[35] high-resolution ultrasonic spectroscopy, IR spectroscopy and NMR spectroscopy[36-38] can also be used to study such phase transition process. Often, several of these instruments are used together in an effort to achieve a more comprehensive understanding of LCST phenomena. For example, Maeda used using IR, viscometry, and DSC methods together to study the interaction of water with poly(vinyl methyl ether) (PVME) around the phase transition temperature.[39] By analyzing the concentration dependence of endothermic enthalpy changes and the near IR spectral changes around the cloud point temperature, he determined that there was a cooperative formation of PVME-water complex above a

critical concentration of PVME. He was also able to show that there was a temperature-induced cooperative destruction of this same complex around 36 °C, resulting in the aggregation of the polymer chains due to the exposure of their hydrophobic groups.

Additive Effects on the Responsiveness of Thermoresponsive Polymers

The phase transition temperature of an aqueous solution of a stimuli-responsive polymer is known to be influenced by the addition of other substances such as cosolutes,[40-42] cosolvent,[43] surfactants[44] and other macromolecules.[45] The effects of such additives can alter the LCST so that it becomes higher or lower. The changes in the LCST depend on the interactions among the polymer, water and the additive. Salt and other cosolute effects are the most studied of the additive effects. This is in part a result of the fact that the changes in the LCST of a stimuli-responsive polymer in response to salts are paralleled by salt effects on the protein cold denaturation and enzyme activity.

The studies of salt effects began over 100 years ago in the late 1880 – when Franz Hofmeister, a pharmacologist, discovered that salts had different effectiveness in precipitating protein suspensions. Their effectiveness could be arranged in a sequence – that is now called a Hofmeister series. These effects have later been shown to be broadly applicable to many sorts of macromolecules. While the original Hofmeister series ranked anions or cations in their relative ability to precipitate a mixture of hen egg white proteins, later works showed that salt identity and concentration affected enzyme activity, protein stability and protein crystallization in the same fashion. Recent work has even shown Hofmeister effects for salts on bacterial growth. A 1985 comprehensive review of the Hofmeister effect includes nearly 1000 references and concludes that the

Hofmeister effect has the following characteristics: 1) it becomes important in the concentration range of 0.01-1.0 M; 2) different measurements of the Hofmeister series typically give similar ranking order; 3) there is usually a sign inversion at about NaCl; 4) anion effects are dominant; and 5) mixture of different salts have an effect that is approximately additive.[46] Typically, the Hofmeister anion series in terms of stabilizing proteins has the following order:

$$CO_3^{2-} > SO_4^{2-} > S_2O_3^{2-} > H_2PO_4^- > F^- > Cl^- > Br^- \approx NO_3^- > I^- > ClO_4^- > SCN^-.$$

The anions on the left side of Cl^- are historically called kosmotropic (water structure making) and the ones to the right are called chaotropic (water structure breaking). Whether the influence of anions on the macromolecular properties is caused at least in part by 'making' or 'breaking' bulk water structure has been debated over the past three decades. With the emergence of advanced experimental techniques, new data and evidence has suggested alternative explanations for such effect. Freitag and Garret-Flaudy had studied the effects of six potassium salts and two series of cations (five alkali-metal hydroxides and chlorides, respectively) on the cloud point temperature of PNIPAM oligomers. They found that all salts, with the exception of low concentrations (<0.5 M) of KI, lowered the cloud point temperature. Also, the relationship between the cloud point temperature and the concentrations of the added salt tended to be linear. The intensity of the anion effects corresponded to their position in the Hofmeister series. They interpreted the salt effect on PNIPAM oligomers based on the structure making/structure breaking potential of the involved ions as well as on the solvophobic theory which took into account the contribution of both electrostatic and hydrophobic

interactions.[47] The Bergbreiter and Cremer group also examined the salt effect of eleven sodium salts on the LCST of PNIPAM by using the temperature gradient microfluidics apparatus mentioned earlier. From these studies, they found that the ability of anions to lower the LCST followed the Hofmeister series. The effect of the anions was explained based on three direct interactions of the anions with the macromolecule and its immediately adjacent hydration shell. First, the anions could modulate the surface tension of the polymer/water interface. Second, anions (especially the kosmotrophic anions) polarized solvation water molecules that were directly hydrogen bonded with the amide moieties of PNIPAM. Last, certain chaotropic anions had an apparent binding constant for PNIPAM that created a 'salting-in' effect.[29]

Even though there is not a united theory to explain the anion effect, the ranking order of anions on LCST is widely accepted. The effects of cations on LCST are more complicated in terms of their ranking order and their overall importance relative to anions. As mentioned in Collin and Washabaugh's review, the Hofmeister effect is dominated by anions and the effects of cations are more modest. Freitag and Garret-Flaudy also investigated the effects of two series of cations (five alkali-metal hydroxides and chlorides, respectively) on the cloud point temperature of PNIPAM oligomers. Their results showed that variation of alkali cations, with the exception of Li^+, had little difference in depressing PNIPAM's LCST. In the experiment conducted by Hofmeister in 1888, the relative effectiveness of the cations of metal sulfate salts in salting-out of euglobulins from aqueous solution was ranked: $Li^+ > Na^+ \approx K^+ > NH_4^+ > Mg^{2+}$.[48] The only divalent cation that he examined was magnesium (II) and it was less effective in

salting-out protein than monovalent cations. In the study of the effects of salts on helix ↔ coil transition in fibrous protein collagen, von Hippel and Wong[49] found that the effectiveness of the cations on stabilizing the native helical structure of the collagen followed the order:

$$(CH_3)_4N^+ > NH_4^+ > Cs^+, Na^+, K^+, Rb^+ > Li^+ > Mg^{2+} > Ca^{2+} > Ba^{2+}.$$

This ranking was somehow correlated with cation charge density in such way that the cation with less charge density had a larger effect on stabilizing the helical form of collagen. Warren *et al.*[50,51] studied the salt effect on the activity of highly charged and uncharged enzymes and found that the ability of the cations of metal chlorides to maintain the enzyme activity followed:

$$(CH_3)_4N^+ > Cs^+ > K^+ > Na^+ > Rb^+ > Li^+.$$

Only monovalent cations were examined in this study and the ranking order of cations was similar to that of von Hippel and Wong. However, in the studies of the salt effect on the stabilization of halophilic malate dehydrogenase, Ebel *et al.* found that anions and cations were independently important in affecting the protein stability.[52] The order of cation efficiency depended on the salt concentration. At low salt concentration, the order of cations in stabilizing the folded protein form was:

$$Ca^{2+} \sim Mg^{2+} > Li^+, NH_4^+, Na^+ > K^+ > Rb^+ > Cs^+.$$

While at high salt concentration, the order reversed to

$$NH_4^+, Na^+, K^+, Cs^+ > Li^+ > Mg^{2+} > Ca^{2+}.$$

Divalent cations were most efficient in stabilizing protein only at the lower salt concentrations and tended to denature the protein at higher salt concentrations. The

anion effect however followed the Hofmeister series as $SO_4^{2-} \sim OAc^- > F^- > Cl^- > Br^- > I^-$ both at low and high concentrations.

The aforementioned examples suggested that the effects of cations on macromolecule solubility are complicated. The effectiveness of the cations seems to depend on the structure of the macromolecules used to probe the cation effects and on the nature of the counter ions. Most studies of cation effects have also been focused on monovalent cations, only a few divalent or higher valent cations have been investigated. In the research discussed in this dissertation, effects of cations such as Al^{3+}, Zn^{2+}, Mg^{2+}, Cu^{2+} and Ni^{2+} on PNIPAM solubility in solution and on wettability of PNIPAM-grafted nanocomposite surfaces have been studied. The details will be discussed in Chapter IV. These studies showed significant cation effects both on solution LCSTs and on graft surface wettability with sulfate ion as a common counter ion. Furthermore, if the salt activity was taken into account, the cation effect was correlated with the cation charge numbers in a way that their effectiveness follows order of trivalent > divalent > monovalent.

A recent report from Guo and Friedman also suggested that cation effects are charge density dependent.[53] They used Gadolinium (Gd^{3+}) vibronic sideband luminescence spectroscopy (GVSBLS) as a probe to study cation effects on the changes of OH stretching frequency derived from first-shell waters of aqueous Gd^{3+} and of Gd^{3+} coordinated to other molecules. Typically, the frequency of vibronic sideband (VSB) of this OH stretching mode was inversely correlated with the strength of the hydrogen bonding of Gd^{3+} coordinated water molecules to their neighboring waters. They found

out that the addition of cation chloride or acetate salts to aqueous solution of EDTA, structured peptides, or a calcium-binding protein increased the VSB in a cation identity and concentration dependent fashion. The cation effects on increasing VSB frequency were determined by the charge density of the cations. They also found out that the cation effects were modulated by the specific anion used. They concluded that high charge density cations sequestered waters in a configuration that precluded strong hydrogen bonding to neighboring waters. Anion effects emerged as anions competed for hydrogen-bonding sites with the remaining free waters on the surface of the hydration shell.

Several groups have studied the effects of surfactants (anionic, cationic and nonionic) on the phase transition of PNIPAM solutions or PNIPAM gels.[54-56] In solution, anionic surfactants such as sodium dodecyl sulfate (SDS) usually increase PNIPAM's LCST with increasing surfactant concentrations. At higher concentrations, the addition of SDS can even lead to the disappearance of this clouding phenomenon. Cationic surfactants only cause slight LCST increase while nonionic surfactants have almost no effect on the LCST.[57,58] Schild and Tirrell had systematically studied the interaction of PNIPAM with sodium *n*-alkyl sulfates in experiments where they varied the alkyl chain lengths to include alkyl groups that had 1-16 carbons.[55] Surfactants with chain lengths ≤ 4 depressed the LCST of PNIPAM and exhibited no evidence of enhanced aggregation in PNIPAM solutions. Surfactants with intermediate chain lengths of 5-10 carbons depressed the LCST at low surfactant concentrations but increased the LCST at concentrations that exceed the critical aggregation concentrations. Sodium *n*-dodecyl

sulfate elevated the LCST even at low concentrations and formed aggregates in PNIPAAM solutions at a concentration 10-fold lower than its critical micelle concentration. They concluded that PNIPAM promoted the surfactant aggregation and formed complexes with the so- formed surfactant micelles. This effect became most apparent with longer surfactant alkyl groups and was not seen for surfactants containingt chain lengths of four carbons or less. Elevation of the LCST with longer chain sodium *n*-alkyl sulfates was a result of electrostatic repulsion between charged polymer-micelle complexes, which prevent polymer collapse and aggregation.

An anionic biological surfactant, sodium cholate has also been applied to PNIPAM solution to understand the biocompatibility of PNIPAM's biomedical applications.[59] DSC studies showed that the presence of sodium cholate broadened the phase transition endotherm of PNIPAM solution and shifted the PNIPAM LCST to lower temperature. The effect of the sodium cholate on the LCST of PNIPAM was in contrast to the effect of conventional anionic surfactants that generally shifted the LCST to higher values.

As mentioned earlier, stimuli-responsive polymers, especially PNIPAM have received attention for their biomedical applications in drug delivery and in biosensors. Given the presence of biological macromolecules in aqueous solutions, various studies have been reported that examine the influence of macromolecular species on the phase transition temperatures of PNIPAM. Housni and Narain examined the influence of macromolecular species, polyethylene glycol (PEG with M_n of 3400 Da) and ionic bovine serum albumin (BSA with M_n of 63000 Da), on the LCSTs of PNIPAM prepared

by RAFT polymerization process.[45] The effects of the macromolecular species on LCSTs of PNIPAM samples with different degree of polymerization were listed in Table 1. These data showed that the addition of both PEG and BSA raised the LCSTs of all PNIPAM samples. The effect of PEG did not vary with the molecular weight of PNIPAM samples while the effect of BSA was most noticeable for the lower molecular weight PNIPAM samples. Dynamic light scattering and surface tensiometry were used to probe the interactions between the added macromolecules and the PNIPAM chains. The results showed that adding macromolecules increased the surface activity (low surface tension) of PNIPAM solutions and decreased the hydrodynamic radius of the PNIPAM molecules at 25 °C. They proposed that the macromolecular additives stabilized dehydrated PNIPAM chains by forming hydrogen bonds with them. Overall, they concluded that macromolecular additives had effects on the coil to globular transition of PNIPAM samples, especially with the lower molecular weight PNIPAM.

Table 1. Effect of varying concentrations of polyethylene glycol (PEG) and bovine serum albumin (BSA) on the cloud point temperature of PNIPAM samples with different degree of polymerization. The concentration of all PNIPAM solutions is 5 mg/mL in water.

PNIPAM samples	No additive	Addition of PEG					Addition of BSA		
		1 mg/mL	2 mg/mL	4 mg/mL	5 mg/mL	10 mg/mL	1 mg/mL	5 mg/mL	10 mg/mL
NIPAM(50)[a]	34.2	34.3	34.5	35.3	35.4	36.3	35.6	36.6	37.1
NIPAM(100)[a]	34.2	34.3	34.3	35.1	35.3	36.1	34.5	35.0	36.0
NIPAM(200)[a]	34.1	34.1	34.2	35.4	35.4	36.2	34.8	34.8	36.0

[a] the number in the parenthesis represents the degree of polymerization.

Tjerneld *et al.* investigated the effects of sugars on the cloud points of aqueous poly(ethy1ene glycol) (PEG 20000) solutions with sugars like glucose, maltose, cellobiose, isomaltose, maltotriose, isomaltotriose, and *p*-cyclodextrin. All of these glucose-based sugars, except *p*-cyclodextrin, were found to decrease the cloud points of PEG solution.[60] The 1,6-linked linear oligosaccharides were found to be much more effective in depressing the cloud points of PEG than the 1,4-linked linear oligosaccharides that had the same number of glucose units. The differences between the sugars in their ability to decrease the cloud points in aqueous PEG solutions were explained by their differences in forming intramolecular hydrogen bonds. Studies of the effects of sugars on the LCSTs of PNIPAM aqueous solutions were also carried out by Livney *et al.* in an effect to understand sugar effects on protein stabilization.[61] Their results showed no significant binding of sugars to the polymer occurred and that the LCST of PNIPAM decreased with increasing carbohydrate concentrations. They found a good correlation between a sugar's hydration numbers and its effect on PNIPAM's LCST. The carbohydrates that formed larger and denser hydrated cluster had stronger effect on lowering the coil-to-globule transition temperature.

Design of Stimuli-responsive Polymers

Polymer microstructures will affect the responsive properties of a stimuli-responsive polymer. The design of 'smart' polymers for applications in controlled release or targeted delivery often includes addition of other functional groups or segments to a well-studied thermoresponsive polymer. Responsive random copolymers,[62,63] amphiphilic polymers, grafted copolymer[64-66] and block polymers[67,68]

with different functionalities, shapes and sizes have all been studied in this regard. Generally, incorporation of hydrophobic groups into a thermoresponsive polymer will lower its LCST while the addition of hydrophilic groups will increase its LCST. For example, Kakuchi *et al.* studied the effect of varying the structures of a series of block copolymers consisting of PNIPAM and poly(*N*-hydroxyethylacrylamide) (PHEAA) on the thermoresponsive behaviors of these polymers.[69] Their syntheses used atom transfer radical polymerization (ATRP) to prepare well-defined diblock and triblock copolymers consisting of different fractions of PNIPAM and PHEAA. The number-average molecular weight and mole fraction of each segment were controlled by adjusting the monomer/initiator ratio in feed. The LCSTs of block copolymers with different compositions were then examined by turbidimetry. Their studies showed that the copolymers with lower mole fractions of HEAA units exhibited phase transition phenomenon, in which the LCSTs depended on the mole fractions of HEAA in the copolymer. On the other hand, no LCST was observed for the copolymers with higher mole fractions of HEAA. ^{1}H NMR spectroscopy showed that the disappearance of the LCSTs was due to the formation of the water-soluble micelles. Their studies also showed that structural factors such as position, length and sequence of each block in the copolymers significantly affected the polymers' thermoresponsiveness.

Copolymers that contain functional groups such as acid or base sensitive groups can exhibit dual responsiveness, namely pH and temperature responsiveness.[22] Block copolymers that form core-shell micelles[70,71] or core-shell-corona complex micelles,[72,73] and ABC miktoarm star terpolymer[74] have been studied for their applications on

controlled drug release that can respond both to pH and to temperature changes. Thayumanavan *et al.* designed an amphiphilic block copolymer, which consisted of a hydrophobic tetrahydropyran (THP)-protected 2-hydroxyethyl methacrylate (HEMA) segment and a hydrophilic PNIPAM segment with an intervening disulfide bond (Scheme 4). This block copolymer can self-assemble to form micelles and encapsulate guest molecules inside the micelles at room temperature in water. However, the hydrophobic THP-protected HEMA block is acid sensitive. Under acidic conditions, the THP protection groups can be removed by hydrolysis and the HEMA segment became hydrophilic. The hydrophilic PNIPAM block is temperature responsive and can become hydrophobic when the temperature is above its LCST. Changing of pH or temperature will thus affect the self-assembly of these micelles by changing the hydrophobicity of one of the segments on this block copolymer. Guest molecules in the micelles can then be released by a pH or temperature change. Furthermore, this amphiphilic block copolymer is also redox responsive since the disulfide bond can break under reduction conditions to disassemble the micelle structure. Further experiments also showed that this amphiphilic block copolymer was responsive not just to one single stimulus, but to multiple stimuli.

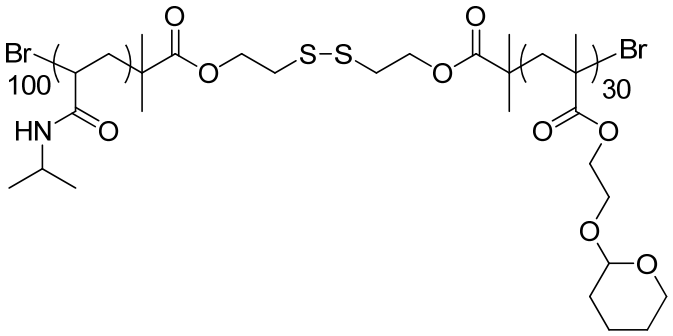

Scheme 4. A multi-stimuli sensitive amphiphilic block copolymer.

Other stimuli-responsive polymers have been designed in order to create materials that can exhibit structural and morphological changes. For example, Fréchet *et al.* designed an amphiphilic polymer that consisted of poly(ethylene glycol) as the hydrophilic component and 2-diazo-1,2-naphthoquinone as the hydrophobic component.[75] The hydrophobic 2-diazo-1,2-naphthoquinone end group could undergo a Wolff rearrangement to form a hydrophilic 3-indenecarboxylate at room temperature in neutral aqueous solution with IR radiation. This amphiphilic polymer was shown to be able to respond to infrared light in such a way that the micelle formed by the polymer was destroyed in a two-photon photoreaction and the encapsulated fluorescent probe molecule was then released. Scheme 5 illustrates the structure of this amphiphilic polymer and the chemical reaction of 2-diazo-1,2-naphthoquinone to 3-indenecarboxylate that is triggered by IR radiation. More examples of light-responsive polymers can be found in other literature.[3,76,77]

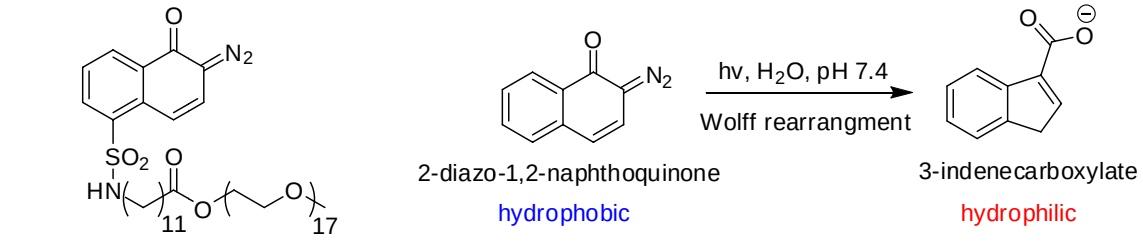

Scheme 5. The structure of a IR light sensitive amphiphilic polymer and the chemical reaction of the 2-diazo-1,2-naphthoquinone triggered by IR radiation.

Spiropyran-containing polymers that respond to mechanical stress and exhibit a colorimetric response have been prepared by Moore and Sottos (Scheme 6).[78] In these materials, a reversible electrocyclic ring-opening reaction of spiropyran to merocyanine is the key reaction in this design and the color changes observed are associated with this reaction. When polymers such as poly(methyl acrylate) or poly(methyl methacrylate) were attached to the 5' and 8 positions of spiropyran, application of mechanical stress such as stretching and compression can induce the ring-opening reaction and lead to visible color changes.

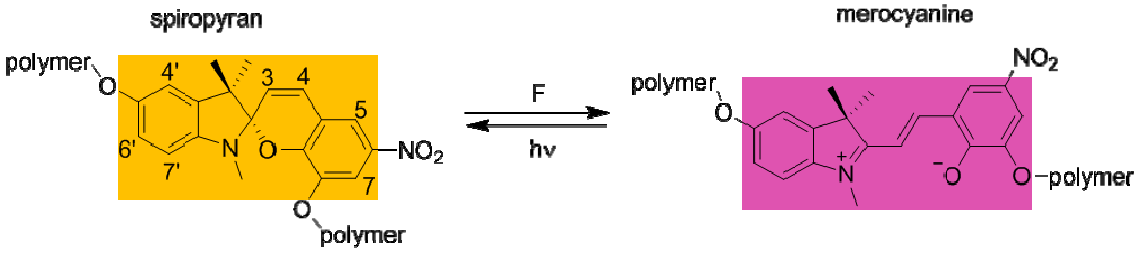

Scheme 6. A spiropyran-containing polymer that can respond to mechanical stress.

As shown in Schemes 4–6, functional groups that undergo specific chemical reactions can be incorporated into polymers and such functionality can alter the product

polymer's physical properties in various ways. Given the wide range of chemical reactions available, the possibilities of designing new smart polymers are endless. A broader spectrum of stimuli-responsive polymers that include not just thermoresponsive polymers but also electric-, magnetic- and mechano-responsive polymers can be anticipated. Part of my research involved incorporating new functional groups into PNIPAM to instigate specific responsiveness on this well-studied thermoresponsive polymer and to alter the LCST in a controlled manner. The details will be discussed in Chapter VI.

Grafting Stimuli-responsive Polymers on Solid Surfaces

Stimuli-responsive polymers have also been grafted on solid substrates to create functional surfaces based on the same sorts of responsiveness observed in aqueous solutions. When grafted onto a surface, the thermoresponsive polymer chains will exist in an expanded conformation at low temperatures. Such hydrophilic grafts lead to hydrophilic surfaces. If at higher temperatures, a thermoresponsive polymer undergoes hydrophobic collapse, the surface can become hydrophobic. Just as PNIPAM is the most commonly studied stimuli-responsive polymers in solution, it is the most studied at surfaces too. Several experimental studies have showed that PNIPAM chains on grafted surfaces undergo coil-to-globule phase transition at temperatures that are close to its LCST.[79-81] These PNIPAM grafts have been used in drug delivery systems, in permeation-controlled filters, and in temperature-controlled actuators. PNIPAM grafts have also been used in liquid chromatography systems and recently temperature-

controlled cell culture dishes where the stimuli-induced hydrophobicity changes of PNIPAM are used to change surface hydrophobicity.

Various surface grafting methods including electrostatic self-assembly, hydrogen bond self-assembly, physical absorption and covalent grafting have been used to prepare responsive surface grafts. These methods can be used on glass, silicon wafers, metals, and even plastics. Our group is interested in the chemical grafting methods especially in covalent layer-by-layer self-assembly. This introduction will discuss different strategies for chemical grafting.

A common chemical grafting strategy is to 'grow' polymer chains from the surface. This method has been referred as the 'graft-from' method since the polymerization is initiated from the surfaces. By using this method, surfaces with long chains and high densities of polymer grafts can be prepared. In order to carry out this graft-from method, the substrate surfaces are first chemically modified to attach active groups. These groups can include initiators, transfer agents, or monomers. Conventional radical polymerizations or living radical polymerizations are most commonly used in the surface initiated polymerizations. Atom transfer radical polymerization (ATRP) is the most common procedure among these methods for the controlled synthesis of polymers on surfaces as it is applicable to different monomers and reaction media (aqueous or organic). Another advantage of using ATRP is that the end of the polymer chains is capped with an active functional group. Such groups can be used to form block copolymer brushes by the addition of fresh catalyst and a new monomer.

For example, NIPAM was grafted onto mixed self-assembled monolayers (SAMs) on gold by ATRP using a CuBr and Me_4Cyclam (1,4,8,11-tetramethyl 1,4,8,11-azacyclotetradecane) catalyst system at room temperature.[82] The thermally induced hydration transition of these PNIPAM brushes was then studied by surface plasmon resonance spectroscopy (SPR) and contact angle measurements. SPR measurements showed that the PNIPAM brush collapsed over a temperature range of ~10−40 °C. The contact angle measurements, however, indicated a sharp wettability transition at a temperature of ~32 °C with advancing water contact angles changing from ~65° to 78°. The results showed that polymer segments in the outermost region of the brush remained highly solvated until the solution lower critical solution temperature (~ 32°), while densely packed, less solvated segments within the brush layer underwent dehydration and collapse over a broader range of temperatures.

PNIPAM brushes have also been prepared on quartz crystals by ATRP. The PNIPAM grafted crystals were then used to determine the effect of salts on the volume phase transition of thermoresponsive polymer brushes by using quartz crystal microbalance with dissipation monitoring (QCM-D) analyses.[83] Changes in mass and viscoelasticity of PNIPAM brushes were measured as a function of temperature, upon contact with NaCl solutions. The phase-transition temperatures of PNIPAM brushes derived from QCM-D measurement were found to decrease as the concentrations of NaCl increased. This observation paralleled the inverse relationship between the concentration of salt and the LCST of PNIPAM in aqueous solution. However, in contrast to the linear decrease in LCST upon increasing salt concentrations observed for

PNIPAM solutions, the trend in phase-transition temperature for PNIPAM brushes was non-linear. Specifically, at low salt concentrations, the phase-transition temperature decreased more rapidly and tended to level off at elevated concentrations. This phenomenon was explained by the tendency of salt ions to affect the water structure around PNIPAM chains.

Surface-initiated aqueous ATRP using PMDETA/CuCl and HMTETA/CuCl catalysts has also been used to synthesize PNIPAM brushes on polystyrene latex particles.[84] First, functionalized anionic polystyrene latex particles with ATRP initiators were synthesized by surfactant-free shell-growth emulsion polymerization of styrene and 2-(2'-chloropropionato)ethyl acrylate. NIPAM was then polymerized from these particles by ATRP in water. The molecular weight of the PNIPAM chains, grafting density, and hydrodynamic thickness of the grafted polymer layer were then measured. The M_n and grafting density of the grafted PNIPAM chains increased with increases in the monomer concentration and decreased with addition of copper (II) complex and external initiator. Molecular weights from about 50 kDa to 800 kDa with low polydispersities (between 1.25 and 1.4), were achieved. A further polymerization of *N*,*N*-dimethylacrylamide onto a PNIPAM-grafted latex established that the original PNIPAM chains were terminated with a reactive end group. The hydrodynamic thickness (HT) values for PNIPAM brushes were sensitive to temperature and salt concentration. The hydrodynamic thickness of the brushes decreased from ~ 580 nm to 100 nm when the temperature was increased from 22-36 °C suggesting a broad transition region. The HT values of PNIPAM grafted PS particles were also measured in NaCl and Na_2SO_4 with varied salt

concentrations. The HT decreased with increases in salt concentrations in both cases. Na_2SO_4 induced a HT transition at around 0.2 M while NaCl effects were only seen at ~ 1.0 M. These results showed that effects of salts on the HT of PNIPAM brushes were similar to the effects of those salts on the LCST of PNIPAM solution.

Nitroxide-mediated controlled polymerization (NMP) was also used by Wolfgang *et al.* to grow PNIPAM directly from iron oxide nanoparticles. This lead to the formation of magnetic iron oxide core/shell nanoparticles with a defined PNIPAM shell around the nanoparticles (Scheme 7).[85] In this chemistry, a 1,2-diol functionalized NMP initiator was attached to the Fe_2O_3 nanoparticles by ligand exchange with an octylamine stabilized Fe_2O_3 nanoparticle. The resulting nanoparticles (**NP1**) were then used to initiate the controlled polymerization of NIPAM in DMF at 150 °C to form Fe_2O_3 nanoparticles coated with a thermoresponsive organic shell (**NP2**).

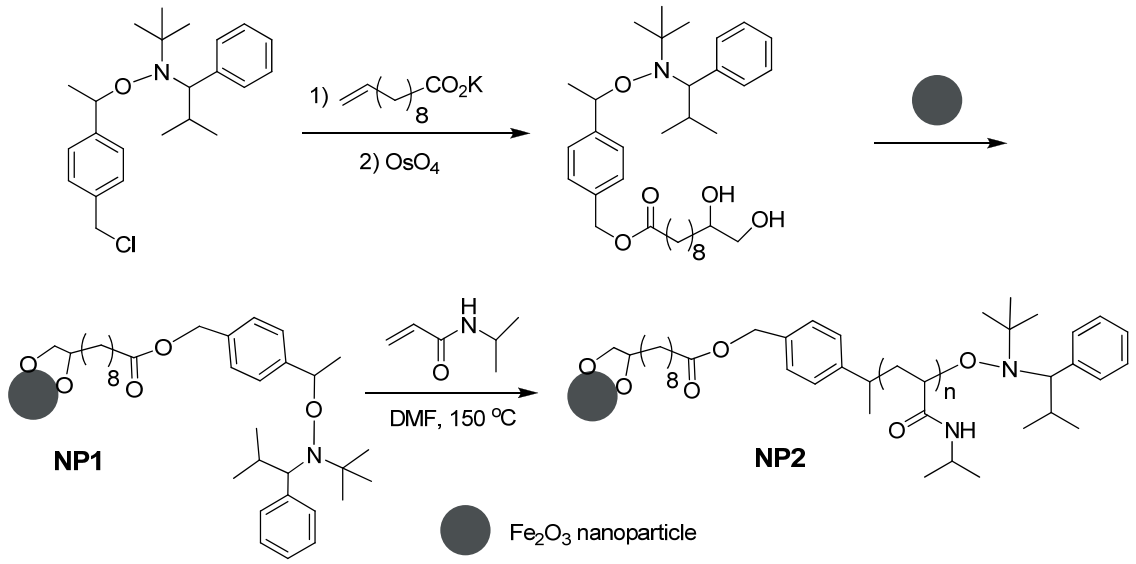

Scheme 7. PNIPAM chains grow from Fe_2O_3 nanoparticles by surface-initiated nitroxide-meditated control polymerization.

Other polymerization techniques such as plasma polymerization,[86] electron beams irradiation,[87] and electrochemically induced free-radical polymerization[88] have also been used to graft thermoresponsive polymers on surfaces. For example, PNIPAM deposited onto silicon wafers and capillary glass tubes from a plasma glow discharge of NIPAM both have a phase transition temperature of about 29 °C. Plasma polymerization of NIPAM as described in this study is a one-step, solvent-free, vapor-phase coating technique that can be applied to fabricate thermally responsive coatings on a variety of biomaterials, avoiding the need for specially prepared substrates and functionalized polymers.

Alternatively, chemical grafting can be achieved by allowing functionalized surfaces to react with stimuli-responsive polymers that bear reactive group(s). This method is also called 'graft-to' method since the polymer is premade before grafting it to the surface. The advantage of this method is that the to-be-grafted polymer can be characterized beforehand. The reactive groups can be incorporated into the polymers as terminal groups, pendant groups or in the main chain of the polymer. Different chemical reactions can be used for grafting. For example, Iwata *et al.* demonstrated the preparation of ultrathin thermo-sensitive layers on substrate surfaces by allowing a PNIPAM copolymer that contained < 2% isocyanate units to react with a hydroxyl-functionalized gold surface (Scheme 8).[89] Ye et al. synthesized PNIPAM protected CdS quantum dot by using terminal thiolated PNIPAM to react with CaS particles directly.[90] Thiol-terminated polymers have been frequently used in the 'graft-to' method because

such polymers with narrow molar mass could be conveniently prepared by RAFT polymerization process followed by the reduction of the dithioester end groups.[91]

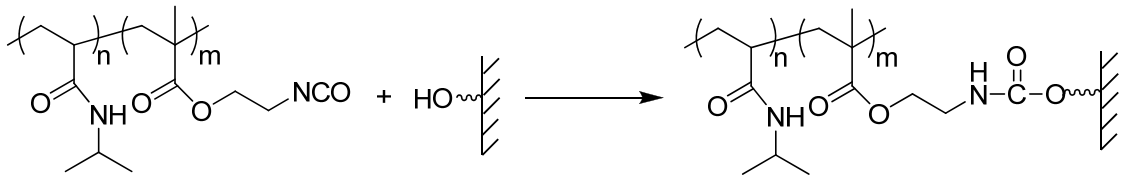

Scheme 8. The grafting of PNIPAM to a gold surface by allowing isocyanate containing PNIPAM copolymer to reacted with surface hydroxyl group.

Condensation reactions of nucleophiles and carbonyl derivatives that result in stable bonds can also be used to graft functional polymers to the substrate surfaces. Either the nucleophiles or the carbonyl derivatives can be incorporated into the to-be-grafted polymers as terminal groups, in backbones, in pendant groups, or as side chains. Such polyvalent polymers can be grafted to surfaces sequentially via a covalent layer-by-layer (LbL) assembly method. Our group has successfully used this chemistry to graft polyfunctional polymers to surfaces like silica nanoparticles, silicon wafers, metals, polyethylene films, and multiwall carbon nanotubes.

This chemistry typically uses polyvalent electrophiles and nucleophiles to build a polymer network on substrate surfaces. For example, commercially available poly(maleic anhydride)-*c*-poly(methylvinyl ether) (Gantrez, **1**) is a polyvalent electrophile that can be used with nucleophilic amine-terminate generation five (G5) poly(amidoamine) dendrimers (**2)** to form a polymer graft. By alternately treating the activated surface with **1** or **2**, ultrathin multilayer grafts were assembled successfully on Au, Al, Si, or polyethylene. Furthermore, the amic acids generated during the grafting

process could be imidized by mild heating to form impermeable monolithic films. If a hydrophobic octadecyl layer were attached as a top layer at the end of this covalent LbL assembly, the imidized monolithic film could serve as a protective layer for a substrate like Al. The passivation of Al against corrosion in alkaline solution or from pitting in neutral chloride-containing solution was demonstrated.[92]

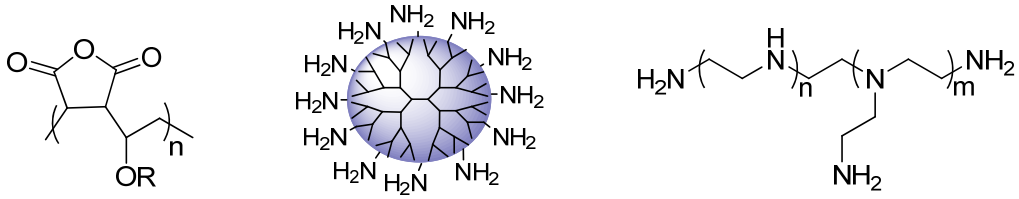

1 **2** **3**

The experimental procedure for covalent LbL assembly of PEI (**3**)/Gantrez (**1**) on oxidized PE substrates by this method is shown in Scheme 9. In this chemistry, the first step is oxidation of the PE substrates with chromic acid to generate carboxylic acid groups at the surfaces. The so formed carboxylic acid groups are subsequently activated to form electrophilic mixed anhydride groups by treatment with ethyl chloroformate. The nucleophilic polyvalent polymer, PEI, is then attached to the activated PE surface by reaction with the anhydrides to form amide bonds. The newly formed surface is rich in nucleophilic amine groups. Those groups are then allowed to react with electrophilic Gantrez. Repetition of this amine-anhydride condensation reaction yields a surface graft covered with a network of PEI and Gantrez.

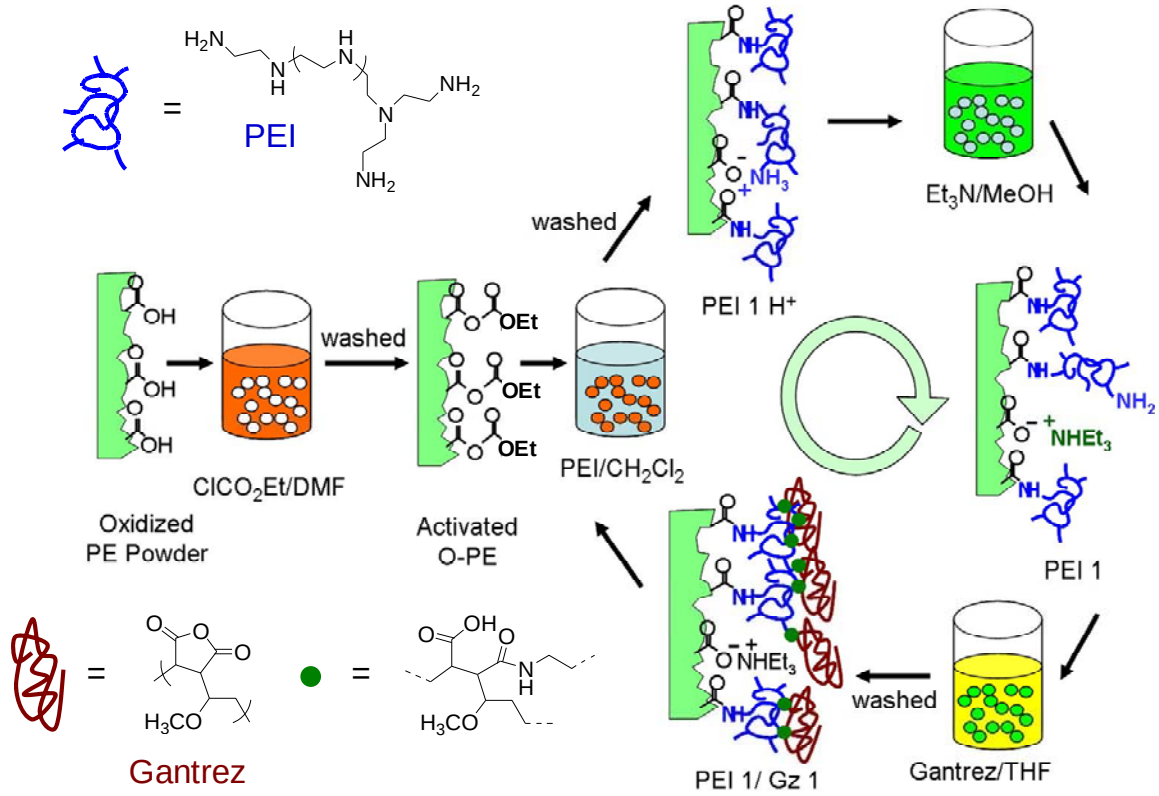

Scheme 9. The grafting procedure of covalent LbL assembly of PEI/Gantrez on oxidized PE substrates.

The progress of this synthetic process on surfaces can be analyzed by ATR-IR spectroscopy that shows the disappearance of a small carboxylic acid peak of oxidized PE at 1710 cm^{-1} and the appearance of an amide peak at 1650 cm^{-1}. The subsequent treatment by Gantrez leads to the appearance of anhydride peaks at 1790 and 1730 cm^{-1}. The reaction of Gantrez and PEI and the presence of ammonium carboxylate groups can be confirmed by observing the disappearance of anhydride peaks and the appearance of amide and carboxylate peaks at 1650 and 1560 cm^{-1} respectively. Fluorescence analysis can also be used to monitor surface growth by covalently tagging a small percentage of a

fluorophore, dansyl amine to the surface during the process when the surface is treated with PEI. For example, a graft with six (PEI+ dansyl amine)/Gantrez bilayers were assembled on oxidized PE and the fluorescence was measured after each of the bilayer assembly. Except for the first bilayer assembly, the fluorescence analyses showed linear fluorescence intensity increase between the second bilayer and the sixth bilayer assembly.

This dansyl amine-tagged $(PEI/Gantrez)_6$ graft was also alternately treated with acid (1.0 M HCl) and base (1.0 M NaOH) to test the stability of such surface grafts prepared by covalent LbL assembly method. These acid/base conditions are known to lead to delamination of electrostatic assembled LbL grafts. The results showed that the fluorescence intensity dropped significantly after acid treatment because protonation of the tertiary amine group on the dansyl group diminished the fluorescence. However, the fluorescence did not completely disappear suggesting that not all the dansyl groups reacted with HCl. The fluorescence intensity increased to almost the original value after subsequently treatment of NaOH due to the deprotonation of the tertiary amine salts. The reversible changes in fluorescence intensity through repeated HCl/NaOH treatments showed that this covalent surface graft was stable to such acid/base treatments.

This covalent LbL assembly method can also use functionalized inorganic materials as a reagent. For example, we successfully prepared a nanocomposite thin film on functionalized PE films by covalently assembling PEI functionalized multiwall carbon nanotubes (MWNT-NH-PEI) (**4**) and Gantrez. The surface consisting of five MWNT-NH-PEI/Gantrez bilayers was modified to be superhydrophobic by treating with

ethyl chloroformate and octadecanoic acid. The resulting octadecylated surface had a water contact angle of 165° and a sliding angle of less than 5°. These surfaces also exhibited a nanoscopic roughness based on AFM studies.

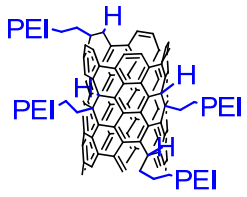

4

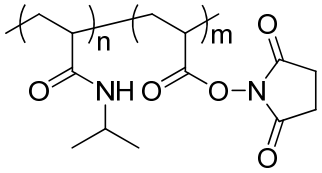

5

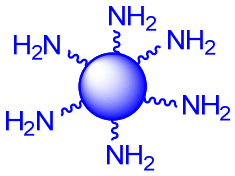

6

In this dissertation, the same covalent LbL self-assembly procedure has been used to graft PNIPAM/SiO_2 nanocomposites on either organic or inorganic surfaces. In these syntheses, an active ester-containing PNIPAM copolymer **5** and aminated silica nanoparticles **6** are used as polyvalent electrophiles and nucleophiles respectively. These PNIPAM/SiO_2 nanocomposite surfaces show significant solute-induced wettability changes that depend on the solute identity and solute concentration. For example, a $(PNIPAM/SiO_2)_6$/PNIPAM nanocomposite grafted PE film had an advancing contact angle (θ_α) of 76° in water while in 1.0 M Na_2SO_4 the θ_α was 144°. In 1.2 M NaSCN, the θ_α was 72°. These large differences in advancing contact angles enabled us to study the effects of salts on the wettability of surfaces. This has included studies of both anions and cations. Details of these results will be discussed separately in the later chapters.

CHAPTER II

THERMODYNAMIC CLOUD POINT ASSAYS*

Introduction

Cloud points and clouding behavior are widely used as visual probes of phase separation in macromolecular systems.[12,93] We and others have used measurements of clouding to study lower critical solution temperature (LCST) behavior for a variety of materials including polymers like poly(*N*-isopropylacrylamide) and poly(alkene oxide)s.[69,94] This work most commonly requires several milliliters of a solution and most often the phase separation process is followed by observing changes in transmittance of a sample using a visible spectrometer. Apparati that use smaller volumes (e.g., 20 μL of sample) have also been described.[95] More recently our analyses of these phenomena were greatly facilitated by the application of a new microscale temperature gradient apparatus developed by the Cremer group.[29] This simple instrument setup has the advantage of only requiring 10 μL of solution in a capillary tube and affords significantly greater precision than prior assays that monitor transmittance changes. The advantage of assaying as many as 6 or 7 samples at once without the delays associated with waiting for an apparatus to heat from below the LCST to above the LCST make this method a high throughput method for analysis of samples with LCSTs in the 20-50 °C

---

*Part of the data reported in this chapter is reprinted with permission from "Thermodynamic Clouding Assays" by D. E. Bergbreiter and H. Fu, *J. Polym. Sci., Part A: Polym. Chem.*, 2007, **46**, 186, Copyright [2007] by Wiley Periodicals, Inc., A Wiley Company.

range. Several other techniques have also been used to study such phase separation processes. These include dynamic light scattering,[96] differential scanning calorimetry,[97] NMR spectroscopy,[98-100] dynamic rheology,[101] IR spectroscopy,[102] solvatochromatic effects,[103] and fluorescence spectroscopy.[104,105] Nonetheless, while all of these techniques have been used from time to time, simple assays of clouding behavior remain the most common approach to studying these sorts of phase separation processes that are important in a variety of applications of thermally responsive polymers.[68,106-112]

Here we describe another approach to assay clouding behavior for polymer solutions exhibiting LCST behavior. This microscale assay of LCSTs uses 10 μL or less of a sample solution and a commercially available automated melting point apparatus to measure and record LCST clouding curves at temperatures from ambient to over 250 °C. Although this apparatus sacrifices some of the high throughput features of Cremer's temperature gradient apparatus,[113] it can still assay up to three samples at once at temperatures that are defined by a calibrated instrument. As a bulk assay, it advantageously monitors phase changes of these stimuli-responsive materials in a fashion that exposes these materials to temperature changes like they would encounter in typical applications. The apparatus uses samples that can be sealed in capillary melting point tubes so samples can be easily saved and reanalyzed. Moreover, since the instrument is computer controlled and automatically saves the experimental data to a computer, it is experimentally practical to use different temperature rates to assay and record the change in clouding behavior. This can reveal very complex sorts of phase behavior. As discussed later, manipulation of the data also allows one to determine what

the clouding process would look like with an infinitely slow heating rate and to obtain a corrected clouding temperature that is a more accurate thermodynamic measure of the entire phase separation process. These assays use the same methodology used to determine 'corrected' melting points in analysis of pharmaceuticals to obtain 'corrected' clouding curves.[114]

Melting Point Apparatus and LCS Measurements

An OptiMelt apparatus from Stanford Research Systems was used for analyses of LCST in this study.[114] This apparatus uses a digital image processor to detect the light scattering that occurs as a sample changes from a scattering solid to a liquid. Since an aqueous solution of PNIPAM during an LCST process exhibits analogous changes in its optical characteristics, this same melting point apparatus can determine an LCST and a clouding curve. Other features of this apparatus include linear temperature ramping and accurate temperature readings with 0.1 °C resolution. In a typical experiment, 10 μL of a polymer solution was introduced to a regular capillary melting point tube (Kimble 1.5-1.8 X 90-mm) using a microsyringe and the tube was sealed before placing it into the sample holder. Three sealed sample tubes were placed into the sample holders for simultaneous measurements of their clouding curves at the desired heating rate. During the heating process, the thermosensitive polymers underwent phase transitions that changed the optical characteristics of the sample. The reproducibility of phase transition behavior was monitored by carrying out a second clouding curve assay. The second sample could be obtained either by removing the tube from the apparatus and letting the polymer redissolve or by preparing a fresh sample. Repetition of the LCST measurement

the same day or after several days using the same heating rate gave curves that were identical to the original curves. This is illustrated in the figures below. The digital image processing on board the melting point apparatus analyzed the intensity changes and produced a graph of the percent light scattering versus temperature. The resulting usually sigmoidal curve of the extent of clouding versus temperature and the data for specific scattering percentages were then used in our LCST studies. The supplied MeltView software transferred and stored the real-time images of the samples to a computer during the analysis. The software bundles all sample images together as a single package file and the file can be recalled at anytime to play back the phase transition process frame-by-frame or as a continuous movie. Such movies provide a visual record of the phase changes and allow qualitative differentiation of the phase separation process in milieu as similar as H_2O, 50/50 (v/v) H_2O/D_2O, and in pure D_2O (see supplementary material).

Studies of LCSTs by an Automatic Melting Point Apparatus

The utility of a digital melting point apparatus for the analysis of clouding curves is illustrated by the results in Figure 1. This figure displays a series of raw data measuring scattering of a 10 mg/mL sample of PNIPAM (M_w = 322 kDa, PDI = 1.06 by GPC) in water as a function of heating rate as capillary tubes containing about 10 μL of this aqueous polymer solution were heated from 30 to 34 °C. The analyses used heating rates of 0.1, 0.2, 0.5, 1.0, 2.0, and 5.0 °C/min. Just as true in a melting point determination, higher heating rates produce different clouding behavior with the curves progressively moving to higher temperature as the heating rate increases.

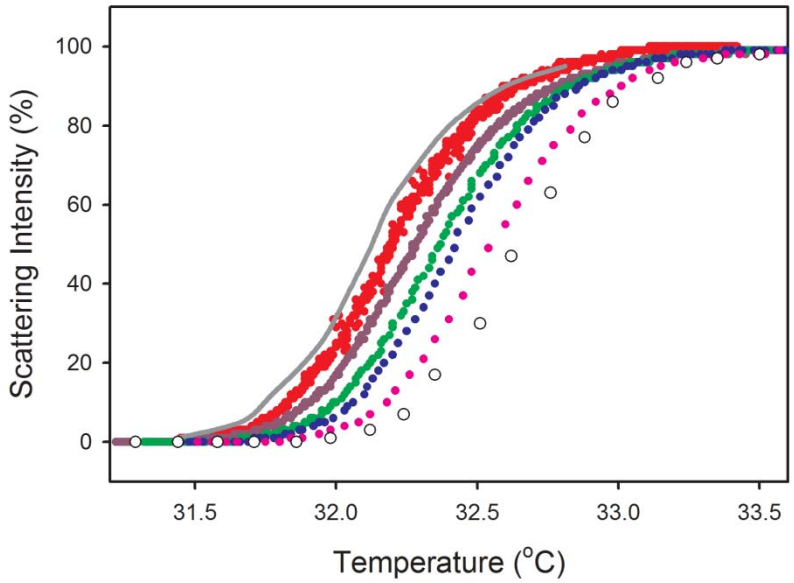

Figure 1. Scattering curves showing the percentage of light scattered versus temperature for a 10 mg/mL solution of poly(N-isopropylacrylamide) in water as a function of heating rate: red color (0.1 °C/min); magenta color (0.2 °C/min); green color (0.5 °C/min); blue color (1.0 °C/min); pink color (2.0 °C/min); (○) (5.0 °C/min). The solid gray line is the 'corrected' clouding curve (see text).

The observation in Figure 1 that the observed LCST value depends on the heating rate is not unexpected. Such effects are seen in most methods that assay a polymer's LCST. As is true in melting point analyses, a 'corrected' clouding curve would be one that would be measured at an infinitely low heating rate. That of course poses an experimental problem akin to that faced in measuring specific viscosity for an infinitely dilute polymer solution. We addressed this problem reasoning that the changes in the observed clouding curve associated with varied heating rates could arise because of the inefficiency of the heat transfer between the sample and the heating stand at least in some cases. In analogy to the reasoning used to obtain corrected melting points, 'corrected' thermodynamic cloud point temperatures ($LCST_{actual}$) could be measured at varying extents of clouding. Such data when plotted would then produce a 'corrected'

cloud point curve which would correspond to the thermodynamic LCST clouding curve that would be obtained at an infinitely slow heating rate. Such data and such a curve should be calculable if the light scattering because of the phase transition is proportional to the square root of the ramp rate as is the case in a melting point assay.

Using the same reasoning used to calculate a thermodynamic melting point,[114] the amount of heat (d$Q(t)$) transferred from the block to the sample by a melting point apparatus during an LCST analysis in a given time dt is given by eq 1.

$$dQ(t) = \alpha\,(T_{obsd} - T_{actual})\,dt \tag{1}$$

This amount of heat depends on a constant α that reflects heat transfer properties of the apparatus and sample, the time, and the temperature difference between the block and the stand (T_{obsd} - T_{actual}). If the phase separation process acts like a first order phase transition, the sample temperature will be essentially constant during the period the block is being heated. The temperature ramping rate of the instrument r is equal to dT/dt, so eq 1 can be rewritten as shown in eq 2.

$$dQ(t) = \alpha\,(T_{obsd} - T_{actual})(dT/r) \tag{2}$$

Integration of this expression over the observed temperature range for the visible clouding phase transition gives eq 3 where the integral term can be related to the thermodynamics of the phase transition (the term designated ΔG_{LCST} in eq 3).

$$\Delta G_{LCST} = \int_{LCST_{actual}}^{LCST_{obsd}} \left[\frac{\alpha(T - T_{thermo})}{r}\right] dT \tag{3}$$

$$\Delta G_{LCST} = (\alpha/2r) \cdot (LCST_{obsd} - LCST_{actual})^2 \tag{4}$$

$$LCST_{actual} = LCST_{obsd} - (2\Delta G_{LCST}/\alpha)^{1/2}\, r^{1/2} \tag{5}$$

Solving this integral term then leads to eq 4 which can be rearranged to the form of a linear equation (eq 5) where the difference in the clouding temperature that is correlated with the LCST, $LCST_{obsd}$, and the $LCST_{actual}$ will be directly related to the square root of the temperature ramp rate with a slope that is determined by the thermodynamics for the transition and the aforementioned constant α that reflects the heat transfer properties of the apparatus and sample.

Application of eq 5 to various points in a clouding transition for PNIPAM does indeed show that there is a linear relationship between the square root of temperature ramp rate and the $LCST_{obsd}$ for various levels of clouding in several phase transitions (Figure 2). When these linear correlations are extrapolated to the intercept on the ordinate of the graph, they generated a set of data ($LCST_{actual}$) that are in effect cloud point measurements at an infinitely slow heating rate - data that when plotted produce a thermodynamic clouding curve. The representative $LCST_{actual}$ values for the clouding temperature studies of PNIPAM in H_2O and D_2O are listed in Table 2. The standard errors for each of the $LCST_{actual}$ values at 95% confidence are also listed in the same table. As shown in Table 2, the standard errors for the $LCST_{actual}$ are generally between 0.01-0.03 °C for 5-80% level of scattering. Compared to the clouding temperature ranges of PNIPAM in either H_2O or D_2O (~ 1.5 °C), the uncertainty for the values of $LCST_{actual}$ resulted from this linear regression approach is less than 2% and should not affect the outcome of the corrected clouding curve. This approach has thus been used to generate the corrected clouding curves shown on Figures 1 and 2 (gray line) and in some of the other figures in this chapter.

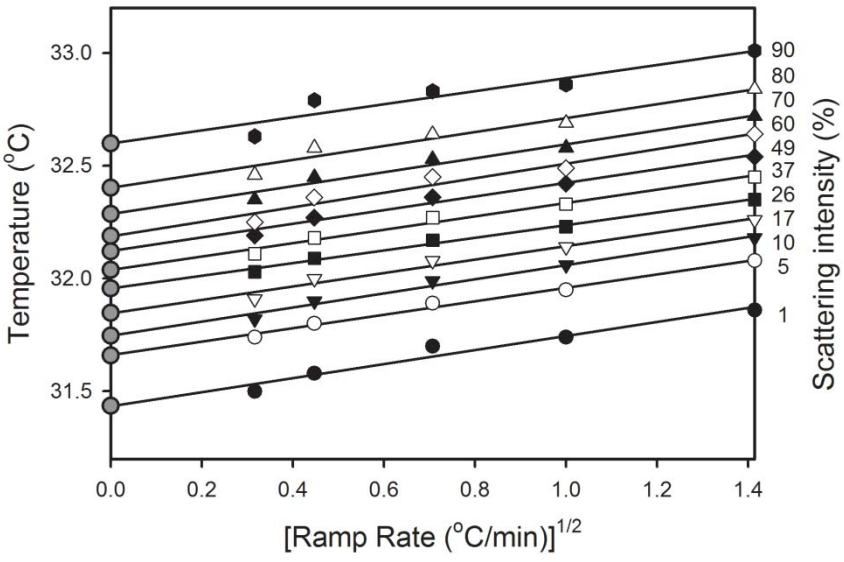

Figure 2. The temperature $LCST_{obsd}$ for a particular scattering intensity plotted versus the square root of the heating rate, $r^{1/2}$, at various scattering intensities for a sample of 10 mg/mL of PNIPAM in water. The lines shown for a linear regression analysis for these data at the various percentages of clouding lead to extrapolated LCST values for a particular percentage of clouding or light scattering (•) that would in principle be obtained with an infinitely small heating rate. A resulting 'clouding curve' generated based on these extrapolated points is shown in Figure 1 above.

In the correlations shown in Figure 2, good linear correlations were observed for 1-80% levels of scattering. The values of the best fitted slopes and the standard errors of each slopes obtained from the linear regression analyses for a series of scattering intensity are listed in Table 3. The slopes are consistent with an endothermic phase transition. There are about 5-10 % uncertainty for the values of the best fitted slopes between 5 -80 % scattering intensity as seen in Table 3. It is somehow difficult to assess how parallel these linear regression lines are. But as the values of each of the best fitted slopes are in a close range, we can still use the average values of the slopes to estimate the solvent isotope effect for PNIPAM's phase transition process as described later. The

correlation works well for levels of scattering (clouding) below 90% and for ramp rates below 5 °C/min. Linear plots of scattering > 90% versus $r^{1/2}$ in our experience had larger errors and were usually not used in determining the slope of the correlation. The clouding curves for ramp rate larger than 5 °C/min had too few data points to be included in these linear plots.

Table 2. $LCST_{actual}$ Obtained from the Linear Regression Analyses of $LCST_{obsd}$ Versus $r^{1/2}$ at Various Levels of Scattering in the Cloud Point Curves for PNIPAM in H_2O or D_2O.

PNIPAM in H_2O			**PNIPAM in D_2O**		
Scattering (%)	**$LCST_{actual}$ (°C)**	**Standard error**	**Scattering (%)**	**$LCST_{actual}$ (°C)**	**Standard error**
1	31.43	0.033	2	32.41	0.022
5	31.66	0.015	9	32.64	0.025
10	31.75	0.021	21	32.78	0.016
17	31.85	0.025	41	32.94	0.016
26	31.96	0.014	60	33.09	0.018
37	32.04	0.019	78	33.27	0.022
49	32.12	0.023	89	33.44	0.015
60	32.19	0.026			
70	32.29	0.023			
80	32.40	0.030			
90	32.60	0.054			

Table 3. Slopes for Plots of $LCST_{obsd}$ Versus $r^{1/2}$ at Various Levels of Scattering in the Cloud Point Curves for PNIPAM in H_2O or D_2O.

PNIPAM in H_2O			PNIPAM in D_2O		
Scattering (%)	**Slope**	**Standard error**	**Scattering (%)**	**Slope**	**Standard error**
1	0.310	0.038	2	0.378	0.025
5	0.298	0.017	9	0.351	0.028
10	0.313	0.024	21	0.365	0.019
17	0.297	0.029	41	0.366	0.018
26	0.280	0.016	60	0.358	0.021
37	0.296	0.022	78	0.335	0.025
49	0.302	0.026	89	0.312	0.017
60	0.322	0.041			
70	0.309	0.033			
80	0.308	0.031			
90	0.29	0.062			
Average	0.302			0.352	

This new procedure for assay of cloud points has quite high precision. This is illustrated by the very modest scatter in the data in Figure 1 for the individual points in the 0.1 and 0.2 °C/min heating rate clouding curves shown. These assays are also sensitive enough to probe the same sort of subtle effects of solution components on PNIPAM LCSTs that we have probed previously using a temperature gradient apparatus. Figure 3 illustrates this for PNIPAM in H_2O, 50/50 (v/v) H_2O/D_2O, and pure D_2O at ramp rates of 0.1 °C/min. Comparison of the results for the three solvent mixtures shows that the solvent isotope effects on the LCST of PNIPAM are nearly linearly dependent on the mole fraction of deuterated solvent as we noted earlier. However, while the earlier analyses only compared the onset of the LCST process to show a roughly linear dependence of the LCST with the mole percent D_2O, the results obtained in this new

procedure show that solvent isotope composition effects on LCSTs are essentially the same for all points on the clouding curve. Figure 3 also includes both a corrected LCST curve obtained for PNIPAM in pure H_2O and pure D_2O, showing that in D_2O as in H_2O that there only a modest difference between the 0.1 °C/min curve and the 'corrected' curve.

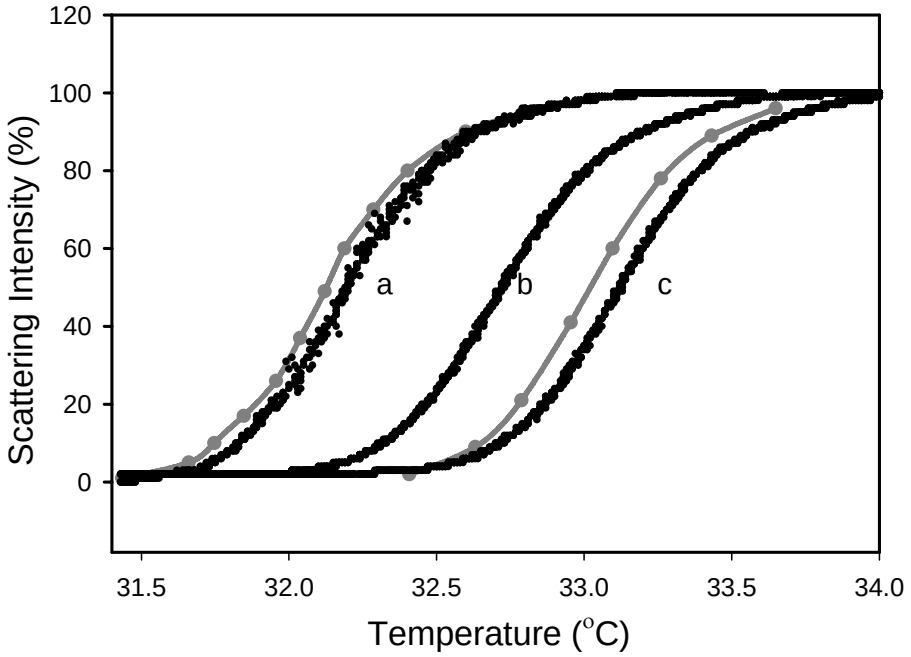

Figure 3. Scattering curves showing clouding of a 10 mg/mL solution of PNIPAM in mixtures of H_2O and D_2O measured at a heating ramp rate of 0.1 °C/min: (a) pure H_2O (lowest temperature curve); (b) 50/50 (v/v) H_2O/D_2O (intermediate temperature curve); (c) pure D_2O (highest temperature curve). The gray lines for the lowest and the highest temperature clouding curve are the 'corrected' clouding curves for H_2O and D_2O, respectively with the points showing the calculated $LCST_{actual}$ at various scattering values.

The plots of $LCST_{obsd}$ versus $r^{1/2}$ measured in the D_2O case can be compared with similar plots measured in H_2O to determine the solvent isotope effect. This comparison shows that the slope, $(\Delta G_{LCST}/\alpha)^{1/2}$, is greater in D_2O than in H_2O as would

be expected since the reported LCST of PNIPAM is higher in D_2O than H_2O. The difference in the $LCST_{D2O}$ versus the $LCST_{H2O}$ in the present work is about 1 °C over most of the clouding curve. Our earlier work had estimated this difference to be 0.7 °C.[30] The Winnik group observed a difference of about 2 °C in measurements based on pressure perturbation calorimetry.[115] The Winnik group also determined the difference in heat capacity for the LCST process in D_2O versus H_2O and found that the $\Delta c_{p(D2O)}$ was twice as large as the $\Delta c_{p(H2O)}$. In our case we can also calculate a solvent isotope effect for the LCST process. The slopes of the curves that correlate the $LCST_{actual}$ with the $LCST_{obsd}$ in the H_2O and D_2O experiments are equal to the ratio of a thermodynamic term for the LCST process and a term for the heat constant for the apparatus and sample that will cancel out when the slope in H_2O correlations of LCST with $r^{1/2}$ is divided by the slope measured in D_2O experiments. Thus, we can use our data to calculate a composite solvent isotope effect on the ratio $\Delta G_{D2O}/\Delta G_{H2O}$for the PNIPAM phase separation in H_2O versus D_2O. This value is 1.36 and is similar to the twofold difference in Δc_p previously noted by the Winnik group.[115]

While PNIPAM has a higher LCST in D_2O versus H_2O, the effect of isotopic substitution in the solvent on LCSTs can vary. The use of a melting point apparatus to determine LCSTs in such cases has the advantage of being useful over a broad temperature range. Moreover sealed samples can be used. Thus we were able to study the effect of D_2O versus H_2O on the LCST of a poly(ethylene oxide) (PEO). Using a PEO sample with an average molecular weight of 300 kDa the onset of the $LCST_{H2O}$ was about 99 °C. The onset of the $LCST_{D2O}$ for this same sample was about 94 °C. Thus,

PEG's LCST has a solvent isotope effect that is opposite with that of PNIPAM (Figure 4a). The solvent isotope effect for a triblock poly(alkene oxide) polymer Pluronic® 10R5 (**7**) was also analyzed. This polymer too had a lower LCST in D_2O than H_2O (Figure 4b).

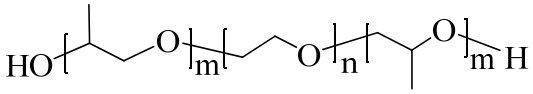

7 (n = 22, m = 8) Pluronic 10R5

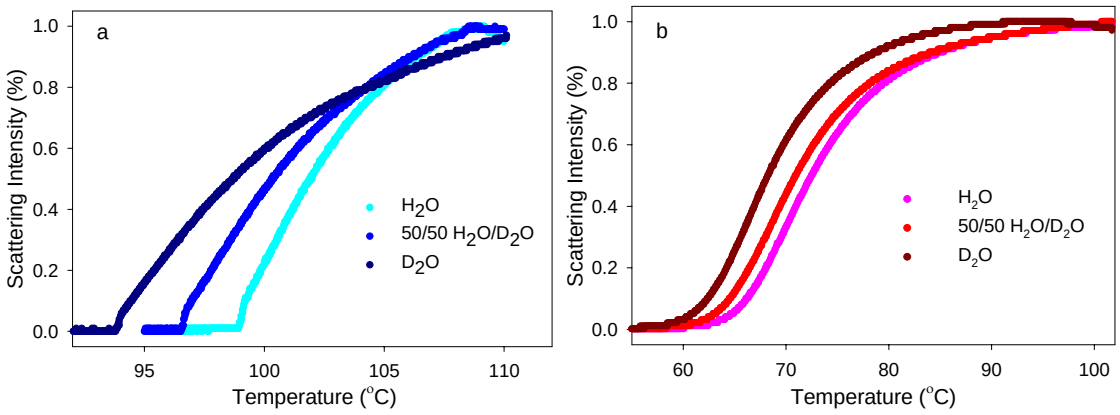

Figure 4. Scattering curves showing clouding of a) a 1 wt % solution of PEO (300 kDa) in mixtures of H_2O and D_2O and b) a 1 wt % solution of Pluronic® 10R5 (**7**) in mixtures of H_2O and D_2O. All the clouding curves were obtained at a heating ramp rate of 2 °C/min.

The concentration of sample necessary to measure cloud points with this automated melting point apparatus varied depending on the sample. Although most of the analyses in the case of PNIPAM used 10 mg of PNIPAM/mL of solution, we were able to analyze cloud point curves for PNIPAM samples with as little as 1 mg of PNIPAM/mL of solution. As the concentration of polymer in solution decreased, the precision of the analyses decreased because the scatter intensity of the sample decreased.

However, 'corrected' clouding curves could still be obtained even with the 1 mg of PNIPAM/mL sample. The data obtained using our apparatus were compared with data obtained from clouding curves measured using Cremer's temperature gradient apparatus. The two clouding curves are shown in Figure 5 and are nearly identical.

The Hofmeister effect of salts on phase separation and solvation phenomena is an effect that is ubiquitous in many solutions or suspensions of synthetic and biological macromolecules. As expected, addition of NaCl to PNIPAM lowered the phase transition temperature and LCST process. Just as was true in pure water, the clouding curve depends on the heating rate of the analyses in a regular fashion. We were also able to calculate a corrected clouding curve in this system (Figure 6) for PNIPAM in the presence of 0.4 N NaCl. Thus the same procedures used above to determine a clouding curve at an infinitely slow heating rate in pure H_2O and D_2O can be used successfully with salt solutions too.

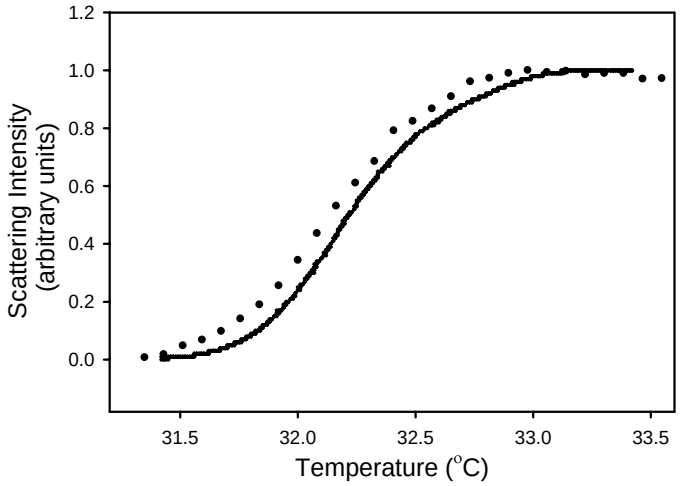

Figure 5. Scattering curves showing clouding of a 10 mg/mL solution of poly(*N*-isopropylacrylamide) measured by the OptiMelt melting point apparatus at a heating ramp rate of 0.1 °C/min (solid Line) and by the temperature gradient apparatus (dotted line).

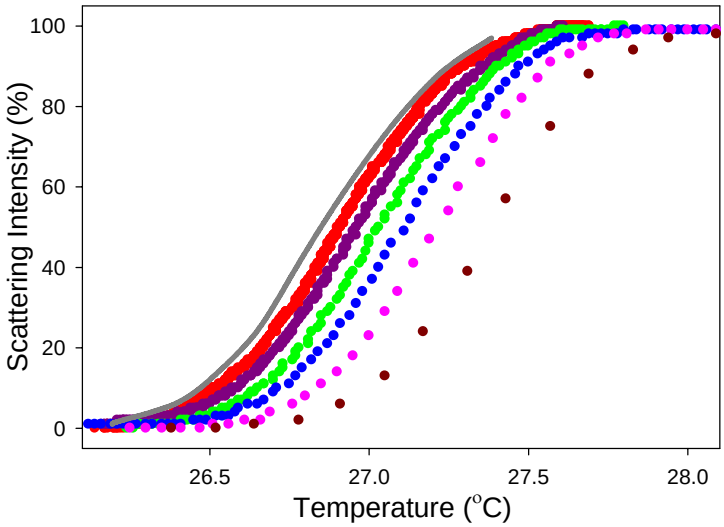

Figure 6. Scattering curves showing clouding of a 10 mg/mL solution of poly(*N*-isopropylacrylamide) in 0.4 M NaCl as a function of heating rate: red dots (0.1 °C/min); purple dots (0.2 °C/min); green dots (0.5 °C/min); blue dots (1.0 °C/min); pink dots (2.0 °C/min); dark red dots (5.0 °C/min). The solid gray line is the 'corrected' clouding curve.

The temperature range for the melting point apparatus used in these studies allowed us to assay LCSTs that can only be observed at higher temperature and provided a way to examine different materials' phase transitions that can involve temperature ranges of only a few degrees or tens of degrees. It also allowed us to determine how phase transitions of such materials are affected by solution components or heating rates. The study of PEO LCST isotope effects discussed earlier provides one example where we were able to readily examine solvent isotope effects near 100 °C. Brief studies described below of phase separation of several other poly(alkene oxide) Pluronic® surfactants (**7**, **8**, and **9**) afford additional examples that illustrate how this apparatus can be used to detect complicated phase separation behavior of thermally responsive polymers. The Pluronic® surfactants **8** and **9** are like the surfactant **7** described earlier and are triblock polymers or oligomers containing poly(ethylene oxide)-poly(propylene

oxide)-poly(ethylene oxide) blocks where the length of the hydrophilic poly (ethylene oxide) and hydrophobic poly(propylene oxide) blocks varies. They differ from **7** also in that they are terminated by primary hydroxyl groups.

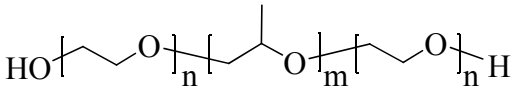

8 (n = 17, M = 60) Pluronic P103
9 (n = 27, M = 61) Pluronic P104

The complicated phase transition behaviors that can be seen with these Pluronic® materials are illustrated by the clouding curves in Figures 7 and 8. Figure 7 illustrates this with studies that assay the phase behavior of a 1 wt % solution of Pluronic® 10R5 (**7**) in water in the presence of Na_2SO_4 - a kosmotropic salt known to affect LCSTs and phase transitions. In these examples, assays of a 1 wt % aqueous solution of **7** in various Na_2SO_4 concentrations were carried out using a 2 °C/min heating rate. As would be expected, these experiments yielded a series of clouding curves which progressively moved to the lower temperature with increasing salt concentration. This is consistent with the Hofmeister effect. However, while the onset of the phase separation consistently moves to lower and lower temperatures, irregular clouding behavior was seen at higher salt concentrations. At these higher salt concentrations, **7** clouded normally in the 30-40 °C range but exhibited complex solubility behavior on heating further above 50 °C. Assays of LCSTs that depend solely on measuring the initial clouding temperature do not detect these more complicated phase behaviors. Such effects are a result of both the presence of the salt and are altered by the heating rate. For example, in this case, lower heating rates of 0.1 °C/min led to the formation of a

liquid/liquid biphasic system where the clouding and the resultant light scattering does not uniformly increase as the temperature is increased. Clouding curves observed for **7** in the presence of different concentrations of NaCl likewise shifted to lower temperatures as the NaCl concentration was increased (Figure 8). In these cases too, **7** exhibited complex clouding behaviors at high NaCl concentration (above 2.14 M NaCl) at higher temperature after an initial phase separation event.

Together with Cremer's group, we had studied the anion effects on the LCST of PNIPAM by using the temperature gradient apparatus and the results showed that the anion effects followed the Hofmeister series. Figure 7 and 8 show that additions of Na_2SO_4 or NaCl progressively shift the clouding curves of Pluronic® 10R5 (**7**) to lower temperature with increasing salt concentrations and Na_2SO_4 has larger effect on lowing the clouding temperature than NaCl. These observations promoted us to study the effects of other sodium salts on the LCST of **7** using this melting point apparatus to see if the Hofmeister effects are also applied on the LCST of this triblock copolymer. The results are presented in Figure 9 and the effects of salts follow the Hofmeister series in a order of citrate^{3-} > SO_4^{2-} > H_2PO^{4-} > Cl^- > Br^- >> SCN^-. The chaotropic NaSCN shows distinct 'salting-in' effect and addition of NaSCN increased the LCST of **7** about 10 °C even at concentration of 3 M.

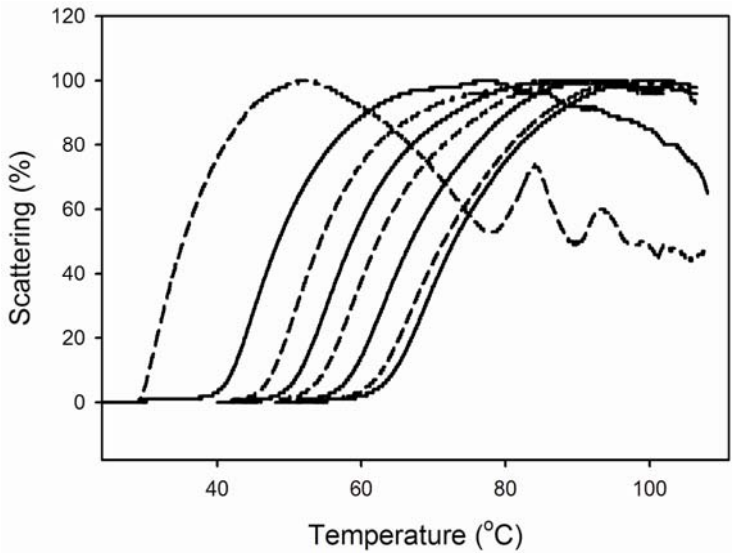

Figure 7. Scattering curves showing clouding of a 1 wt % solution of **7** (Pluronic® 10R5) in water in the presence of various concentrations of Na_2SO_4. The plots from right to left have the following concentrations: (-) 0.033 M; (---) 0.067 M; (-) 0.133 M; (---) 0.200 M; (-) 0.267 M; (---) 0.333 M; (-) 0.476 M; and (---) 0.714 M. These analyses were carried out at a heating rate of 2°C/min. A clouding curve of this polymeric surfactant in the absence of Na_2SO_4 is indistinguishable from the curve for the 0.033 M Na_2SO_4 solution.

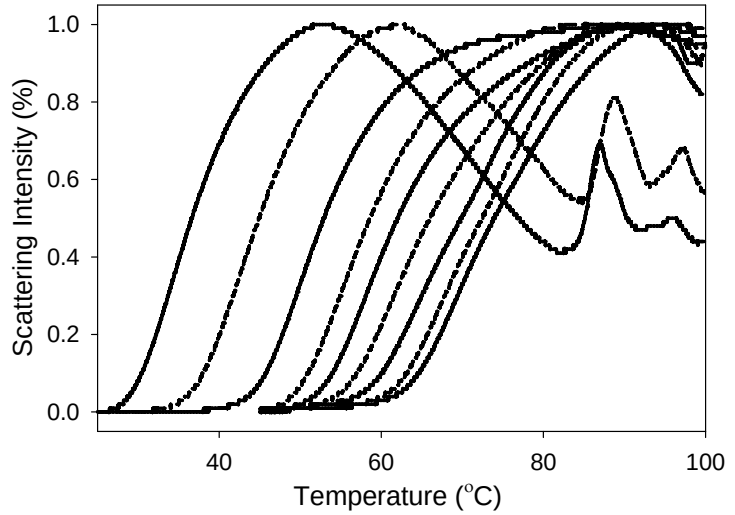

Figure 8. Scattering curves showing clouding of a 1 wt % solution of **7** (Pluronic® 10R5) in water in the presence of various concentrations of NaCl. The plots from right to left have the following concentrations: (-) 0.1 M; (---) 0.2 M; (-) 0.4 M; (---) 0.6 M; (-) 0.8 M; (---) 1.0 M; (-) 1.43 M; (---) 2.14 M; and (-) 2.86 M These analyses were carried out at a heating rate of 2°C/min. A clouding curve of this polymeric surfactant in the absence of NaCl is indistinguishable from the curve for the 0.1 M NaCl solution.

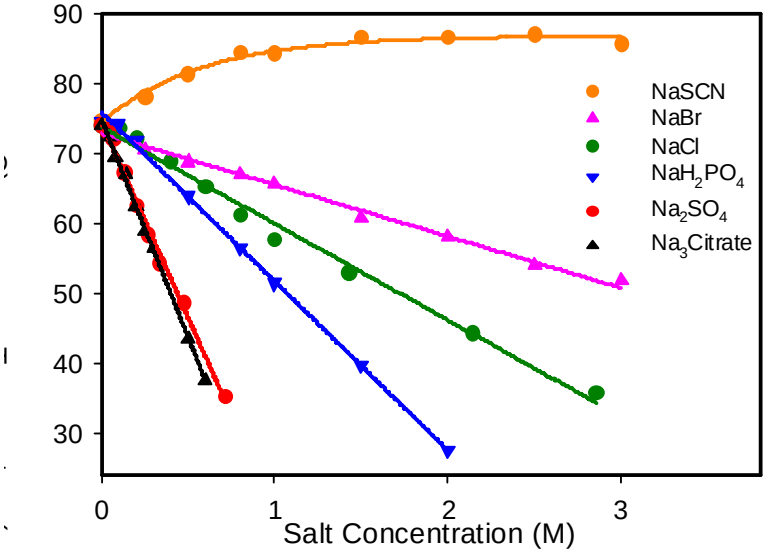

Figure 9. Effects of anions on the LCST of 1 wt% Pluronic® 10R5 aqueous solution. The temperatures at 50% scattering intensity of the clouding curves were used to construct this graph.

The less regular clouding behavior seen for a poly(propylene oxide)-co-poly(ethylene oxide) triblock copolymer **7** at high-salt concentrations is one illustration how this small scale bulk assay of LCST phenomena can detect more complex phase selective solubility. These effects are not unique to this particular polymer or to the presence of salt. Even more complicated phase behavior is seen in plain water with the other Pluronic® copolymers **8** and **9**. The results for **8** and **9** shown in Figure 10 show that these other poly(alkene oxide) copolymers have phase behavior that contrasts with that of **7** in pure water. As shown in Figure 10, such effects, while complicated, are quite reproducible (a movie showing these complicated clouding behaviors can be found in the supplementary material).

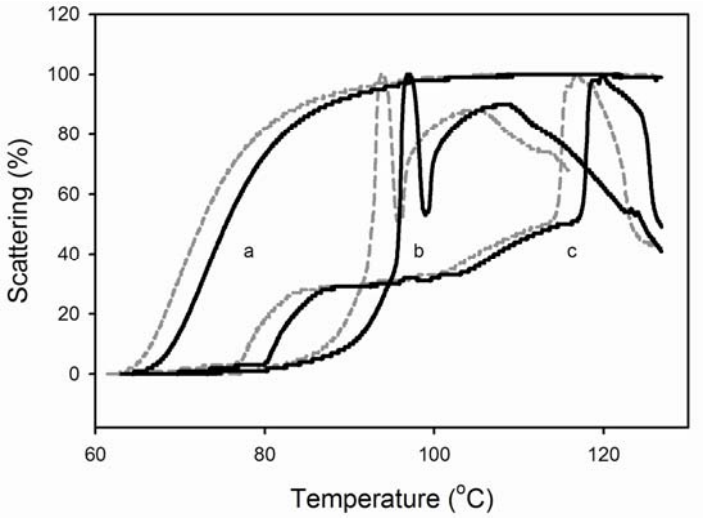

Figure 10. Scattering curves showing clouding of three different Pluronic® copolymer surfactants in water (1 wt %) at 2 °C/min: (a) **7** (initial clouding at 63 °C); (b) **8** (initial clouding at 76 °C); and (c) **9** (initial clouding at 83 °C). The reproducibility of these complex clouding curves was measured by analysis of a freshly prepared second sample. A repetition of the initial experiment (a second clouding curve measured for each of the three samples) is shown for the sake of clarity as a gray dashed line that is offset from the corresponding original curve by 3 °C.

Conclusion

The results shown above show the broad utility of a simple digital melting point apparatus for analysis of phase separations that generate clouding curves. In cases where the clouding simply shifts as a function of the heating rate of the analysis, it is possible to use the data from these analyses to generate 'corrected' clouding point curves that approximate the phase separation at an infinitely slow heating rate. The temperature range of the apparatus also allows for analyses at much higher temperatures and provides a simple way to examine irregular clouding behavior in more complex systems.

CHAPTER III

DESIGNING SURFACES WITH WETTABILITY THAT VARIED IN RESPONSE TO SOLUTE IDENTITY AND CONCENTRATION*

Introduction

'Smart' surfaces[116,117] that respond to external stimuli such as pH, temperature, or solvent are of interest in many applications. Surfaces with stimuli-responsive wetting properties have been used in applications such as self-cleaning coatings, microfluidics devices, and cell culture dishes. Surfaces grafted with thermoresponsive polymers such as poly(*N*-isopropylacrylamide) (PNIPAM) can exhibit tunable wettability changes upon changing temperature and pH value.[92,118-120] These wettability changes derive from the fact that at their lower critical solution temperature (LCST), thermoresponsive polymers like PNIPAM undergo phase transition leading the polymer chains to change from a hydrophilic coil conformation to a hydrophobic globular conformation. When these polymers are grafted on textured substrates, large wettability changes can be obtained by changing temperature and pH value.[121,122] Similar responsive behavior can also been seen with polyelectrolytes which change solubility depending on the protonation state of pendant acidic or basic groups. Just as PNIPAM grafts can change wettability with temperature changes, polyelectrolyte grafts too can have pH responsive wettability.

---

*Part of the data reported in this chapter is reprinted with permission from "Designing Surfaces with Wettability That Varies in Response to Solute Identity and Concentration " by K. Liao, H. Fu, A. Wan, J. D. Batteas and D. E. Bergbreiter, *Langmuir*, 2009, **25**, 26-28, Copyright [2008] by American Chemical Society.

However, while responsive surfaces that exhibit changes in surface wetting due to temperature and pH changes are known, surfaces that change their wetting behavior without undergoing a chemical reaction solely in response to the solute identity in a given solvent or to varied concentrations of the same solute have not been reported.

While solute or salt induced changes in surface wettability are not known, the effects of salts on the solubility of polymers like PNIPAM are well known. Indeed, Hofmeister effects of salts on the LCSTs of thermoresponsive polymers such as PNIPAM have been extensively studied both by our group and others.[31,32,48,123] Given the sharp and visually obvious phase transitions seen for PNIPAM at its LCST and the varied effects of salts on this LCST value, we envisioned that PNIPAM-grafted surfaces with proper constructed nanostructure could exhibit significant Hofmeister-like anion-responsive wetting properties. In this chapter, we describe PNIPAM nanocomposite grafts prepared by covalent layer-by-layer assembly that exhibit striking changes in surface wetting in response to changes in solute identity or concentration, changes in wetting that follow a Hofmeister series.

We prepared these responsive nanocomposite surfaces by covalent layer-by-layer grafting chemistry. These syntheses drew inspiration from our prior work on the assembly of superhydrophobic surfaces.[124,125] In that work, we had shown first that condensation of an electrophilic anhydride-containing polymer with polyvalent nucleophilic polymers or aminated MWNTs (multiwall carbon nanotubes) led to covalent grafts that exhibited significant pH-responsive wettability. We had also shown that nanocomposite grafts formed with polydisperse MWNTs were topologically

complex and that these grafts when chemically modified could be either superhydrophobic or superhydrophilic depending on whether the grafts were modified with hydrophobic or hydrophilic reagents.[126] We reasoned that similar nanocomposite grafts whose hydrophobic or hydrophilic character changes in response to solute concentration could also be prepared without chemical derivatization if they were prepared with a responsive polymer. This proved to be the case, and we saw responsive solute dependent wettability for grafts formed by covalent layer-by-layer assembly of a copolymer of NIPAM and *N*-acryloxysuccinimide (NASI) (PNIPAM-*c*-PNASI) with an aminated silica nanoparticle mixture. Silica nanoparticles are used in this synthesis as building blocks to create a desired nanoscale roughness on the surfaces.

Preparing the Solute-responsive PE/(PNIPAM/SiO_2)$_6$/PNIPAM Nanocomposite Surfaces by Covalent Layer-by-layer Self-assembly Method

Our synthesis of these responsive nanocomposite grafts involved assembling a covalent graft using the copolymer of PNIPAM-*c*-PNASI (M_n = 30,000 Da) and an admixture of aminated 10 and 100 nm fused silica particles as polyvalent electrophilic and nucleophilic reagents, respectively. The assembly process is illustrated in Scheme 10. In the first step of this process, the NASI groups in the PNIPAM-*c*-PNASI copolymer are allowed to react with the amine groups of an aminated surface derived from the reaction of an activated, oxidized polyethylene with polyethyleneimine (PEI). This leads to covalent binding of PNIPAM-*c*-PNASI copolymer to this surface via amide bonds. However, spatial constraints preclude complete consumption of all of the NASI groups of PNIPAM-*c*-PNASI. This results in a surface having unreacted

electrophilic NASI groups that can react with amine groups of amine-functionalized 10 and 100 nm diameter silica nanoparticles in a second step. As shown in Scheme 10, this second step produces a nucleophilic amine-rich surface. While this surface could be used as is for further grafting, we treated this surface with excess *i*-$PrNH_2$. This quantitatively converts any unreacted NASI groups into NIPAM groups. The covalent layer-by-layer assembly then continues with further stages of PNIPAM-*c*-PNASI/10 and 100 nm aminated silica nanoparticle/*i*-$PrNH_2$ treatments.

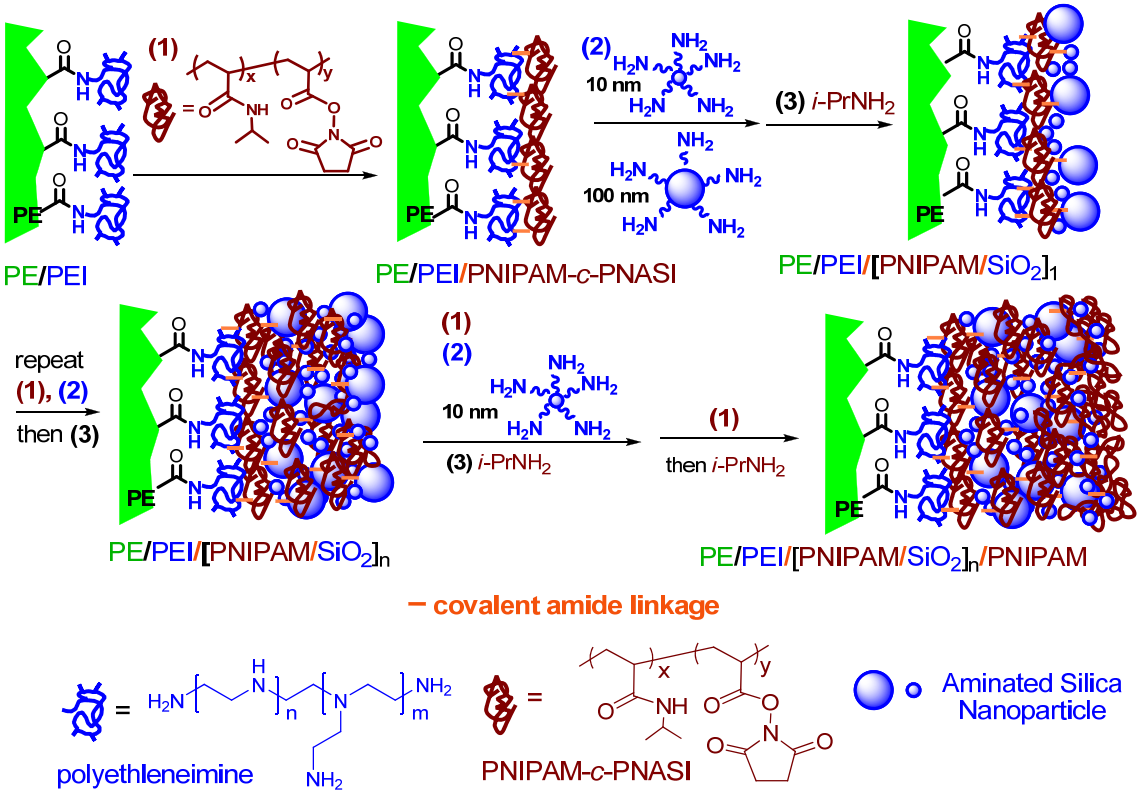

Scheme 10. Covalent layer-by-layer assembly of a $(PNIPAM/SiO_2)_n$/PNIPAM nanocomposite graft on a PEI modified PE film. The final structure is not drawn to scale.

At the sixth stage, a similar procedure is carried on except that this time, only the 10 nm aminated silica nanoparticles are used instead of using the mixture of 10 an 100 nm aminated silica nanoparticles. Once the sixth stage is assembled, the surface is capped with PNIPAM-*c*-PNASI. A final treatment with excess *i*-$PrNH_2$ ensures that the outmost layer of this graft is covered with PNIPAM. We denote this nanocomposite surface as PE/(PNIPAM/SiO_2)$_6$/PNIPAM.

This PE/(PNIPAM/SiO_2)$_6$/PNIPAM nanocomposite surface contains carboxamides based on the observation of absorption peaks at 1670 and 1640 cm^{-1} in the attenuated total reflection infrared (ATR-IR) spectrum (Figure 11). In addition, a large Si-O absorption peak at around 1100 cm^{-1} is seen in Figure 11 for the silica nanoparticles. The absorption intensity of both the carboxamide and Si-O peaks relative to the C-H absorption peaks at ~2900 cm^{-1} increases as the numbers of deposition bilayers increase. This surface was further characterized by atomic force microscopy (AFM) (Figure 12) and it had an average surface roughness of ~ 287 nm in air based on analysis of a random series of 2.5 μm × 2.5 μm regions. The 100 nm nanoparticles are discernable at the surface of the film and define the local surface roughness. These PE/(PNIPAM/SiO_2)$_6$/PNIPAM nanocomposite surfaces combine the property of responsive polymer and surface roughness. The surface roughness is expected to enhance the responsiveness of the surface leading large changes in surface wettability upon the changing of external stimuli, in our case, the changing of salt concentrations or salt identity.

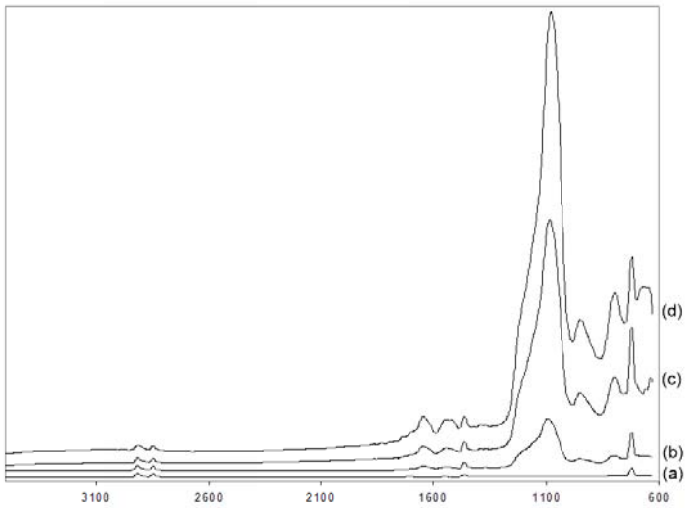

Figure 11. ATR-IR spectra of (a) oxidized PE and PE/(PNIPAM/SiO_2)$_n$ /PNIPAM surfaces with (b) n=2; (c)=4; (d)=6.

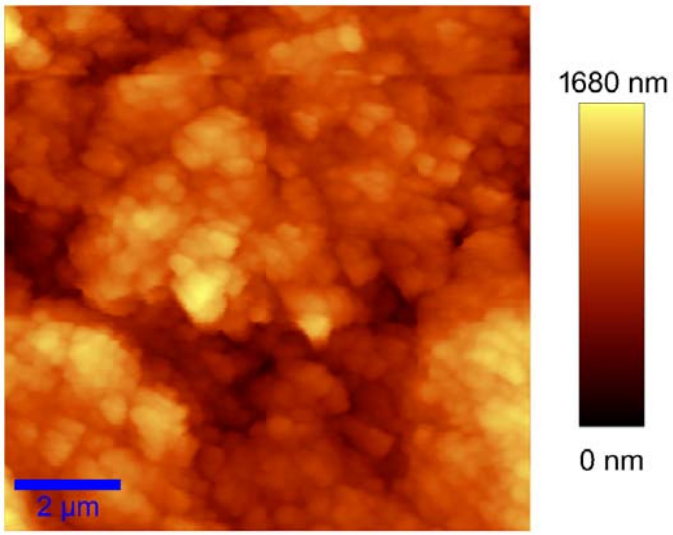

Figure 12. Tapping mode AFM topographic image of a covalent layer-by-layer assembled PE/(PNIPAM/SiO_2)$_6$/PNIPAM nanocomposite surface with an rms roughness of ~ 287 nm.

Studies of the Solute-responsive Wettability

The changes in wettability as a function of solute ion and concentration on a prepared PE/(PNIPAM/SiO_2)$_6$/PNIPAM nanocomposite surface are illustrated in Figures

13 and 14. In these figures, drops of water or salt solutions that are allowed to stand for 3 minutes on the same PE/(PNIPAM/SiO_2)$_6$/PNIPAM nanocomposite surface have distinctly different static contact angles (Θ). As shown in Figure 13, the same PE/(PNIPAM/SiO_2)$_6$/PNIPAM nanocomposite surface is reversibly either hydrophilic or hydrophobic depending on the identity of the solute in the water. Moreover, these solute-induced wettability changes are also found to be sensitive to the concentration of the given solute with significant differences in contact angle (Θ) for even dilute aqueous solutions of a solute such as sodium citrate (Figure 14). These visually apparent changes in wettability for this PE/(PNIPAM/SiO_2)$_6$/PNIPAM nanocomposite surface are not only large, they are also reversible and reproducible. The same surface can be treated with dozens of different solute solutions but still has similar wettability on subsequent re-examination with water.

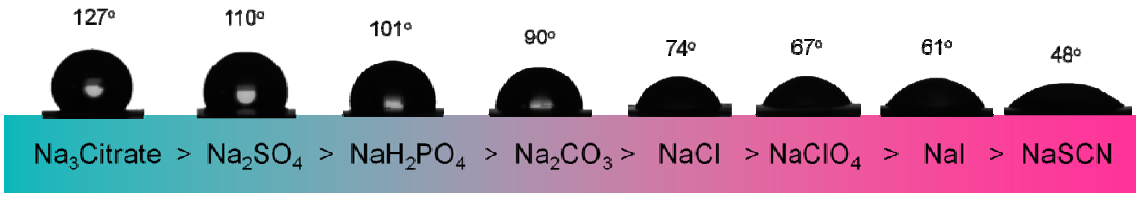

Figure 13. Static contact angles for various sodium salt solutions at 1.2 M measured on a PE/(PNIPAM/SiO_2)$_6$/PNIPAM nanocomposite surface 3 minutes after a 10 μL droplet of corresponding solutions was placed on this surface.

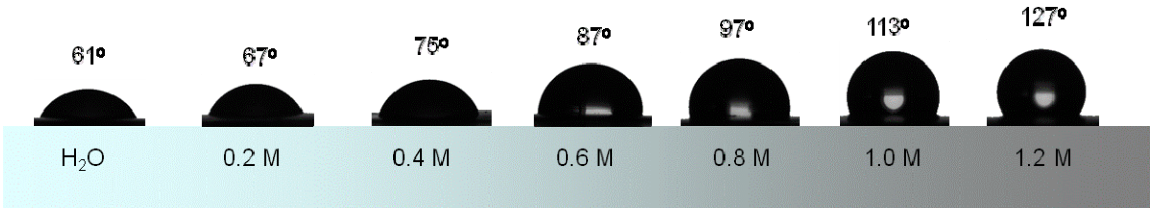

Figure 14. Static contact angles for sodium citrate aqueous solutions with varied concentrations on the same PE/(PNIPAM/SiO_2)$_6$/PNIPAM nanocomposite surface 3 minutes after a 10 μL droplet of corresponding solutions was placed on this surface.

While the visually different wettabilities in Figures 13 and 14 illustrate the responsiveness of this PE/(PNIPAM/SiO_2)$_6$/PNIPAM nanocomposite surface, these static contact angles are time dependent. Figure 15 shows how static contact angle changes with time when droplets of a series Na_2SO_4 solutions with different concentrations are placed on a PE/(PNIPAM/SiO_2)$_6$/PNIPAM nanocomposite surface. Such changes are expected to be dependent not only on time as shown here but on other factors like ambient temperature or relative humidity. In Figure 15, the Θ values decrease sharply for all solutions at the first 20 seconds which are largely due to the surface reorganization. Later, the Θ values decrease more slowly with time and the changes in Θ after the first 60 seconds are due in part to evaporation of the water drops at the surface. Advancing contact angle (Θ_a) measures the largest contact angle possible without increasing a sessile drop's solid/liquid interfacial area by adding volume of liquid dynamically. The Θ_a value is a property of the measured surface and does not change with time. Thus, to avoid any time dependent or experimentally dependent changes in contact angle, wettability is discussed using measurements of advancing contact angle for the various solute ions throughout the rest of this chapter.

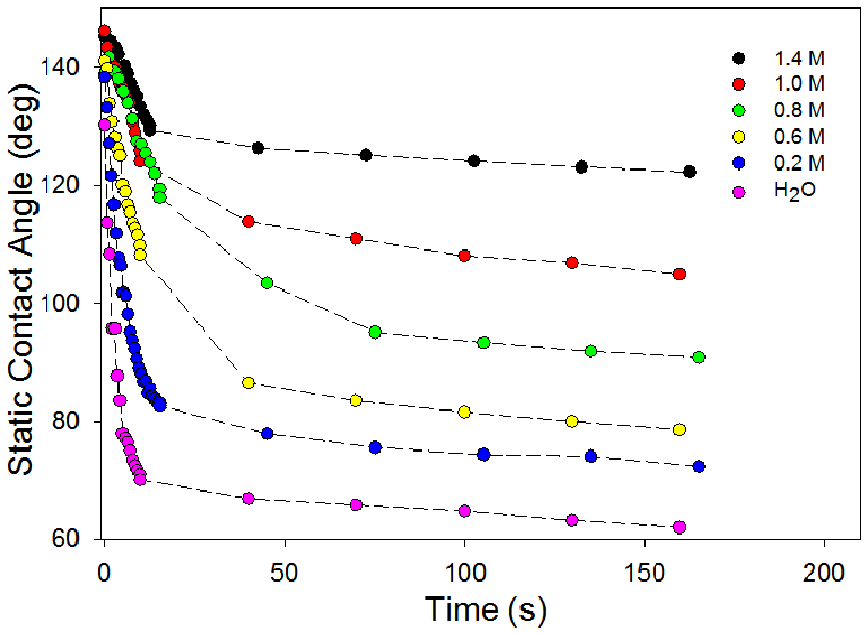

Figure 15. Static contact angles of a series of Na_2SO_4 solution with different concentrations on a PE/(PNIPAM/SiO_2)$_6$/PNIPAM nanocomposite surface measured as a function of time.

Most interestingly, this surface exhibited large solute dependent wettability changes. With pure water, the advancing contact angle Θ_a was 76°, while with 1.4 M Na_2SO_4 (a Hofmeister kosmotrope) the Θ_a was 144°. This 68° difference in Θ_a between water versus 1.4 M Na_2SO_4 ($\Delta\Theta_a$) was much larger than the $\Delta\Theta_a$ seen using these same solutions on glass grafted with PNIPAM brushes, unfunctionalized PE, oxidized PE, or a PEI/Gantrez graft on PE that was grafted with PNIPAM. Those surfaces had smaller $\Delta\Theta_a$ values of 14°, 0°, 8°, and 25°, respectively.

The large solute responsive wettability of these PE/(PNIPAM/SiO_2)$_6$/PNIPAM nanocomposite surfaces allowed us to examine the concentration dependence of wettability changes with solute anions. We measured the advancing water contact angle of several sodium salt solutions with varied concentrations and the results are shown in

Figure 16. For the kosmotropic anions, the results generally show a gradual increase in Θ_a values with increased salt concentration until a certain critical concentration of salt is reached. This is illustrated by the results for sodium citrate, Na_2SO_4, NaH_2PO_4, and NaCl, where the increase in Θ_a with increased salt concentration exhibited sigmoidal behavior with inflection points that varied from around 0.6 M (sodium citrate) to 1.2 M (NaCl). In the case of chaotropic anions such as thiocyanate, salting-in behavior similar to that seen in the LCST behavior of PNIPAM, hydroxymethylcellulose,[40] and other macromolecules occurred. Salt-enhanced wetting is also seen for NaI, though the changes in Θ_a in this case are close to the error in contact angle measurements. All these surfaces had Θ_r values of <10°.

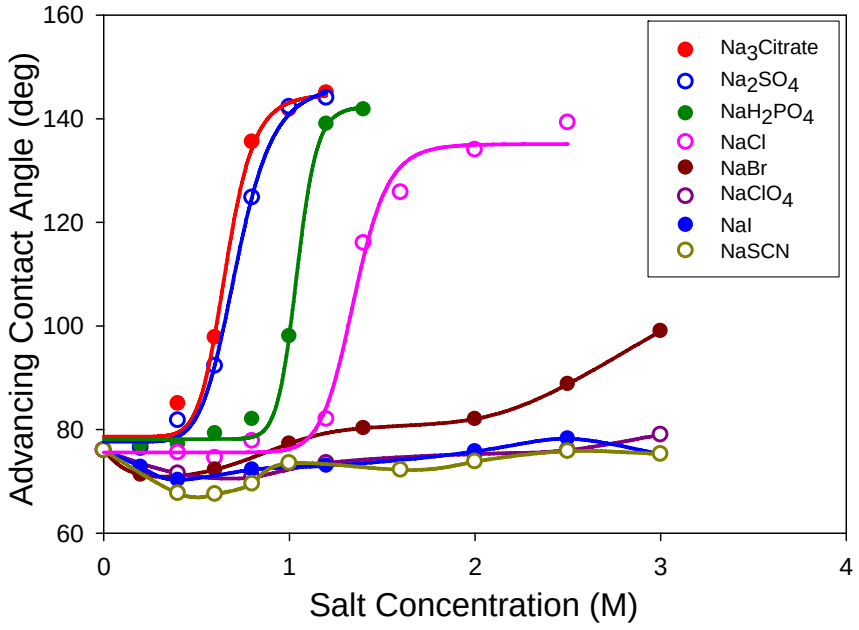

Figure 16. Changes in advancing contact angle (Θ_a) of a PE/PNIPAM/$SiO_2)_6$/PNIPAM nanocomposite surface measured with solutions of various salts as a function of salt concentration. Each data point is the average of three individual measurements and has an error of ±2°.

Atomic Force Microscopy Studies

The AFM Studies of the PE/(PNIPAM/SiO_2)$_6$/PNIPAM nanocomposite surfaces were done by Mr. Albert Wan from Batteas's group. The results from AFM measurements show visible changes in surface texture when changing from one solute to the next (Figure 17). In air, the surfaces are rough and the larger silica particles (ca. 100 nm) dominate the surface morphology. Upon immersion in water, the film swells and the surface roughness decreases from ~287 nm rms to ~170 nm rms. Replacement of water by 1.4 M Na_2SO_4 results in an increase in roughness (ca. 232 nm rms) along with the $\Delta\Theta_a$ of 68°. In 1.2 M NaSCN, the surface roughness decreased to ~145 nm rms and the Θ_a changed to 72° ($\Delta\Theta_a$ of −4°). These changes show that these surfaces reconstruct in response to different solutes and suggest that the changes in water contact angle are likely due to a combination of changes in surface roughness induced by solute dependent swelling or chain collapse that alters the hydrophobicity of the PNIPAM. Hence, the swelling of the polymer on the textured surface follows the expected Hofmeister series which predictably alters the surface roughness and the associated wetting and dewetting of the surface.

The wettability changes and hydration changes seen in AFM are reversible. When a film prepared as shown in Scheme 10 had its Θ_a analyzed using 1.4 M Na_2SO_4, the Θ_a value was 144°. Washing this film with distilled water and tetrahydrofuran (THF), drying, and reanalysis showed it had a Θ_a of 76° with water, the same Θ_a as it had before it was ever exposed to Na_2SO_4. After a month of treatment with various salt solutions, surfaces did exhibit minor changes. After ~100 cycles using various salt

solutions, THF, and water, the $\Delta\Theta_a$ values (1.4 M Na_2SO_4 versus H_2O) gradually decreased from 68° to ~50° though the trends of Figure 15 were still seen.

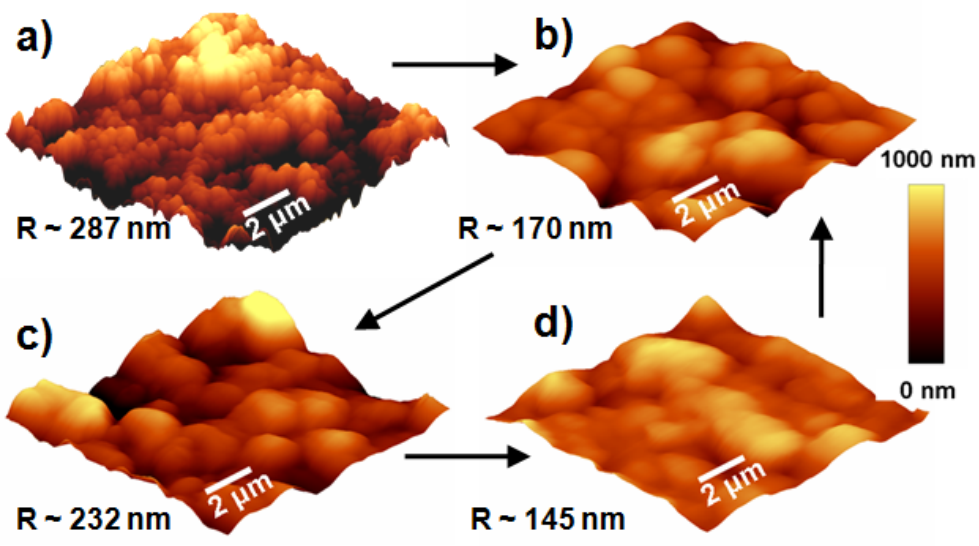

Figure 17. Tapping mode AFM images of PE/(PNIPAM/SiO_2)$_6$/PNIPAM obtained in (a) air, (b) water, (c) 1.4 M Na_2SO_4, and (d) 1.2 M NaSCN. Returning the sample to water yields a surface similar to (b). The average rms roughness of the surface in each environment taken from a random series of 2.5 µm × 2.5 µm regions is listed below each figure.

Conclusion

As noted above, changes in Θ_a values with salts are modest with other surfaces. This may explain why studies of the effect of solute concentration or solute identity on surface wettability are not known, as the errors inherent in studying water contact angles and these modest changes seen in Θ_a values for other surfaces with changes in solute preclude definitive studies of wettability changes. Further improvement in our synthetic procedures to form surfaces with even larger solute responsive $\Delta\Theta_a$ values and further work to study other solutes and to characterize other possible consequences of the solute

responsive morphological changes in these smart surfaces such as modulation of adhesion or changes in surface mechanical properties are continuing. This facile approach to surface modification allows such films to be prepared on virtually any surface and should be a general route to materials with solute responsive wettability.

CHAPTER IV

PARALLEL EFFECTS OF CATIONS ON PNIPAM GRAFT WETTABILITY AND PNIPAM SOLUBILITY*

Introduction

Stimuli-responsive surfaces or switchable surfaces that change their physical or chemical properties in response to external stimuli have been of considerable research interest recently.[127-129] In particular, surfaces that can undergo reversible wettability changes under external stimuli are attractive to applications in microfluidic devices, chromatographic separations, self-cleaning and anti-fog surfaces, and sensor devices.[130] Changes of surface wetting are also used to alter interactions of the stimuli-responsive surfaces with aqueous solutions of biomolecules and biomaterials, which are important in a variety of biological and medical applications of responsive surfaces in biofouling, cell culture, and tissue engineering.[131]

Surfaces grafted with thermoresponsive polymers, such as poly(*N*-isopropylacrylamide) (PNIPAM), elastin-like polypeptides (ELP) are known to reversibly switch between hydrophilic and hydrophobic states in response to temperature changes.[132-136] Such thermoresponsive surfaces have been used in biomedical related applications such as in the controlled capture or release of proteins and cells.[137,138]

---

*Reprinted with permission from "Parallel Effects of Cations on PNIPAM Graft Wettability and PNIPAM Solubility" by H. Fu, X. Hong, A. Wan, J. D. Batteas and D. E. Bergbreiter, *ACS Appl. Mater. Interfaces*, 2010, **2**, 452–458, Copyright [2010] by American Chemical Society.

Their temperature responsiveness of surfaces in these applications derives from the fact that thermoresponsive polymers exhibit lower critical solution temperature (LCSTs). Below the LCST, these polymers are soluble and hydrophilic with an extended coil conformation. Above the LCST, these polymers undergo a sharp phase transition to form a collapsed hydrophobic conformation.[93,139,140] It's well known that the LCST of a thermoresponsive polymer changes upon the addition of salt cosolutes to its aqueous solution[29,31,123] and effects of salts on LCSTs follow the Hofmeister series which ranks various ions towards their ability to affect protein hydration.[141,142] While temperature induced wettability changes of a responsive surface can be sufficient for a particular application, additional triggers such as changes in ionic strength sometimes can enhance the utility of a stimuli-responsive surfaces. For example, ionic strength-induced hydrophilic–hydrophobic phase transitions of ELP have been demonstrated using in reversible capture and release of an ELP fusion protein from an ELP-functionalized surface.[143]

While extensive studies have been done on the effects of salts on the LCSTs of thermoresponsive polymers in aqueous solutions, these studies have largely focused on the effects of anions. Cations are thought to play a minor role. However, few systematic studies have been carried out to study the salt effects on the wettability of thermoresponsive surfaces. In Chapter III, I discussed our studies of salt induced phase transitions of responsive polymers on PNIPAM/SiO_2 nanocomposite grafts on polyethylene (PE) films.[144] These studies showed that changing the anion identity and concentration of various sodium salts had a significant impact on water contact angles,

an effect similar to that seen in studies of temperature effects on the wettability of PNIPAM grafts on nanostructured surfaces. These anion effects on the wettability of PE_{oxid}-$(PNIPAM/SiO_2)_6$-PNIPAM nanocomposite grafts paralleled the Hofmeister-like effects of these same alkali metal anion salts on PNIPAM LCSTs. We have now investigated how changing cation identity, specifically changing from monovalent cations to divalent metal cations to a trivalent cation like Al(III) affects surface wettability of these PNIPAM-containing nanocomposite grafts. These wettability studies show that the effects of varying cation identity and concentration on a graft surface's wettability can be as large as the effects of anions. In addition, studies of the effects of these cation sulfate salt solutions on LCSTs show that LCST effects and surface wettability effects are comparable. A correlation between cation valence and the cation's effect on both LCSTs and surface wettability is seen when solution activity instead of concentration is examined. Using activities, the intensity of the cation effect on wettability follows the order: trivalent > divalent > monovalent. Similar analyses of LCSTs show that at similar activities, trivalent and divalent aqueous solutions of metal sulfates induce more salting out than aqueous solutions of monovalent sulfates.

Studies of Cation Effects on PE/$(PNIPAM/SiO_2)_6$/PNIPAM Nanocomposite Surfaces

We recently showed that it was possible to use covalent layer-by-layer assembly of nanoparticles and functional polymers to prepare surfaces that have wettability that changes dramatically based on whether the surface is functionally hydrophilic or hydrophobic.[144,145] Such materials are analogous to thermally responsive grafts of

PNIPAM and related polymers on nanostructured surfaces.[146,147] Notably, these wettability changes for a surface could be reversibly induced without the need for covalent modification with a hydrophobic or hydrophilic group. Likewise, the assembly of these nanocomposite grafts with silica nanoparticles avoided the need for physical patterning of the underlying substrate to create a topologically complex surface. Since the polymer matrix of these grafts used PNIPAM, the grafted surfaces changed from hydrophilic to hydrophobic much like PNIPAM's solubility in water changed as one varied the identity and concentration of a sodium anion solute. The large anion effect seen for PNIPAM/SiO_2 nanocomposite grafts on PE films and the effects of changing the identity of the anions on LCSTs of PNIPAM prompted us to study how varying cation identity could affect surface wettability. Since surface wettability was particularly sensitive to the concentration of a solution of a kosmotropic salt like sodium sulfate, we focused out attention on various cation salts of this common anion to determine if other cation salts would be more or less effective at altering surface wettability. The results showed that changing cations could affect surface wettability in an equally dramatic fashion. Moreover, the analyses of the effects of various sulfate salts on wettability using activity instead of concentration provided a contrasting picture of the effect of these various metal sulfate salts.

The nanocomposite grafts used in this study are prepared on polyethylene films the same way as described in Chapter III by following the procedure shown in Scheme 10. Studies of the effects of aqueous solutions of trivalent, divalent and monovalent cations on wettability of the prepared PE/(PNIPAM/SiO_2)$_6$/PNIPAM nanocomposite

surfaces were then carried out. In these studies, we opted to investigate cation salts of a common anion. These studies are more complicated in some ways than studies that use simpler sodium salts because the divalent and trivalent metal cations have relatively more complex and concentration-dependent structures in aqueous solution.[148,149] For example, the identity of the metal cationic species in aqueous solutions in the 0.1-1.0 M regime is complicated with a trivalent salt like $Al_2(SO_4)_3$. While Al^{3+} species like $Al(H_2O)_6^{3+}$ can be present, changes in pH or the presence of additives can lead to formation of a variety of other species.[150,151] The situation with divalent metal salts is somewhat less complex as these species are more likely also to be present in many forms, often as hexahydrates.[152] Moreover, depending on the cation and anion, varying amounts and varying types of ion pairs are present. The complexity of such solutions over the concentration range of 0.05-1.0 M is seen in studies of divalent sulfates where both contact and solvent separated ion pairs are present.[153-155] Similar complexity is seen in NMR studies where metal cationic species form various types of contact and solvent separated ion pairs with anions that range from halides to sulfates.[156-158] The solvated cationic species that are likely present at a solid/solution interface are certainly no less complex.[53] Given that such complications affect studies of the effect of an aqueous solution of any trivalent and divalent metal salt,[159] we opted to focus on a common anion that has a large effect on wettability. Since the kosmotropic sulfate anion was found to have a large effect on surface wettability in our prior studies of sodium salts, we examined the effect of varying the identity and concentration of the cation in sulfate salts on wettability.

To avoid any time dependent changes in contact angle as we discussed in Chapter III, these studies measured advancing water contact angles (Θ_a) as a function of the concentration of the various sulfate salt solutions. The results shown in Figure 18a show that changing the identity of the cation in aqueous solutions of sulfate salts did indeed have a large effect on surface wettability. The effects were seen in comparing trivalent, divalent and monovalent as well as in comparing monovalent sulfate salts alone. These effects were also reversible. For example, a PE/PNIPAM/$SiO_2)_6$/PNIPAM nanocomposite surfaces analyzed with a 1.0 M $Al_2(SO_4)_3$ solution had a Θ_a of 145°. Washing this surface first with water and then with THF yielded a film was then dried and reanalyzed with water. That analysis showed that the film had a Θ_a of 76°, a value that was identical to that of the Θ_a for water on the film before the original analysis with $Al_2(SO_4)_3$. Similar reversible wettability was seen in reanalysis with all of the other cation salts. This sort of reversible behavior was also seen in Chapter III for the effects of anions on surface wettability.

While the effect of changing cation identity in Figure 18a was significant, the results in Figure 18a suggested that the changes in wettability were not correlated with the cation valence. Specifically Na_2SO_4, $(NH_4)_2SO_4$, and Li_2SO_4 had a greater effect on surface wettability than $MgSO_4$, $CuSO_4$ or $NiSO_4$. $ZnSO_4$ was however very much like the monovalent sulfate salts in its effect on wettability. The wettability of these grafts was most sensitive to the concentration in $Al_2(SO_4)_3$ solutions. Plots of advancing water contact angle (Θ_a) versus SO_4^{2-} concentration (Figure 19) also showed the effects of divalent salts and monovalent salts on surface wettability are intermingled. We also

plotted advancing water contact angle versus ionic strength (Figure 20) and the plots showed that mono-, di-, trivalent cations' effects on wettability increase with solution ionic strength though Zn^{2+} is nearly indistinguishable from NH_4^+. Given the complexity of cation species in these solutions, we thus also looked at the variation in Θ_a for various cation sulfates versus salt solution activity. The activity coefficients for the various sulfate salts were obtained either directly from the literature[160-162] or were calculated by using Pitzer's method (which was used mainly for salt concentrations lower than 0.1 M for which the activity coefficients were not listed).[163,164]

The resulting plot of Θ_a versus activity shown in Figure 18b differed from the analogous plot of Θ_a versus concentration in that the divalent cations and monovalent cations were both slightly distinguishable from one another but also were present in distinct groupings. The single trivalent cation examined exhibited similarly distinct behavior. The differences seen for plots using concentration (Figure 18a) or activity (Figure 18b) were not observed in similar studies of various sodium salts. Plots of Θ_a *vs.* concentration and Θ_a *vs.* activity in Figures 21a and 21b showed only modest differences. In these cases, the activity coefficients of the various sodium salts did not change appreciably as the concentration of the anion changes from 0.1 - 1.0 M. Since the changes in activity over this concentration range paralleled the changes in anion concentration, the shape and sequential order of the curves in the activity plot are generally similar to what is seen in plots of Θ_a versus concentration.

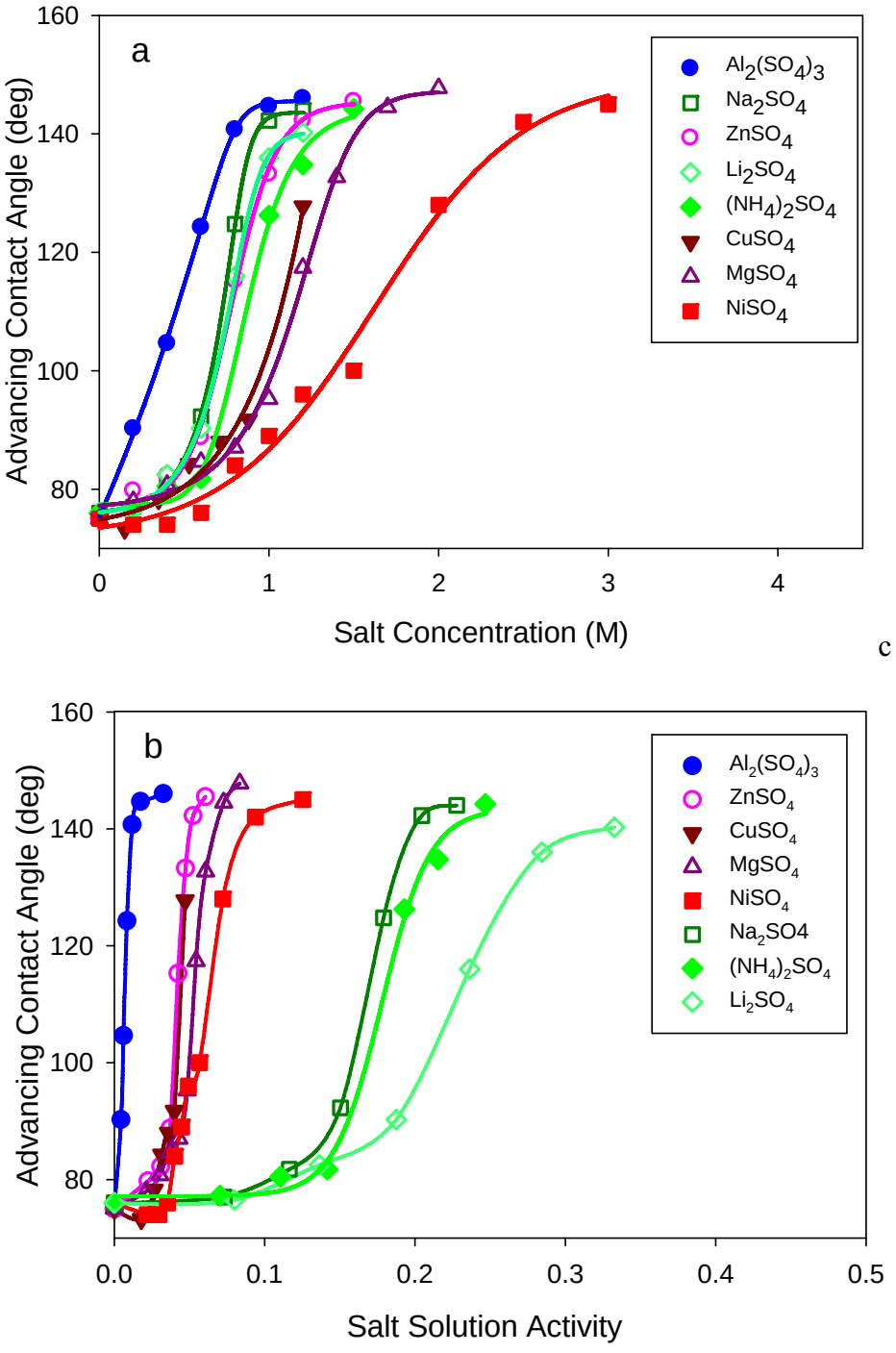

c

Figure 18. Cation effects on wettability of a PNIPAM/SiO_2 grafted nanocomposite surface: a) The advancing contact angles of various cation sulfate salts versus salt concentration; b) The advancing contact angles of various cation sulfate salts versus salt solution activity.

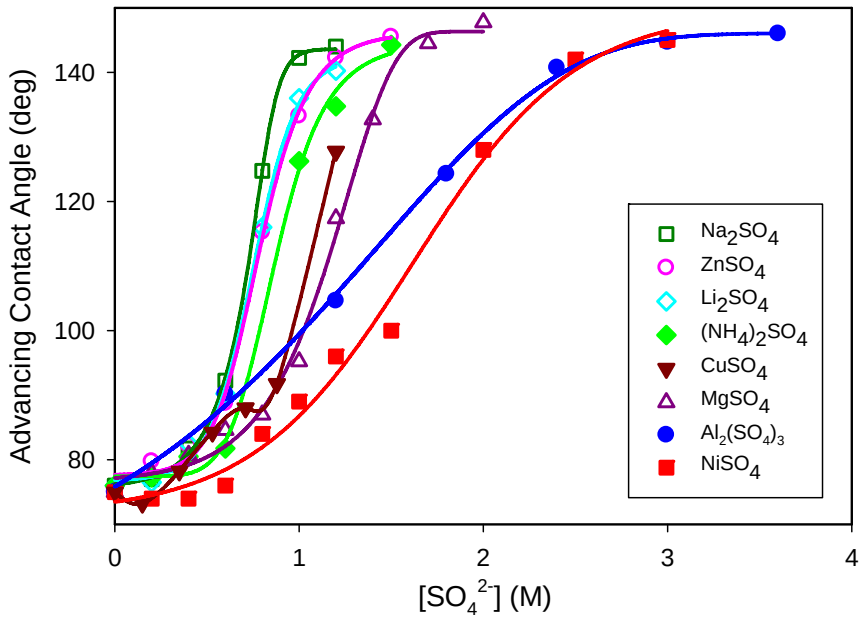

Figure 19. Cation effects on wettability of PNIPAM grafted nanocomposite surface. This figure was plotted over the advancing contact angles of various cation sulfate salts versus concentration of the sulfate ion.

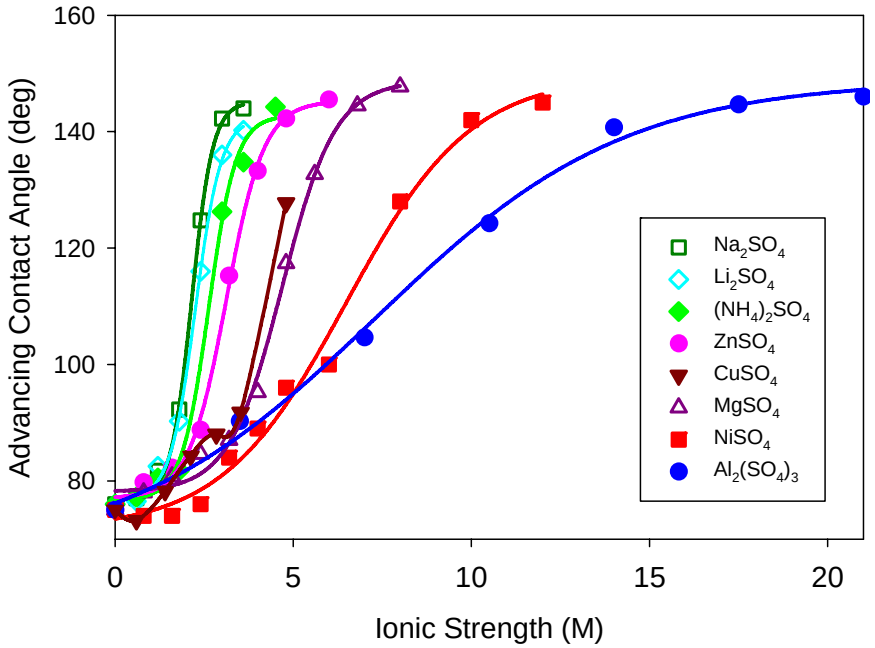

Figure 20. Cation effects on wettability of PNIPAM grafted nanocomposite surface. This figure was plotted over the advancing contact angles of various cation sulfate salts versus ionic strength of the salt solutions.

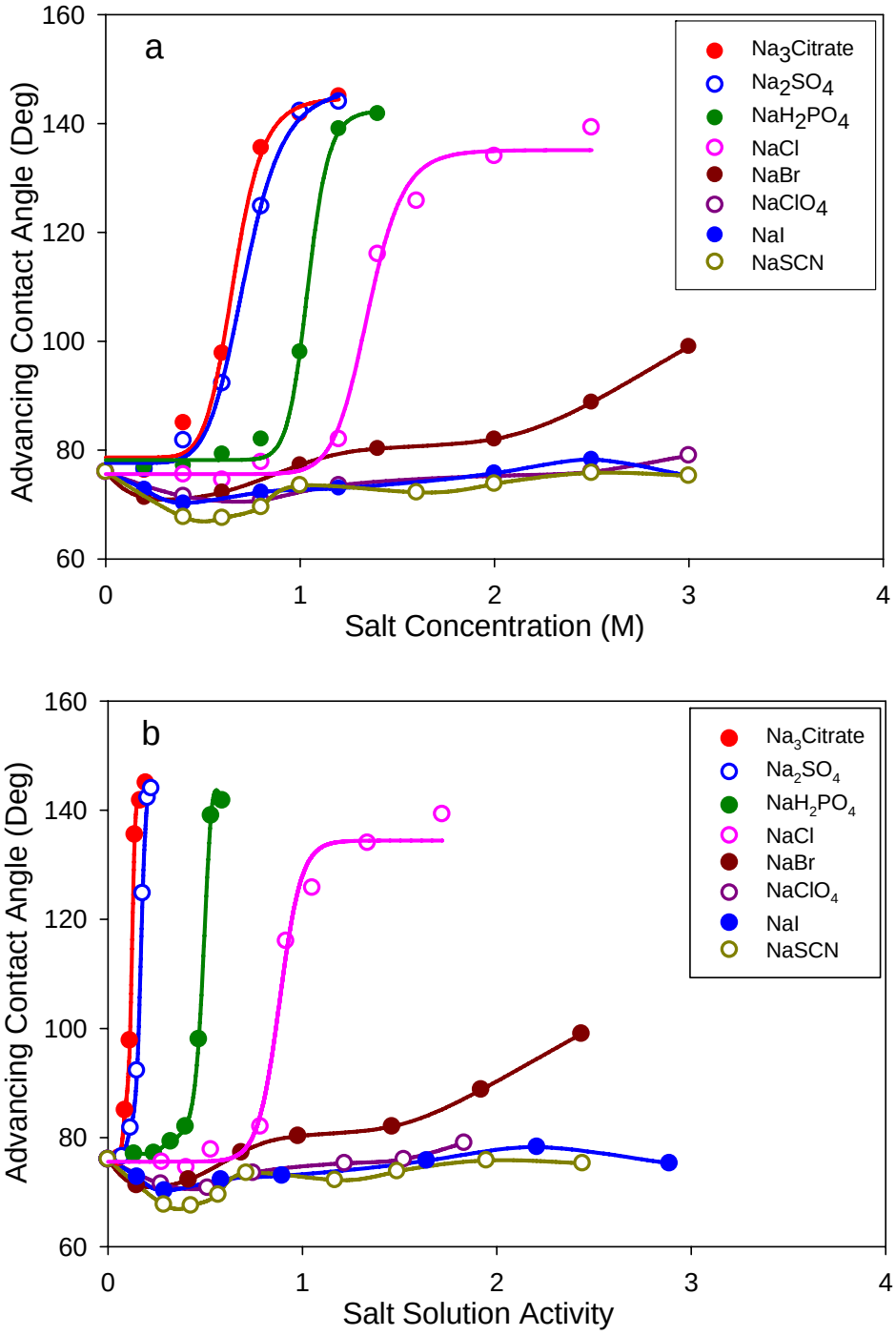

Figure 21. Anion effects on wettability of PNIPAM grafted nanocomposite surface: a) The advancing contact angles of various sodium salts versus salt concentration; b) The advancing contact angles of various sodium salts versus salt solution activity.

As was true for our earlier studies where anion identity and concentration were varied, the change of Θ_α with salt activity or concentration produced a curve similar to a titration curve with an inflection point that was significantly different with different salts. This effect was most striking in a plot of Θ_α for different cations on the wettability of these PNIPAM nanocomposite grafts and was greatest in comparison of groups of cations of different valence. For example, in Figure 18b, the inflection point for wettability change of the trivalent Al(III) was about 0.01 while the average inflection points for the di- and monovalent sulfate salts were 0.05 and 0.19 respectively. It was also notable that significant differences could be found for cations that have the same valence. For example, the wettability curves in Figure 18b for Na_2SO_4, $(NH_4)_2SO_4$ and Li_2SO_4 had inflection points at solution activities of 0.17, 0.18 and 0.23 respectively.

Atomic Force Microscopy Studies

Our prior studies of the effect of varying anion identity and concentration in reversibly changing wettability of PNIPAM/SiO_2 nanocomposite grafts showed that the wettability changes were correlated with changes in surface roughness presumably due to solvation/desolvation of the PNIPAM matrix. A similar correlation between surface roughness and surface wettability with different cation sulfate solutions was also found by AFM on the PE/(PNIPAM/SiO_2)$_6$/PNIPAM surfaces here (Figure 22). As shown in Figure 22a, this PNIPAM/SiO_2 nanocomposite surface inherently had both macro- and nanoscale roughness like the samples we prepared previously in air (224 nm compares to 287 nm rms). This 224 nm rms roughness changed when the surface was exposed to water, dropping to a value of ~157 nm rms. This 157 nm rms roughness did not change

significantly in the presence of 0.2 M aqueous $ZnSO_4$ (134 nm rms). However, treatment with a 0.8 M $ZnSO_4$ solution increased rms roughness to ~257 nm rms which further increases to ~307 nm in the presence of 1.2 M $ZnSO_4$. As described above, these changes in roughness likely corresponded to changes in solvation of the nanocomposite graft. Akin to the changes in surface morphology seen in our earlier work, they paralleled changes in wettability induced by the solute responsive swelling or chain collapse that altered the hydrophobicity of the PNIPAM component of the nanocomposite graft.[165-167]

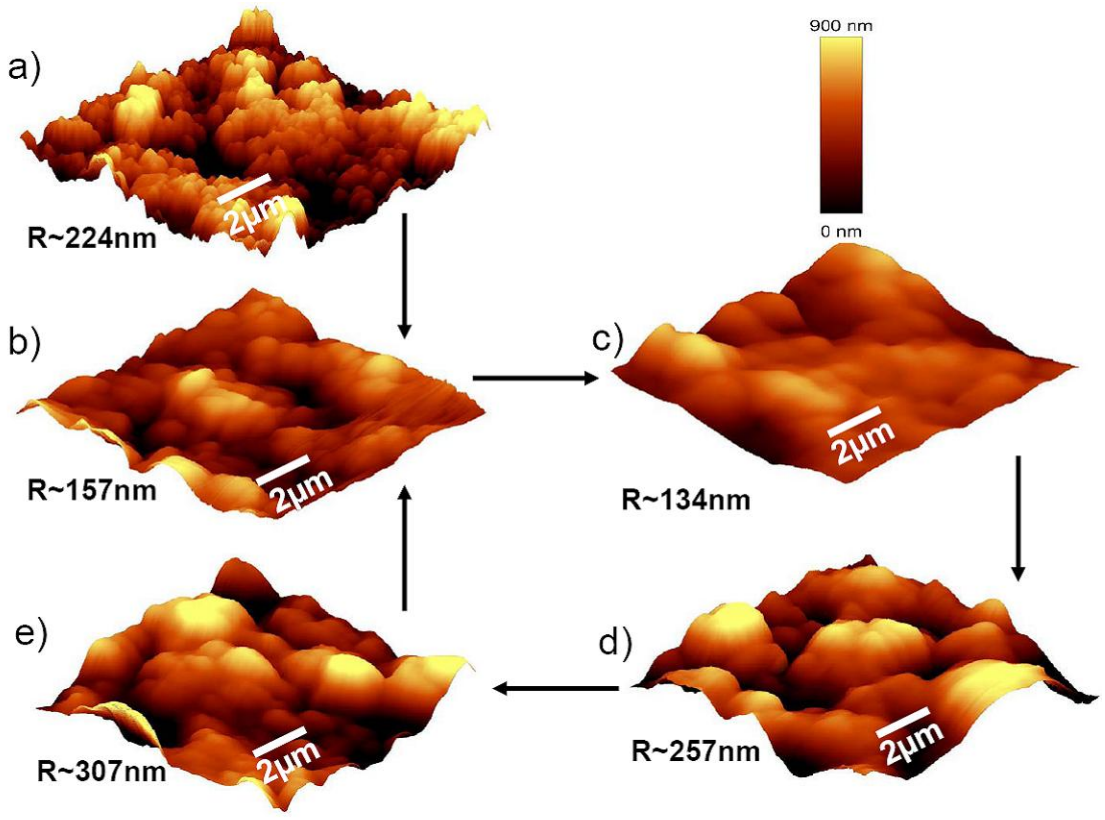

Figure 22. Tapping mode AFM images of PE/PEI/(PNIPAM/SiO_2)$_6$/PNIPAM obtained in (a) air, (b) water, (c) 0.2 M $ZnSO_4$, (d) 0.8 M $ZnSO_4$ and (e) 1.2 M $ZnSO_4$. The average rms roughness of the surface in each environment was taken from six random 2.5 μm × 2.5 μm regions and the data was listed below each image(scale bar: 2 μm).

Studies of Cation Effects on LCST of PNIPAM Solution

Since our earlier studies of the effects of changing the identity and concentration of anions on wettability of responsive grafts were based on prior studies of LCSTs of PNIPAM in sodium salt solutions, we chose to also study the effect of varying the identity and concentration of these sulfate salts on PNIPAM LCSTs. These studies employed the same automated melting point apparatus and procedures we used previously to study clouding curves for solutions of these and other thermoresponsive polymers.[168] As was true in our prior work, we used a fractionated sample of atactic PNIPAM with a M_n of 322 kDa (PDI = 1.06) as the polymer substrate. This PNIPAM was made by conventional radical polymerization and was purified by solvent precipitation. The sample solutions were prepared as mentioned in the experimental section and each sample had a constant PNIPAM concentration of 10 mg/mL. Plots of the LCST versus sulfate salt concentration and activity are shown in Figures 23a and 23b, respectively. The LCSTs in these curves were based on the temperature at which 50% clouding was observed. Plots of the LCST versus sulfate salt concentration or activity based on the 10% value for clouding were roughly similar (Figure 24). In either case, distinguishable cation effects were also seen on the phase transition temperature of PNIPAM solutions when we plotted the LCSTs versus salt concentrations (Figure 23a and 24a). Just as was true in studies of surface wettability, plots of the LCST versus salt concentration did not distinguish between divalent and monovalent sulfates, *e.g.* Na_2SO_4 and $ZnSO_4$ are quite similar. $NiSO_4$, $MgSO_4$, and $CuSO_4$ in contrast, behaved like 'salting in' cations in accord with conventional Hofmeister effects.[142] Plots of salt

concentration versus LCST with $Al_2(SO_4)_3$ showed this salt is the most kosmotropic. However, just as seen earlier for the cation effect on advancing contact angle, a plot of LCST versus salt solution activity showed distinctly different behavior for monovalent, divalent and trivalent sulfate salts (Figure 23b and 24b). Because the activity coefficient of the tri- and divalent cations was less than that of the monovalent cations, the intensity of the effects of different cations followed the order: trivalent > divalent > monovalent. More linear plots though were obtained when sulfate solution concentrations were plotted versus LCSTs.

While it is possible to speculate about the origin of these differences (*e.g.* Al^{3+} bears the most positive charge, $Al_2(SO_4)_3$ has the highest ionic strength,[40] and $Al_2(SO_4)_3$ produces the most ions when it dissociates), this speculation is likely to have to be oversimplified given the complexity of species present in aqueous solutions of these tri-, di- and monovalent sulfate solutions. Given this complexity, a simplified picture where cation hydrates of whatever structure affect the ability of water to hydrate the macromolecules seems to be a reasonable way to try to understand the different effects seen here.[169]

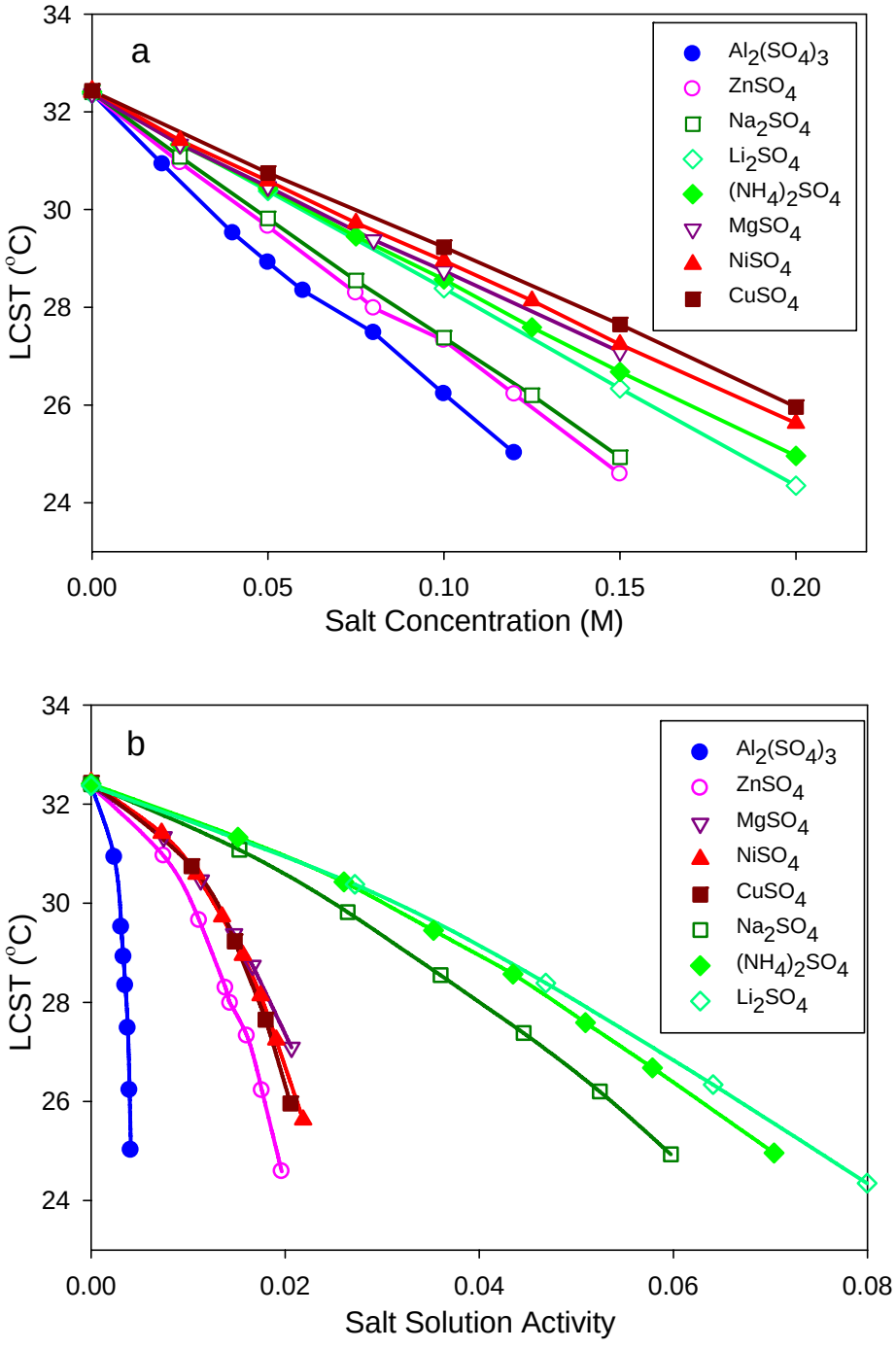

Figure 23. Cation effects on the LCSTs (based on the temperatures at which 50% clouding were observed) of PNIPAM in aqueous solution: a) The LCSTs of PNIPAM in various cation sulfate salt solutions versus salt concentration (M); b) The LCSTs of PNIPAM in various cation sulfate salt solutions versus salt activity. The concentration of PNIPAM was fixed to 10 mg/mL for all samples.

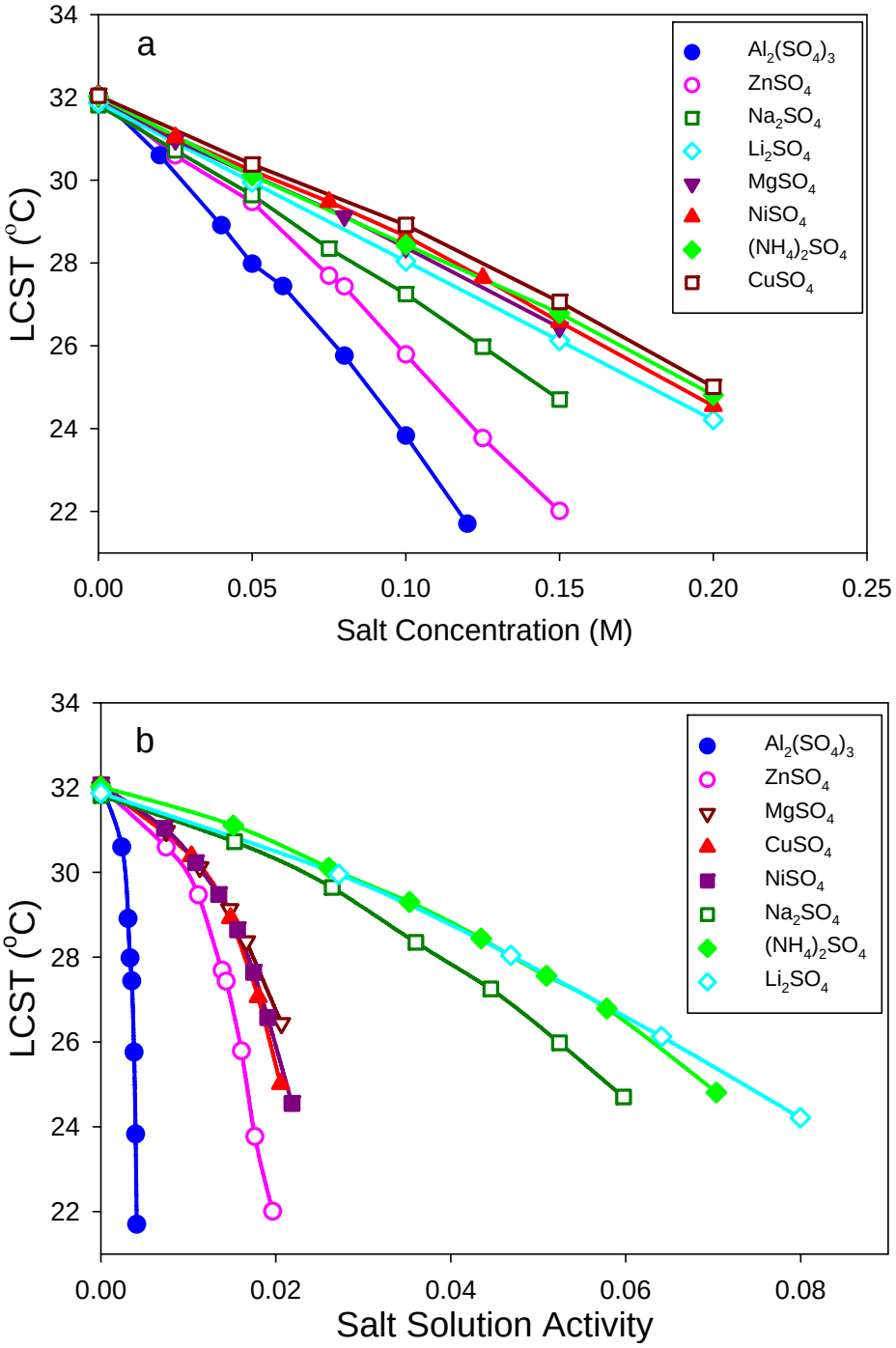

Figure 24. Cation effects on the LCSTs (based on the temperatures at which 10% clouding were observed) of PNIPAM in aqueous solution: a) The LCSTs of PNIPAM in various cation sulfate salt solutions versus salt concentration (M); b) The LCSTs of PNIPAM in various cation sulfate salt solutions versus salt activity. The concentration of PNIPAM was fixed to 10 mg/mL for all samples.

A similar interpretation of cation effects was advanced by Guo and Friedman in a recent report.[53] From their Gadolinium (Gd^{3+}) vibronic sideband luminescence spectroscopy (GVSBLS) experiments, they concluded that the effect of a cation on an macromolecule hydration was charge density-dependent and that high charge density cations change water configuration which in term weaken its hydrogen bonds to neighboring waters. However, the specific interactions will obviously vary depending on the relative concentrations of the various species present in these complexsolutions. Moreover, these solutions' components' relative concentrations vary in a concentration dependent manner. Thus, the effects are not likely to be linear with concentration, a result that is apparent in plots that use activity but not in those that only look at concentration.

Conclusion

These studies show that cations have large effects on phase separation of PNIPAM solutions and surface wettability of PNIPAM nanocomposite grafts. These effects on surface wettability are correlated with changing solvation/swelling and changing surface roughness of these nanocomposite grafts. Overall, the effects of varying the identity and concentration of cations are as marked as those seen with anions. This suggests that the design of solute responsive interfaces will need to consider cation identity and concentration in addition to anion identity and concentration. As was true in the case of our studies of wettability effects of solute anions, the effect of varying cation identity and concentration seen in wettability are paralleled in studies of changes in LCST for PNIPAM solutions. However, plots of the

physical changes of either the wettability or the LCST of these responsive polymer systems with varying cation concentration and identity vary significantly from plots where activity is used in place of concentration. Such marked differences are not seen for plots of wettability or LCST for less complex solutions where the identity of an anion is varied with a constant cation (Na^+). Generally speaking, the activity coefficients take into account both the dissociation of the electrolytes and the electrostatic forces between the dissociated ions. Thus, it might be more appropriate to use activity than concentration to analyze data especially when complicated electrolytes are under consideration or to at least consider activity as an alternative to concentration in analyses.

CHAPTER V

COVALENT LAYER-BY-LAYER ASSEMBLY OF SOLUTE-RESPONSIVE SURFACES ON SILICON WAFER

Introduction

As described in Chapter III and IV, we have been able to successfully graft PNIPAM/SiO_2 nanocomposites onto the surfaces of polyethylene (PE) films using covalent layer-by-layer assembly method. PE films have inherent roughness and their surfaces can be easily functionalized by oxidation using CrO_3/H_2SO_4.[170] Thus, I have in this chapter described how this method can be extended to covalently assemble layer-by-layer grafts on other types of materials, such as smooth or porous materials. Polished silicon wafers, which have hard and smooth surfaces, have been widely used as substrates for fabrication of microelectronics and solar cells. Two dimensional silicon wafers are also useful substrates when surface grafts are to be characterized by techniques like such as ellipsometry and atomic force microscopy.[171] Polished silicon wafers usually contain a native oxide on their surface and can be functionalized with primary amines by treatment with silanization reagents such as 3-aminopropyltriethoxysilane (APTES).[172,173] Aminated silicon wafers have long been used as substrates to prepare functional surfaces using ionic layer-by-layer self-assembly processes. In this chemistry, the aminated silicon wafers can self-assemble with an acid-containing polymeric reagent.[174,175] Subsequent steps with cationic and anionic polymers then produce a layer-by-layer graft. The chemistry in our covalent layer-by-layer

assembly involves the reaction of a nucleophile with an activated carbonyl derivative and is conceptually similar to the ionic process used by others.[145] For example, we have used the reaction of primary amines with active ester-containing copolymer, PNIPAM-*c*-PNASI to prepare the solute-responsive surfaces described in Chapter III and IV. In both cases, stable covalent amide bonds were formed at ambient temperature in less than 30 minutes. We envisioned that we could use the same condensation chemistry to covalently assemble grafts on surfaces of aminated silicon wafers. In this chapter, I will describe the syntheses of PNIPAM/SiO_2 nanocomposite grafts on polished silicon wafers using this covalent layer-by-layer assembly process. The same grafting materials, PNIPAM-*c*-PNASI copolymer and the 10- and 100-nm diameter aminated silica nanoparticles used in Chapter III and IV were used in this study and the solute-responsive wettability changes of the so-formed surfaces were studied by means of advancing contact angle measurements.

Preparing the PNIPAM/SiO_2 Nanocomposite on Silicon Wafer Surfaces by Covalent Layer-by-layer Self-assembly Method

Functionalization of silicon wafers (SW). A single-side polished silicon wafer (100) (1 x 1.5 cm) was sonicated for 2 minutes successively in hexane, tetrahydrofuran and ethanol to remove any contaminants. The washed silicon wafer was then blow-dried with nitrogen stream and then treated with 7:3 (vol/vol) concentrated sulfuric acid and 30% H_2O_2 for 1 h (*caution: the piranha solution is highly corrosive and extremely reactive with organic substances*). The cleaned silicon wafer was then rinsed with a copious amount of water and ethanol before being immersed into a 5 mM 3-

aminopropyltriethoxysilane (APTES) ethanol solution. The wafer/APTES solution mixture was shaken by a shaker at moderate speed overnight. The APTES treated wafers were then removed from this solution and washed with ethanol and dried in a vacuum oven at 120 °C for 2 h. The resulting amine-functionalized wafer had a hydrophilic surface with an advancing water contact angle of less than 15°. The thickness of the APTES layer was 2 nm as determined by ellipsometry measurement. The ellipsometic data was measured by a Nanofilm EP^3 imaging ellipsometer at 660 nm wavelength with an incidence angle of 75 deg. The film thickness was calculated by fitting the ellipsometric data using the supplied EP^3View software. An AFM image of this ATPES-treated silicon wafer (Figure 25a) was obtained by Mr. Albert Wan in the Batteas group. This image shows a featureless surface with a measured rms roughness of 0.7 ± 0.3 nm. The smooth surface indicated that a monolayer of APTES was attached to the silicon wafer surface.

Covalent layer-by-layer self-assembly of PNIPAM/SiO_2 nanocomposites on silicon wafers. Prior to the PNIPAM/SiO_2 nanocomposite grafting, the APTES-treated silicon substrate was primed by covalently attaching two PNASI/PEI bilayers to its surface. his process was assumed to increase the number of surface amine groups. This priming step was accomplished by allowing the APTES-treated silicon wafer to react first with the electrophilic poly(*N*-acryloxysuccinimide) (PNASI) for 30 minutes. The active ester of NASI was readily converted to an amide upon reacting with an amine. This condensation reaction coupled the polyvalent electrophilic polymers to the originally aminated wafer surface and the remaining unreacted NASI groups could react

further with subsequently introduced nucleophilic polyethyleneimine (PEI) in a similar amide-forming condensation reaction. The surface was amine-rich after one PNASI/PEI bilayer treatment. While the surface could be used directly for a second PNASI/PEI bilayer treatment, we treated this surface with *i*-$PrNH_2$ to quantitatively convert any unreacted NASI groups into NIPAM groups. A second PNASI/PEI bilayer treatment was carried out after the *i*-$PrNH_2$ treatment and the wafer surface by now was covered with a sufficient amount of amine groups. AFM analysis by Mr. Albert Wan showed that small but evenly scattered clusters that were about 4 nm in height appeared on the surface after being primed with one PNASI/PEI bilayer (Figure 25b). AFM analysis also showed that this silicon wafer surface had an rsm roughness of about 1.3 ± 0.3 nm and a thickness of about 6 nm. After the surface was primed with the second PNASI/PEI bilayers, the new surface had a similar rms roughness of 1.2 ± 0.3 nm but an increased thickness of 14 nm (Figure 25c). These results indicated that we were able to increase the amount of surface functional groups without changing the surface roughness. The 'primed' surface is presumed to help to enhance the following covalent layer-by-layer assembly steps.

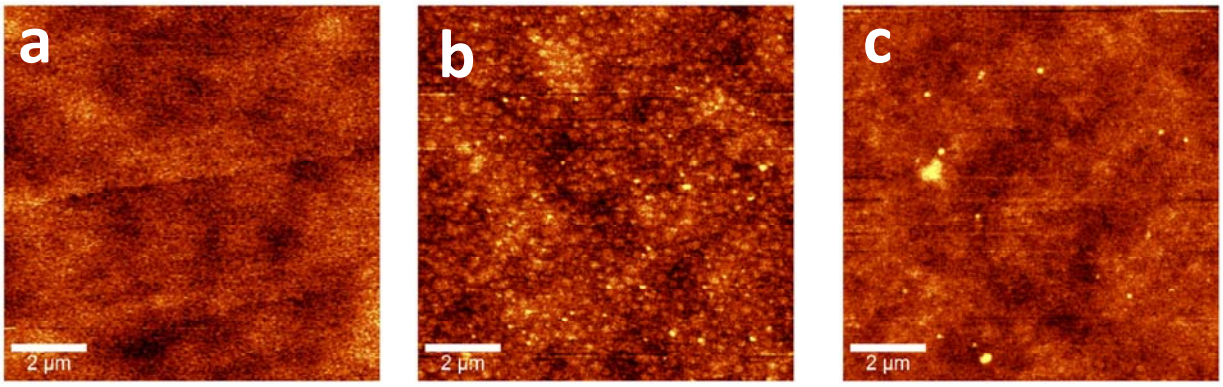

0.7 ± 0.3 nm 1.3 ± 0.3 nm 1.2 ± 0.3 nm

Figure 25. Tapping mode AFM topographic images of surfaces of (a) APTES treated silicon wafer, b) one PNASI/PEI bilayer primed silicon wafer, c) two PNASI/PEI bilayers primed silicon wafer. The numbers under each image are the rms roughness for the corresponding surfaces.

The same covalent layer-by-layer assembly process illustrated in Scheme 10 was then carried out on this 'primed' silicon wafer. As illustrated in Scheme 10, a nucleophilic copolymer, PNIPAM-*c*-PNASI (M_n = 30,000 Da), and electrophilic aminated 10- and 100-nm silica nanoparticles were used in this synthesis. After each PNIPAM-*c*-PNASI/SiO_2 bilayer assembly, excess *i*-$PrNH_2$ was used to convert any unreacted NASI groups into NIPAM groups which led to the formation of a PNIPAM/SiO_2 network on the surface. In most cases, five PNIPAM-*c*-PNASI/10 and 100 nm aminated silica nanoparticles/*i*-$PrNH_2$ treatments were carried out before the surface was treated with one PNIPAM-c-PNASI/10 nm aminated silica nanoparticles/*i*-$PrNH_2$ treatment. Finally the surface was treated with PNIPAM-*c*-PNASI and then *i*-$PrNH_2$ to make a nanocomposite graft with PNIPAM on the top layer. The so-formed PNIPAM/SiO_2 nanocomposite grafted silicon wafers were denoted as

SW/(PNIPAM/SiO_2)$_6$/PNIPAM just as PE/(PNIPAM/SiO_2)$_6$/PNIPAM was used to name the similar nanocomposite graft on a PE film. An AFM image of this SW/(PNIPAM/SiO_2)$_6$/PNIPAM nanocomposite is shown in Figure 26. This image obtained by Mr. Albert Wan reveals the same type of surface texture seen for the PE/(PNIPAM/SiO_2)$_6$/PNIPAM nanocomposite (Figure 12). This SW/(PNIPAM/SiO_2)$_6$/PNIPAM nanocomposite graft has a rms roughness of 287 ± 53 nm which is essentially the same value for the rms roughness of PE/(PNIPAM/SiO_2)$_6$/PNIPAM graft (287 nm).

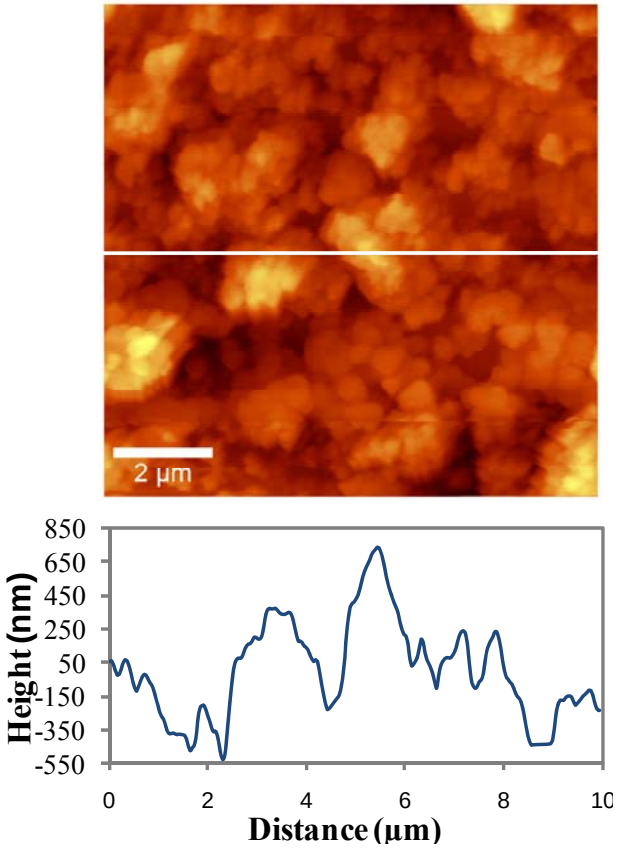

Figure 26. Tapping mode AFM topographic image of a SW/(PNIPAM/SiO_2)$_6$/PNIPAM nanocomposite surface with a rms roughness of 287 ± 53 nm. The bottom graph is the cross-section trace along the white line drawn on the AFM image.

Studies of the Solute-responsive Wettability on the Surfaces of SW/(PNIPAM/SiO_2)$_6$/ PNIPAM Nanocomposite Grafts

In Chapters III and IV, I showed that PNIPAM /SiO_2 nanocomposite grafts prepared on PE films showed distinct responsive wettability for various salt solutions or solutions of one salt with different concentrations. By changing the identity or concentration of a sodium anion salt or a cation sulfate salt, such surfaces can be tuned in such a way that they are alternately and reversibly hydrophilic or very hydrophobic. The propensity of different anions to change the surface wettability paralleled the effects of these anions on LCSTs of soluble PNIPAM and is essentially a Hofmeister effect of salts on wettability. Since this SW/(PNIPAM /SiO_2)$_6$/PNIPAM nanocomposite graft was assembled in the same manner as used for the PE/(PNIPAM /SiO_2)$_6$/PNIPAM graft, we expected that it had similar surface properties as the PE/(PNIPAM /SiO_2)$_6$/PNIPAM graft seen in Chapter III and IV. A series of sodium salt solutions were applied to the newly prepared SW/(PNIPAM /SiO_2)$_6$/PNIPAM nanocomposite graft. As shown in Figure 27, the same sorts of anion effects are observed on this surface. The kosmotropic salts such as sodium citrate and sodium sulfate have greater ability to change the surface wettability than chaotropic salts such as sodium iodide and sodium thiocyanate. Also, larger differences in advancing contact angles ($\Delta\Theta_a$) were seen on this surface with varying solution concentrations. The largest $\Delta\Theta_\alpha$ on surface of this nanocomposite grafted silicon wafer was as high as ~90°. This $\Delta\Theta_\alpha$ is ~20° higher than the largest $\Delta\Theta_a$ (~70°) seen with the PE/(PNIPAM /SiO_2)$_6$/PNIPAM nanocomposite grafts. More interestingly, the surface of SW/(PNIPAM/SiO_2)$_6$/PNIPAM nanocomposite graft

became superhydrophobic with 1.4 M sodium citrate and sodium sulfate. For example, when a 10 μL droplet of 1.4M sodium citrate was applied onto this surface, the droplet would roll on the surface with a sliding angle less than 15°. The same superhydrophobic wettability could also be observed with sodium chloride at higher concentrations (3 M). Just as true for the PNIPAM/SiO_2 nanocomposite grafted PE films, the PNIPAM/SiO_2 nanocomposite grafted silicon wafers showed reversible and repeatable wettability changes in response to changes of salt solution concentrations or solute identity.

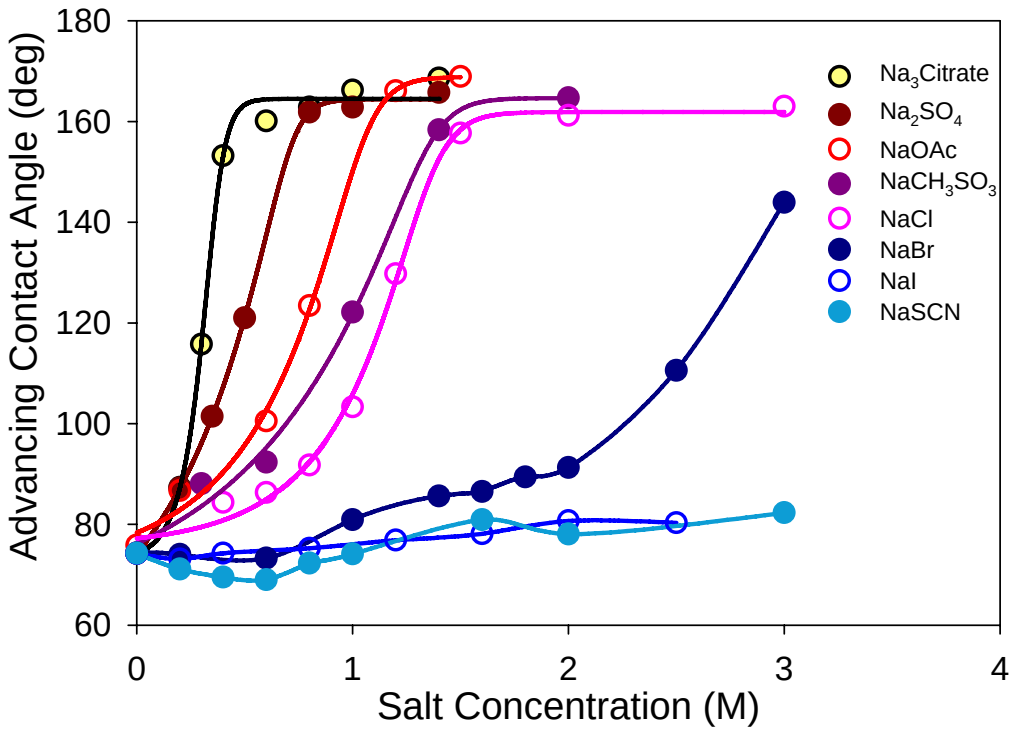

Figure 27. Changes in advancing contact angle (Θ_a) of a SW/(PNIPAM/SiO_2)$_6$/PNIPAM nanocomposite surface measured with solutions of various salts as a function of salt concentration. Each data point was the average of three individual measurements and had an error of ±2°.

We further tested the solute-responsive wettability of the SW/(PNIPAM/SiO_2)$_6$/PNIPAM nanocomposite graft with two organic salts (sodium acetate and sodium methanesulfonate) and a polymeric salt (poly(sodium *p*-styrene sulfonate)). Sodium acetate (NaOAc) and sodium methanesulfonate ($NaCH_3SO_3$) both acted as kosmotropic salts and induced a $\Delta\Theta_a$ of ~ 90° while increasing the solution concentrations (Figure 27). The effect of anions on this solute-responsive SW/(PNIPAM/SiO_2)$_6$/PNIPAM nanocomposite surface follows the order: $C_6H_5O_7^{3-}$ (citrate) > SO_4^{2-} > $CH_3CO_2^-$ > $CH_3SO_3^-$ > Cl^- > Br^- > I^- ~ SCN^-, which agree with Hofmeister series.

The poly(sodium *p*-styrene sulfonate) (PPS) (M_w = 70 kDa) behaved a little differently and it seemed like having a 'salting-in' effect at lower concentrations. Figure 28 showed the changes in advancing contact angle and static contact angle of a SW/(PNIPAM/SiO_2)$_6$/PNIPAM nanocomposite surface measured with aqueous PPS solutions at different concentrations. The droplets of each solution were allowed to equilibrate with the surface for 2 minutes before measuring the advancing and static contact angles. Both the advancing and static contact angle data showed that the surface became more hydrophilic with 0.2 to 0.6 M PPS than with water. This might be due to the interactions between the polymer chains of PNIPAM and the added PSS. Those interactions helped stabilize the coil conformation of PNIPAM chains on the surface and led to a more hydrophilic surface. Similar effects had been reported on the LCSTs of PNIPAM in aqueous solutions with the addition of polyethylene glycol and bovine

serum albumin.[45] As seen in Table 1 in Chapter I, higher LCSTs for PNIPAM solutions were observed with the addition of these macromolecular species.

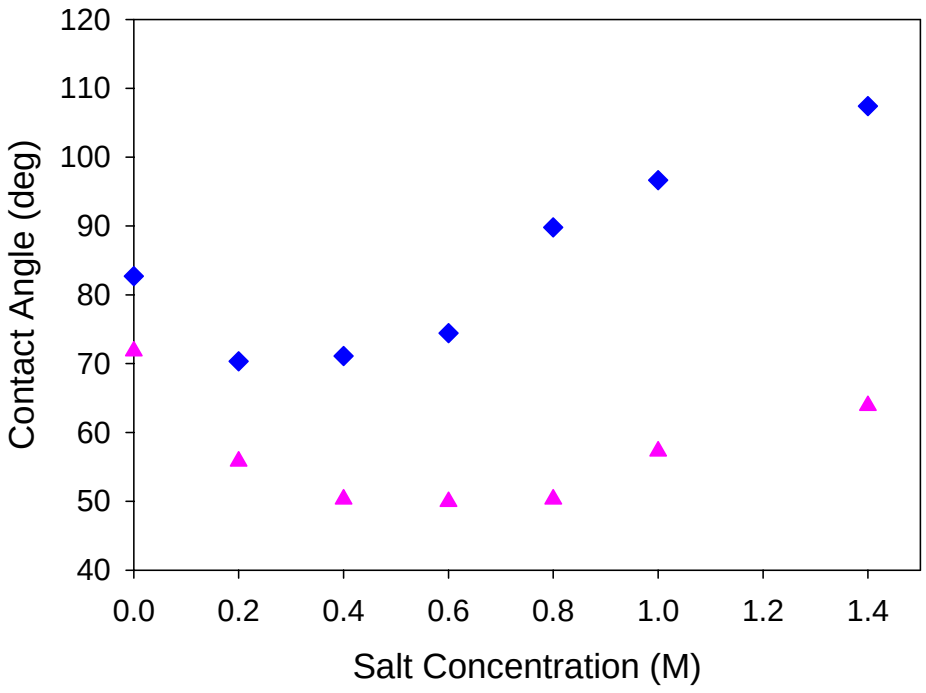

Figure 28. Changes in advancing contact angle (filled diamonds) and static contact angle (filled triangles) of a SW/(PNIPAM/SiO_2)$_6$/PNIPAM nanocomposite surface measured with aqueous solutions of poly(sodium p-styrene sulfonate) in different concentrations. The static contact angles were measured at 2 minutes after each droplet was placed on the surface.

We were also interested in the effect of mixed salts on wettability of this solute-responsive surface. Prior work has suggested mixed salts have an addictive effect on PNIPAM LCSTs.[47] Freitag's group had measured cloud point temperatures of PNIPAM solutions that contained equal amounts of KF/KCl or equal amounts of KF/KI as cosolutes. They found out that either with two salting-out salts (KF/KCl) or with a combination of a salting-out salt (KF) and a salting-in salt (KI), the effect of the two

salt species on the cloud point temperature of PNIPAM solution is additive. In this study, I chose two mixed salt series to test wettability effects of salt mixtures on the SW/(PNIPAM/SiO_2)$_6$/PNIPAM nanocomposite graft: one had a fixed concentration of NaOAc (0.8 M) and a varied concentration of NaSCN; the other had a fixed concentration of NaSCN (0.8 M) and a varied concentration of NaOAc. I chose these two salts because NaOAc and NaSCN had salting-out and salting-in effects respectively as shown in Figure 27. The mixed salt results are shown in Figure 29, which reveals that mixed salts also have an additive effect on the wettability of SW/(PNIPAM/SiO_2)$_6$/PNIPAM nanocomposite grafts.

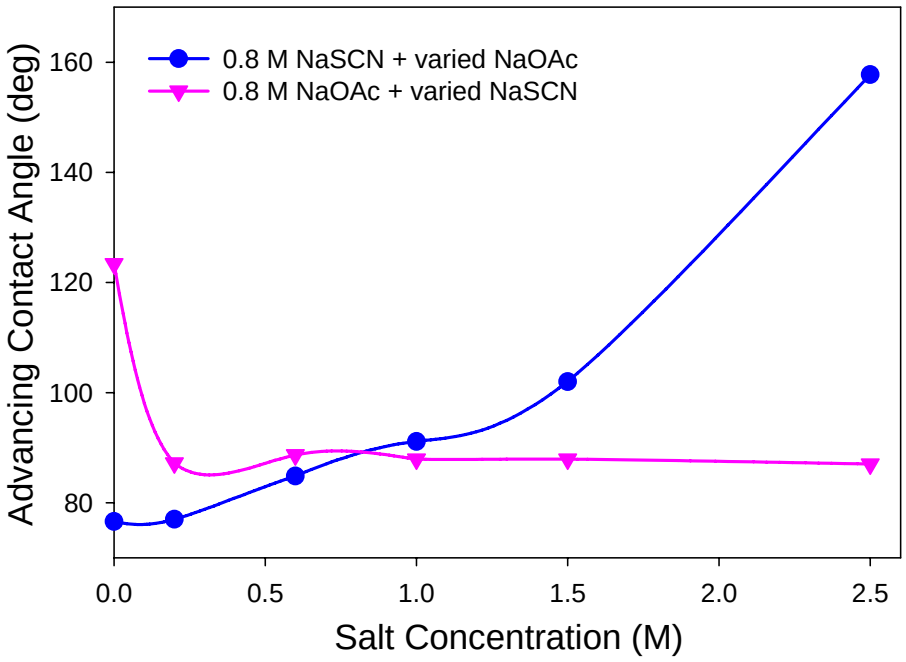

Figure 29. Advancing contact angles measured with solutions of mixed NaOAc and NaSCN on the SW/(PNIPAM/SiO_2)$_6$/PNIPAM nanocomposite surface. The blue circles represent the advancing contact angles obtained using solutions with fixed [NaSCN] (0.8 M) and varied [NaOAc]. The pink triangles represent the advancing contact angles obtained using solutions with fixed [NaOAc] (0.8 M) and varied [NaSCN].

Conclusion

Previously, we have successfully prepared PNIPAM/SiO_2 nanocomposite grafts on soft and rough polyethylene films by a covalent layer-by-layer assembly method. The product PE/(PNIPAM/SiO_2)$_6$/PNIPAM graft showed distinct solute-responsive wettability. In this chapter, we demonstrated that the same covalent layer-by-layer assembly method can be extended to make PNIPAM/SiO_2 nanocomposite grafts on hard and smooth substrates such as silicon wafer. SW/(PNIPAM/SiO_2)$_6$/PNIPAM nanocomposite grafts were successfully grafted on polished silicon wafers and the surfaces of these grafts showed good solute-responsiveness on wettability. When a series of sodium salt solutions were applied to the SW/(PNIPAM/SiO_2)$_6$/PNIPAM nanocomposite surfaces, the same anion effects on wettability were observed as had been seen for PE grafted nanocomposite surfaces. Furthermore, when we applied solutions of mixed sodium acetate (salting-out salt) and sodium thiocyanate (salting-in salt) to a SW/(PNIPAM/SiO_2)$_6$/PNIPAM nanocomposite surface, the mixed salt effects on wettability are additive, which agrees with the additivity of salt on LCST observed in studies of PNIPAM solutions. The ability of grafting a PNIPAM/SiO_2 nanocomposite surface on silicon wafers using the covalent layer-by-layer assembly will also enable us to study the surface growth mechanisms by means of AFM analysis. The thickness and roughness of the grafted surface at different grafting stages can both be measured by AFM. Detailed AFM studies of this covalent layer-by-layer assembly have been carried out with the Batteas group. These results are consistent with an assembly process like that shown in Scheme 10.

CHAPTER VI

PNIPAM-BASED FUNCTIONAL RESPONSIVE POLYMERS

Introduction

Temperature responsive polymers have a lower critical solution temperature (LCST) and are soluble in a cold solution but become insoluble on heating. At their LCSTs, they exhibit reversible coil-to-globule conformational changes and undergo subsequent phase separation in solution. Among all the thermoresponsive polymers, poly(*N*-isopropylacrylamide) (PNIPAM) has been studied in the greatest detail. PNIPAM forms random coils in water at low temperatures and collapses to form solid globules with a sharp phase transition temperature around 32°C. PNIPAM's temperature dependent behavior has been studied in solution, in gels and on surfaces under the influence of various additives and solvents. While this LCST behavior is also affected by the polymer microstructure and polymer stereochemistry, incorporation of modest amounts of other functional groups into the PNIPAM chain allows one to make responsive recyclable polymeric analogs of various functional groups. This allows one to use PNIPAM copolymers in a variety of applications. In this chapter, examples of PNIPAM copolymers with different targeted applications are discussed.

Random PNIPAM copolymers can be easily prepared by two general synthetic approaches (Scheme 11). The first scheme is based on copolymerization of *N*-isopropylacrylamide (NIPAM) with an appropriately functionalized acrylamide or acrylate starting with a desired ratio of two comonomers. Varying the monomer feed

ratios can generate PNIPAM copolymers with different LCSTs which depend on the mole fraction and the nature of substituent R^1 in Scheme 11 a. The second scheme involves the use of an active ester-containing polymer, usually an *N*-succinimidyl-containing polymer (Schemes 11 b and c).[176] Poly(*N*-acryloxysuccinimide) (PNASI) homopolymer or PNIPAM-*c*-PNASI copolymer can both be used to synthesize of functional PNIPAM copolymers.[177] They also have been used as polyvalent electrophiles in our covalent layer-by-layer self assembly procedure for grafting functional nanocomposite surfaces. Both synthetic approaches shown in Scheme 11 are used in the discussions below.

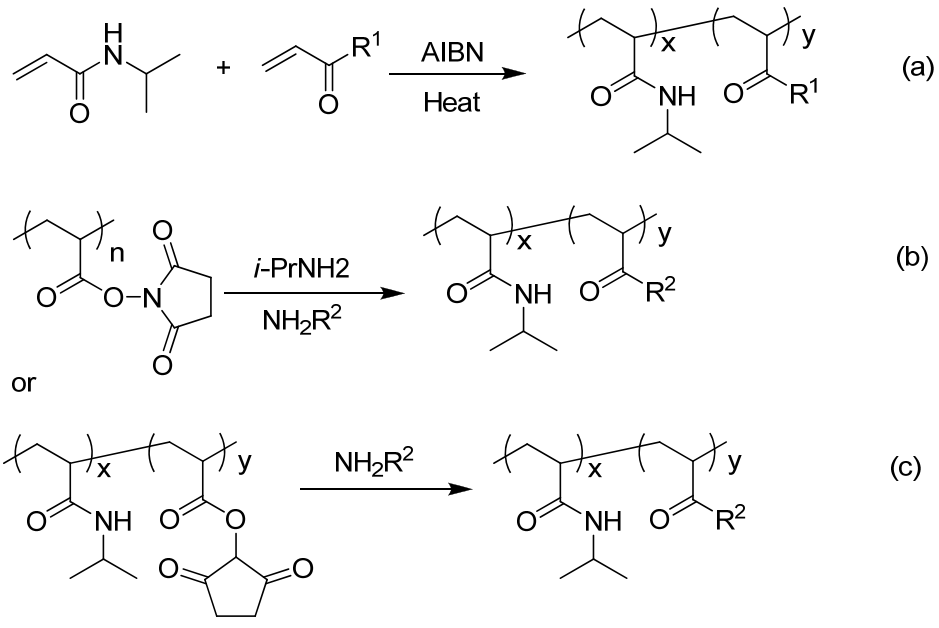

Scheme 11. Syntheses of random PNIPAM copolymers.

Poly(*N*-isopropylacrylamide)-*c*-poly(4-(*N*,*N*-diallylamino)pyridine) (PNIPAM-*c*-PDAAP) – a PNIPAM-supported Organocatalyst

4-*N*,*N*-(Dialkylamino)pyridine derivatives such as 4-(dimethylamino)pyridine (DMAP) and 4-pyrrolidinopyridine (4-PPY) are widely applied as organocatalysts for a variety of nucleophilic addition reactions, such as acylations and silylations of tertiary and hindered hydroxyls, Baylis-Hillman reactions and ester transesterfication or hydrolysis.[178] In order to allow facile recovery and reuse of these catalysts, several approaches for immobilization of 4-*N*,*N*-(dialkylamino)pyridine catalysts on various organic and inorganic solid supports such as polymer beads and silica-based materials, have been reported in the literature.[179,180] Homogeneous polymer-supported 4-*N*,*N*-(dialkylamino)pyridine catalysts using polymers such as linear soluble polymers, dendrimers, and multiarm star copolymers, have also been studied.[181-183]

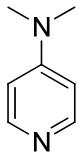

4-(dimethylamino)pyridine

DMAP

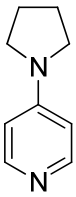

4-(pyrrolidino)pyridine

PPY

Previously, our group had made a soluble polymer-bound version of DMAP using poly(*N*-isopropylacrylamide) (PNIPAM) or poly(4-*tert*-butylstyrene) (PtBS) as a soluble polymer supports. Both the PNIPAM-supported DMAP (**10**) and PtBS-supported DMAP catalysts (**11**) showed activity like that seen for DMAP. The catalyst **10** was successfully recovered and recycled by solvent precipitation or using a liquid/liquid thermomorphic solvent system. The selective solubility of PtBS in heptane

enabled catalyst **11** to be recycled 20 times in a heptanes/EtOH latent biphasic solvent system.

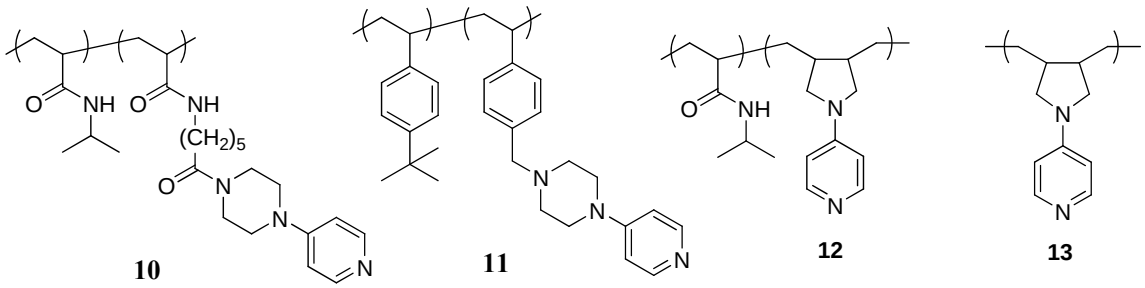

4-Pyrrolindinopyridine (4-PPY) has the highest activity among all the 4-*N*,*N*-(dialkylamino)pyridine catalysts and polymeric versions like poly(4-*N*,*N*-diallylaminopyridine) (PDAAP) **12** have been shown to be more effective in hydrolysis of *p*-nitrophenyl carboxylate in aqueous buffer solutions than 4-PPY. In this section, I describe the synthesis and the kinetic studies of another PNIPAM supported 4-PPY catalyst **13**. The successful recycling of this catalyst with different methods is also discussed.

Using the synthetic route shown in Scheme 12, I first prepared the 4-*N*,*N*-diallylaminopyridine monomer and then copolymerized it with NIPAM in HCl aqueous solution using 2,2'-azobis(2-methylpropionamidine) dihydrochloride (V-50) as initiator to form the poly(*N*-isopropylacrylamide)-*c*-poly(4-(*N*,*N*-diallylamino)pyridine) (PNIPAM-*c*-PDAAP) copolymer **13**.[184] Three PNIPAM-*c*-PDAAP copolymers with NIPAM/DAAP ratios of 5:2, 14:1 and 20:1 were prepared. The mole fractions of comonomers in the product copolymers were determined by ^{1}H NMR spectroscopy. A homopolymer poly(4-*N*,*N*-diallylaminopyridine) (PDAAP) **12** was also prepared by the

same radical polymerization procedure. GPC analyses (Viscotek multidetector GPC system) showed that the 5:2, 14:1 and 20:1 PNIPAM-*c*-PDAAP copolymers had a M_w of 43 kDa, 40 kDa and 42 kDa respectively. The PDAAP homopolymer had a M_w of 35 kDa.

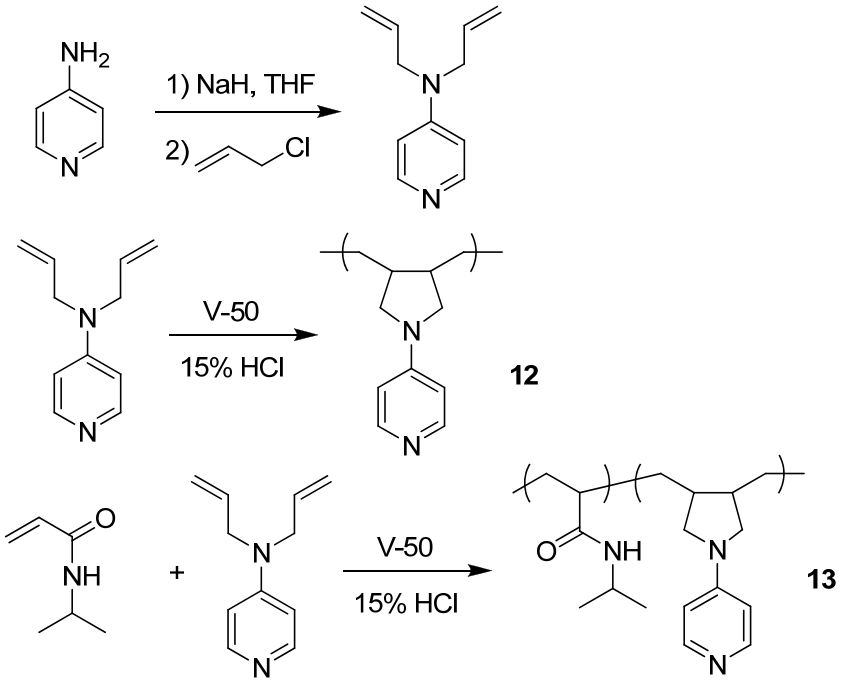

Scheme 12. Syntheses of PDAAP **12** and PNIPAM-*c*-PDAAP **13**.

The catalytic activities of **12** and **13** were studied using hydrolysis reaction of *p*-nitrophenyl octanoate (eq 6).[185] In kinetic studies, the UV absorbance of the hydrolysis product, *p*-nitrophenylate anion, at 400 nm was measured as a function of time using a Varian Carry 100 ultraviolet-visible spectrometer equipped with a temperature controller and a magnetic stirrer. All the catalysts were dissolved in methanol to make stock solutions that had a concentration of 1.5×10^{-3} M. The *p*-nitrophenyl octanoate was

prepared as a $3x10^{-2}$ M solution in acetonitrile. For a typical kinetic analysis, the sample cuvette was filled with 3 mL of a buffer solution to control the pH value and equilibrated for 1 h at 20°C. Then 5 µL each of the catalyst and *p*-nitrophenyl octanoate stock solution was added to this buffer solution. Figure 30 shows the spectra collected during the hydrolysis experiment using PDAAP as catalyst. It's clear to see that when the hydrolysis reaction proceeds, the absorbance at 400 nm wavelength increases.

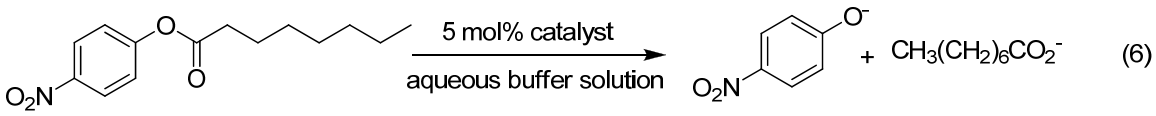

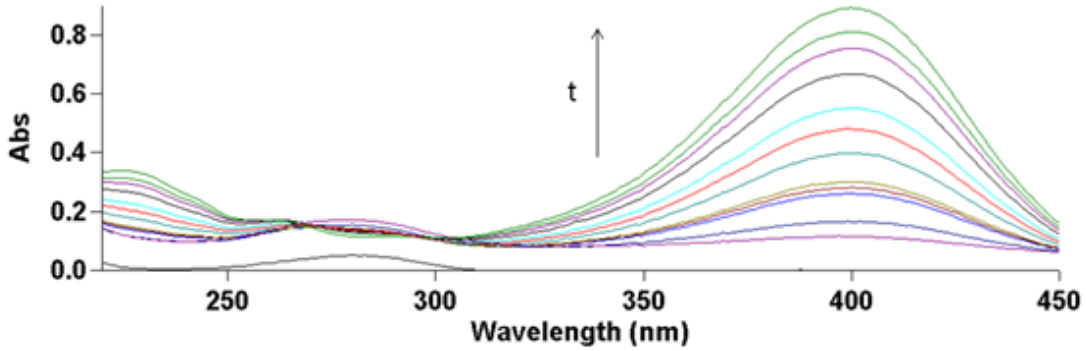

Figure 30. UV spectra collected during the hydrolysis of p-nitrophenyl octanoate catalyzed by PDAAP.

Figure 31 shows the kinetic results obtained for the hydrolysis of p-nitrophenyl octanoate catalyzed by PDAAP and three PNIPAM-*c*-PDAAP copolymers in the pH 8 tris buffer. The same kinetic studies also performed on the 4-PPY catalyzed and uncatalyzed hydrolysis reactions and the results were graphed on Figure 26 for comparison. These results show that all the catalytic hydrolysis reactions are faster than

the uncatalyzed reaction. PDAAP and PNIPAM-*c*-PDAAP copolymers catalyzed reactions are significantly faster than that catalyzed by 4-PPY. This is attributed to the decreased pK_a of macromolecular DAAPs. Of the polymeric catalysts, the homopolymer PDAAP has the fastest rate. The PNIPAM-*c*-PDAAP copolymers' activity decreases as the mole fraction of DAAP in the copolymers decreases.

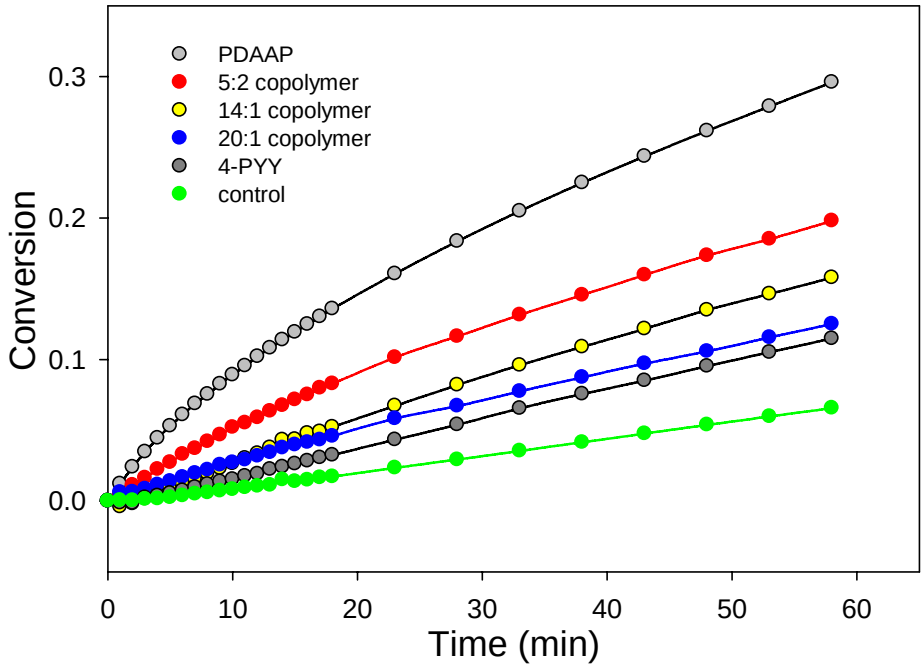

Figure 31. Hydrolysis of 4-nitrophenyl octanoate in pH 8 tris buffer at 20 °C by different 4-*N*,*N*-(dialkylamino)pyridine catalysts.

Kinetic studies were also carried out in a pH 9 tris buffer to determine how pH affects these catalysts' efficiency. Figure 32 shows that all the hydrolysis reactions are accelerated at pH 9. PDAAP and PNIPAM-*c*-PDAAP copolymers catalyzed reactions however are still significantly faster than a reaction using 4-PPY. However, at pH 9, the

14:1 and 20:1 PNIPAM-*c*-PDAAP copolymers have activity that is comparable that of PDAAP and the 5:2 PNIPAM-*c*-PDAAP copolymer.

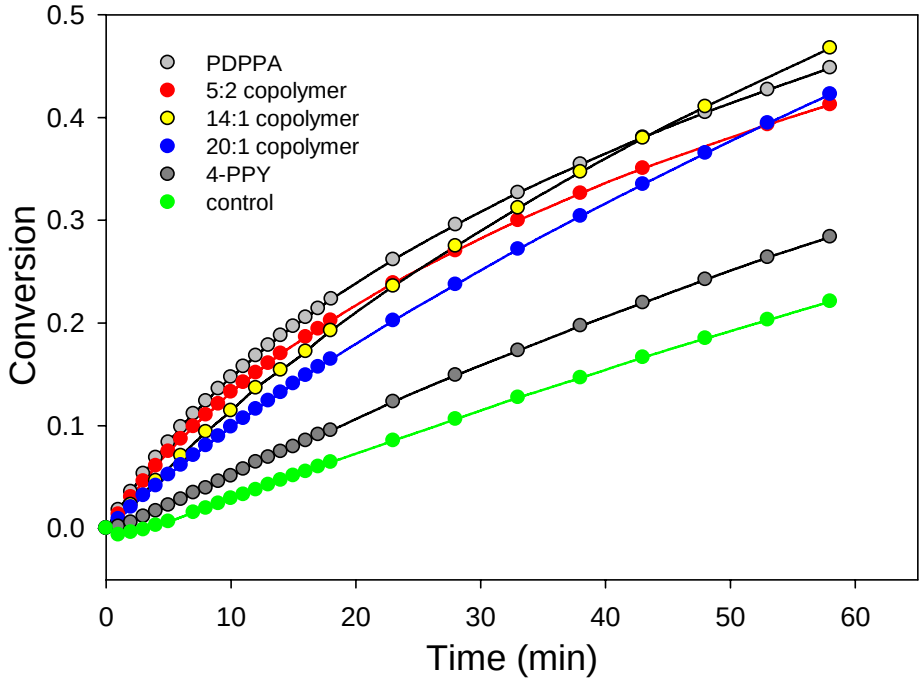

Figure 32. Hydrolysis of 4-nitrophenyl octanoate in pH 9 tris buffer at 20 °C by different 4-*N*,*N*-(dialkylamino)pyridine catalysts.

Both Figures 31 and 32 shows that the PNIPAM supported 4-PPY catalysts **13** have an enhanced catalytic activity compared to the low molecular weight catalyst 4-PPY even with low catalyst loading (20:1). These PNIPAM supported 4-PPY catalysts are also recyclable as shown by using 14:1 PNIPAM-*c*-PDAAP copolymer in the acylation reaction of 2,6-di-*tert*-butylphenol shown (eq 7).

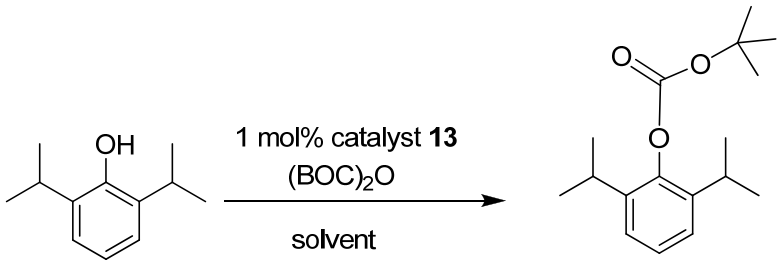

(7)

In this recycling experiment, PNIPAM's solubility properties were used to recover the PNIPAM supported catalyst **13**. PNIPAM has good solubility in most of organic solvents but is insoluble in nonpolar solvents like hexane and ethyl ether. In our previous studies, we had used solvent precipitation to fractionate PNIPAM samples for studies of solute effects on LCSTs. Such techniques also serve to separate and isolate a PNIPAM-supported DMAP catalyst. After we carried out the reaction showed in eq 7 with CH_2Cl_2 as solvent, simple pouring the reaction mixture into hexane served to precipitate the PNIPAM-supported catalyst **13**. This catalyst could be isolated by filtration and then redissolved in CH_2Cl_2 and used again as catalyst. We recycled the 14:1 PNIPAM-*c*-PDAAP catalyst five times by this solvent precipitation method with no loss in activity. GC analyses at 1 h reaction time showed that the product yields of 2,6-diisopropylphenyl carbonate in each cycle were greater than 95%.

Liquid/liquid thermomorphic separation can also be used to recycle the catalyst **13**. A liquid/liquid thermomorphic separation uses two solvents that are immiscible at room temperature but are miscible at elevated temperature. Examples of the thermomorphic solvent systems include N,N-dimethylformamide (DMF)/heptanes and DMSO/cyclohexane. Previous studies carried out by our group had demonstrated that a

dye-labeled PNIPAM-supported catalyst like **10** dissolved selectively in polar DMF-rich phase when it was placed in a liquid/liquid biphasic mixture of DMF and heptane at 25 °C. However, **10** was soluble in the homogeneous solvent mixture of DMF/heptanes that formed on heating this solvent mixture to 70 °C. **10** was successfully used to catalyze the reaction showed in eq. 7 at 70 °C in DMF/heptanes. On cooling of this thermomorphic mixture back to 25 °C, catalyst **10** stayed in the DMF-rich phase while the relatively nonpolar 2,6-diisopropylphenyl carbonate product was enriched in the heptane-rich phase. After a simple separation of the heptanes-rich phase, addition of fresh heptanes and substrates with a second heating and cooling cycle allowed for a simple recycling strategy. The same heating and cooling cycle also worked with the PNIPAM-supported PNIPAM-*c*-PDAAP catalyst **12** (14:1 NIPAM: DAAP). Using **12** on the same acylation reaction showed in eq. 7 in DMF/heptane was successful over four cycles affording 2,6-diisopropylphenyl carbonate product after 40 min in > 95% yield. Physical loss of the catalyst during the separation process was the only recycling problem seen in small scale reaction.

Poly(*N*-isopropylacrylamide)-*c*-poly(2,2,6,6-tetramethylpiperidineoxylacrylamide) (PNIPAM-*c*-PTEMPOAM) – a Temperature and Redox Responsive Polymer

Our earlier studies showed that subtle changes in polymer microstructure can significantly affect PNIPAM solubility. The studies described in this section show that structural it is also possible to design polymers whose solubility can be controlled by reversible oxidation/reduction chemistry. This was accomplished by incorporating nitroxyl groups as redox-sensitive copolymers into a PNIPAM polymer. A nitroxyl

group like 2,2,6,6-tetramethylpiperidinoxyl (TEMPO) can readily be reversibly oxidized to a oxoammonium salt or reduced to a hydroxyl amine under mild conditions (Scheme 13). The reversible oxidation process where a oxoammonium salt is reversibly reduced to a hydroxyl amine is the basis of the chemistry of TEMPO oxidation organocatalysts often used in organic synthesis.[186] This chemistry (shown for TEMPO in Scheme 13) has also been used by Nishide in the design of polymers that are useful as new battery materials.[187] Polymeric versions of the TEMPO species like those shown in Scheme 13 can be used both as recyclable redox catalysts and as materials for rechargeable batteries. This suggests that nitroxyl-containing copolymers are promising targets for the synthesis of copolymers with reversible oxidation/reduction solubility.

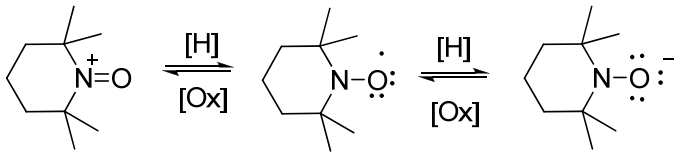

Scheme 13. Redox behavior of TEMPO.

Since the paramagnetic nitroxyl-containing monomers would affect a radical polymerization, we opted to prepare the radical-containing PNIPAM-*c*-PTEMPOAM copolymers (**15)** by using chemistry illustrated in Scheme 11 c. We have used this synthetic approach earlier to prepare libraries of poly(*N*-alkylacrylamide)s to probe the effects of *N*-alkyl group size on poly(*N*-alkylacrylamide) phase selective solubility.[188] This chemistry (Scheme 14) involved the initial synthesis of poly(*N*-acryloxysuccinimide) (PNASI) through AIBN initiated radical polymerization. This PNASI (**14)** was then allowed to react with a mixture of isopropylamine and 4-amino-

TEMPO to form nitroxyl-containing copolymer **15**. While the resulting paramagnetic copolymer **15** could not be analyzed by ^{1}H NMR spectroscopy, a second reaction with the same sample of PNASI could be used to form polymer **16** using the same ratio of isopropyl-amine and 4-amino-2,2,6,6-tetramethylpiperidine. We had earlier shown that the electrophilic active esters in polymers like **14** preferentially react with less hindered amines,[6] so both the 4-amino-TEMPO and 4-amino-2,2,6,6-tetramethylpiperidine were expected to react via their primary amine group to form amides. While the product copolymer **15** of interest in our studies of redox-sensitive LCST behavior cannot be readily analyzed by ^{1}H NMR because it is paramagnetic, the product copolymer **16** was amenable to ^{1}H NMR analysis which showed the ratio of isopropyl/piperidyl groups was 90:10. Copolymer **15** should have a nearly identical 90:10 ratio of isopropyl/TEMPO groups.

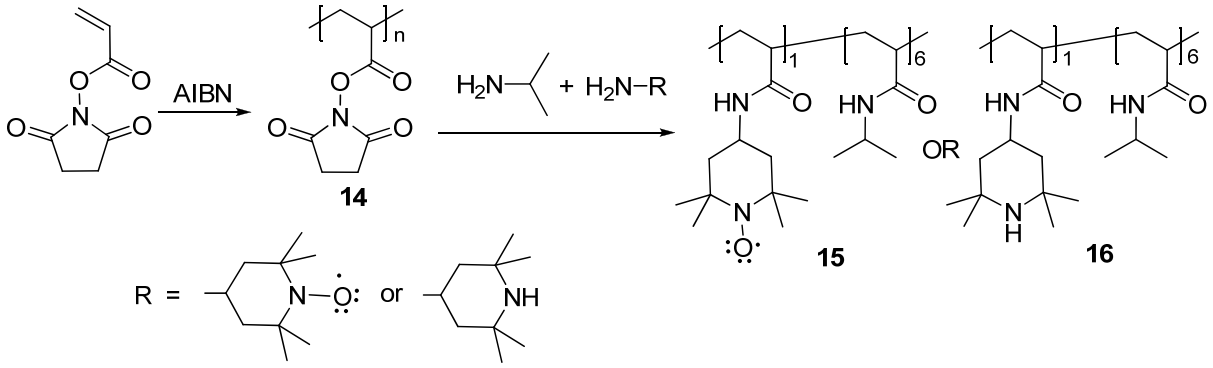

Scheme 14. Synthesis of redox-active PNIPAM copolymers.

GPC analysis of the copolymers **15** and **16** showed that they had a M_n of 179 kDa with a PDI of 1.76. The polymer **15** was also analyzed by cyclic voltammetry and had redox behavior identical to that reported for a low molecular weight TMPO (0.63 V vs.

Ag/AgCl) with potential of 0.66 V *vs.* Ag/AgCl (Figure 33a).[189-191] Polymer **11** was also characterized by ESR spectroscopy and exhibited the characteristic 3-line spectrum of a nitroxyl group (Figure 33b).[192]

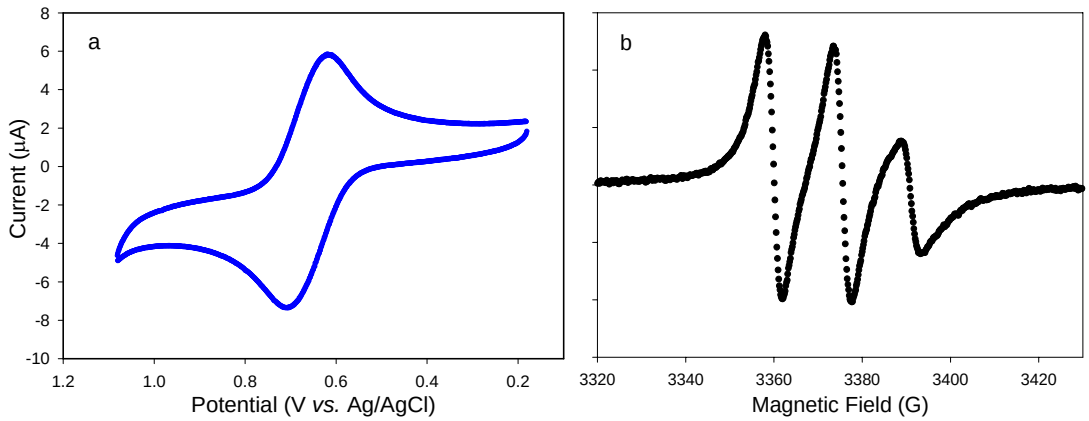

Figure 33. Instrumentation characterization of copolymer **15**: (a) Cyclic voltammogram of **15** in aqueous solution measured with a glassy carbon electrode and a Pt wire electrode at 0 °C. The sweep rate is 10 mV/s and the supporting electrolyte was 0.1 M KCl; (b) Electron spin resonance spectrum of polymer **15** in THF at room temperature.

The LCSTs of the copolymers **15** and **16** were then analyzed using a digital melting point apparatus described in Chapter II. A 10 mg/mL aqueous solution of **15** had a LCST of 23.1 °C at 10% clouding while solution of **16** with the same concentration did not show cloudiness even at boiling temperature. When a kosmotropic salt, in this case, Na_2SO_4 was added to solution of **16**, cloudiness was observed and the clouding temperatures decreased as Na_2SO_4 concentrations increased. On the other hand, when 10 μL 0.8 M ascorbic acid was added to 1 mL 10 mg/mL solution of radical copolymer **15,** only very faint cloudiness was observed. The change of the clouding behavior of **15** suggests that the nitroxyl groups in copolymer **15** have been reduced to

more hydrophilic hydroxylamine groups. In order to observe the effect of reducing agent to the LCST of copolymer **15**, 0.1 M Na_2SO_4 was added to the solution of **15** to enhance the cloudiness, which lowered the LCST of **15** from 23.1 to 18.3 °C. Subsequent analyses of clouding behavior of **15** with the addition of ascorbic acid and then $K_3[Fe(CN)_6]$ were all carried out in the presence of this small amount of Na_2SO_4. Separate LCST analyses using a PNIPAM sample (M_n =322 kDa, PDI=1.06 by GPC) showed that addition of this low concentration of Na_2SO_4 perturbed the clouding curve of PNIPAM by 4.3 °C but did not alter the effect of ascorbic acid or $K_3[Fe(CN)_6]$ to the LCSTs of PNIPAM. The control experiments will be discussed in detail later.

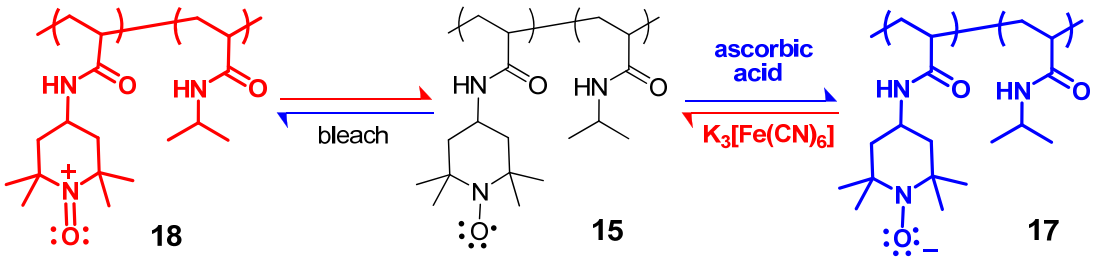

Reduction of the nitroxyl-containing polymer **15** with ascorbic acid forms the hydroxylamine-containing polymer **17** and oxidation of it will form the oxidation product **18**. As expected, this redox chemistry affects the LCST of solutions that initially contained 10 mg/mL of **15**. This is illustrated in Figure 34 that shows a 14 °C change in the solution's LCST behavior as increasing amounts of ascorbic acid are added to **15** to form polymer **17**. Reoxidation of the hydroxylamine-containing polymer **17** by $K_3[Fe(CN)_6]$ largely reverses the changes of the LCST seen on reduction (Figure 35).

Addition of 48 mM of $K_3[Fe(CN)_6]$ to solution presumably containing **17** made a 10 °C decrease of the solution's LCST.

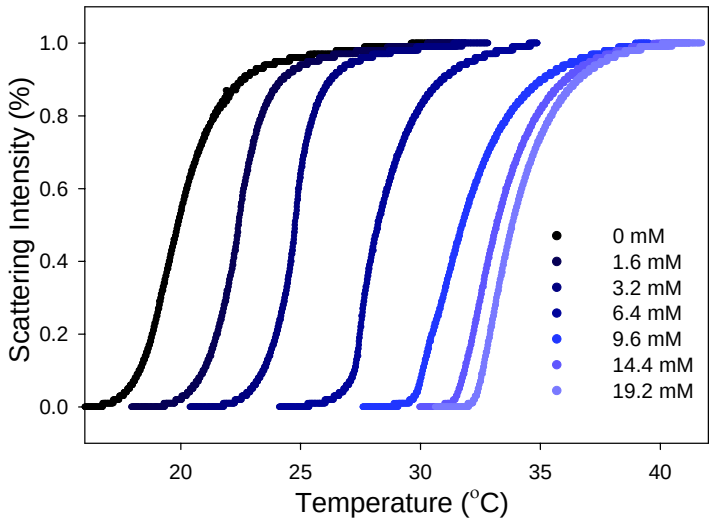

Figure 34. Clouding curves for a 10 mg/mL sample of polymer **15** with 0.1 M Na_2SO_4 in solutions that contain increasing amounts of ascorbic acid. The ascorbic acid concentrations vary from left to right with concentrations of 0, 1.6, 3.2, 6.4, 9.6, 14.4, and 19.2 mM. Na_2SO_4 is used to enhance the samples' cloudiness.

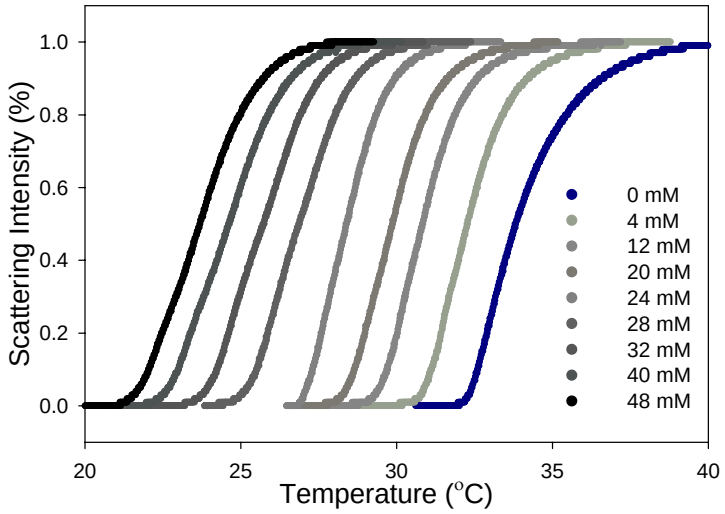

Figure 35. Clouding curves for a 10 mg/mL sample of polymer **15** with 19.6 mM ascorbic acid and 0.1 M Na_2SO_4 in solutions that contain increasing amounts of $K_3[Fe(CN)_6]$. The $K_3[Fe(CN)_6]$ concentrations vary from right to left with concentrations of 0, 4, 12, 20, 24, 28, 32, 40, and 48 mM.

Separate experiments on PNIPAM sample (Figure 36) showed that addition of ascorbic acid and/or $K_3[Fe(CN)_6]$ do not produce such large LCST changes seen for copolymer **15.** Addition of 20 mM ascorbic acid to a 10 mg/mL PNIPAM solution did not change its LCST with or without the addition of 0.1 M Na_2SO_4 while the addition of 48 mM $K_3[Fe(CN)_6]$ to a second 10 mg/mL PNIPAM solution decreased its LCST < 2°C either with or without the addition of 0.1 M Na_2SO_4. Addition of 20 mM ascorbic acid followed by 48 mM $K_3[Fe(CN)_6]$ to a third 10mg/mL PNIPAM solution lowered its LCST about 2.5 °C regardless the PNIPAM solution containing Na_2SO_4 or not.

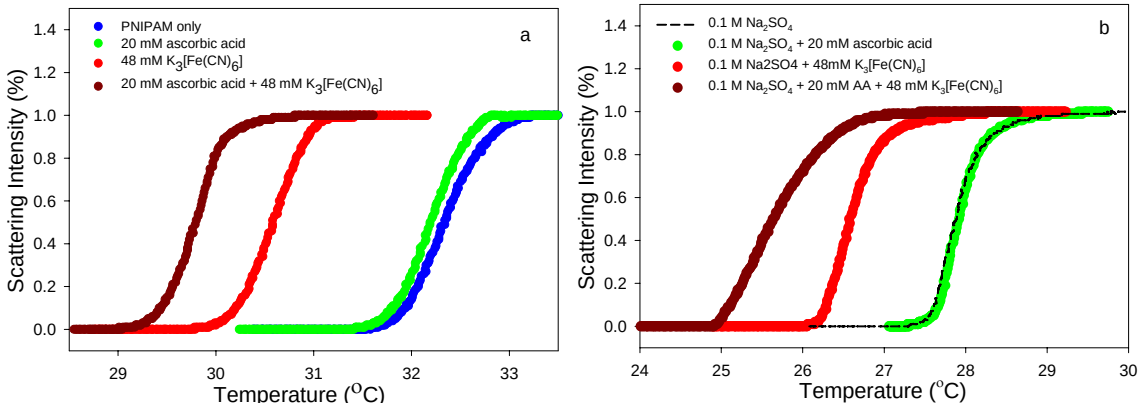

Figure 36. Clouding curves of a 10 mg/mL PNIPAM in the control experiments with ascorbic acid and $K_3[Fe(CN)_6]$: (a) control experiments without addition of 0.1 M Na_2SO_4, (b)control experiments with addition of 0.1 M Na_2SO_4.

Oxidation of **15** to form oxoammonium-containing polymer **18** can be accomplished with household bleach. This oxidation process converts the nitroxyl groups of **15** to oxoammonium groups and also produces a change in LCST as shown in Figure 37. In these studies with bleach, distinct clouding curves were observed without the addition of Na_2SO_4. Increasing amounts of bleach gradually shifted the clouding

curves to higher temperatures. With the addition of 30 µL household bleach straight out of bottle, the clouding temperature at 10 % clouding intensity increased from 23.1 to 39.3 °C. However, reversal of this oxidation process was not successful, perhaps because the NaOCl solution irreversibly modifies the secondary amides present in polymer **15**. Or perhaps reduction of **18** back to **15** will not just stop at **15** but go further to form **17** as well. Separate bleach experiments with PNIPAM solution showed that addition of bleach actually decreased the LCST of PNIPAM solution (Figure 38).

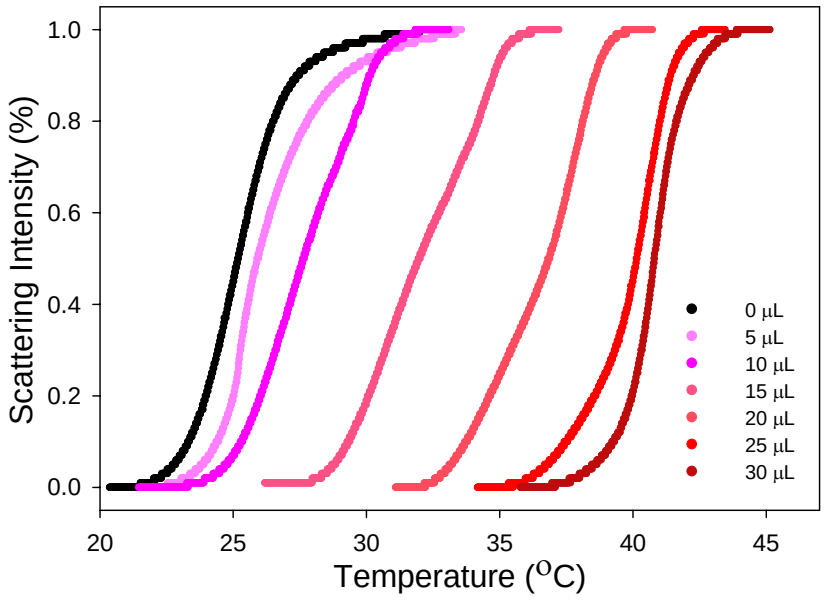

Figure 37. Clouding curves for a 10 mg/mL sample of polymer 15 in solutions that contain increasing amounts of bleach. The amount of bleach varies from left to right with volume of 0, 5, 10, 15, 20, 25, and 30 µL.

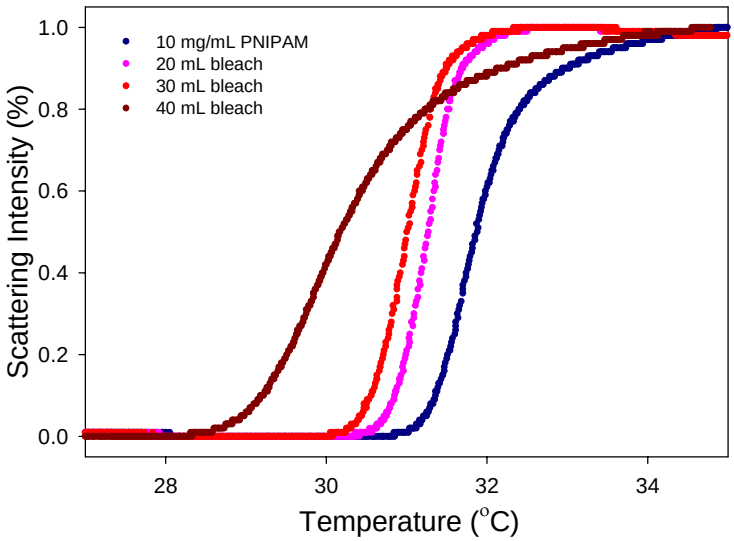

Figure 38. Clouding curves of 10 mg/mL PNIPAM in the control experiments with varied amounts of bleach.

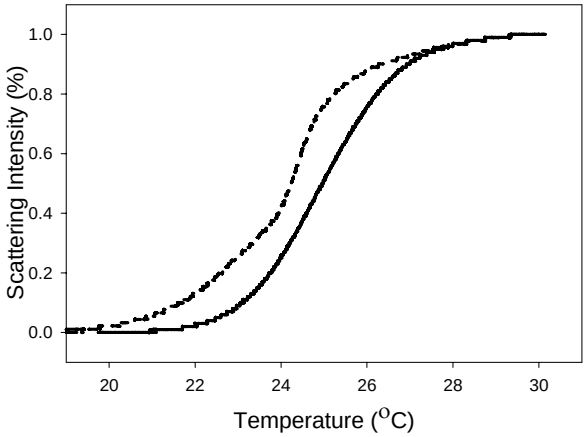

Figure 39. Clouding curves of copolymer **15** with different *i*-PrNH$_2$/TEMPO ratios: solid line, a 90/10 *i*-PrNH$_2$/TEMPO ratio; dashed line, an 85/15 *i*-PrNH$_2$/TEMPO ratio.

The LCST behavior of this nitroxyl-containing PNIPAM copolymer is also dependent on the amount of TEMPO presented. The more TEMPO units present in the copolymer, the lower the LCST is. Figure 39 shows the clouding curves of an 85:15 and a 90:10 *i*-PrNH$_2$/TEMPO copolymers measured with a melting point apparatus. The

shifting of the clouding curves to a lower temperature with a slight increase of the TEMPO amount in the copolymer suggests that the LCST of this nitroxyl-containing PNIPAM copolymer do depend on the polymer composition and the melting point apparatus used in this research is sensitive to detect these differences.

Poly(*N*-isopropylacrylamide)-*c*-poly((*N*-benzo-15-crown-5)acrylamide) (PNIPAM-*c*-PB15C5AM) – an Cation Selective Copolymer for Synthesis of Responsive Surfaces

PNIPAM alone exhibits excellent stimuli-responsiveness to the changes of temperature, cosolutes and solvent compositions. Addition of other kinds of functional groups onto PNIPAM chain as in the copolymer **15** shown above can broaden this chemistry. We also thought it would be of interest to explore molecular recognition based responsiveness. In this section, a crown ether-containing PNIPAM copolymer, poly(*N*-isopropylacrylamide)-*c*-poly((*N*-benzo-15-crown-5)acrylamide) (PNIPAM-*c*-PB15C5AM) **19** was used to prepare nanocomposite graft surfaces using the covalent layer-by-later assembly method describe in earlier chapters. Since crown ethers have been shown that they differentially form complexes with different alkali cations because of the binding constant differences,[193-195] we expected that the nanocomposite surfaces prepared using 15-crown-5 ether-containing PNIPAM might also show some sort of ion-specific responsiveness.

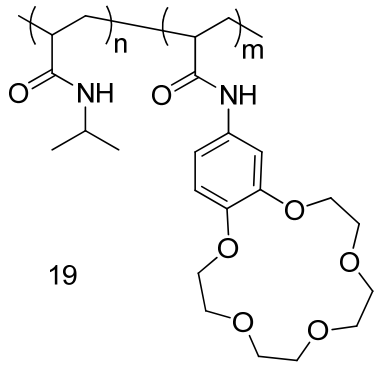

19

The covalent layer-by-layer assembly procedure used in this section to prepare PNIPAM-*c*-PB15C5AM/SiO_2 nanocomposite surfaces is illustrated in Scheme 15. Scheme 15 is different from Scheme 10 in Chapter III in that instead of using *i*-$PrNH_2$ after each PNIPAM-*c*-PNASI/SiO_2 bilayer treatment to convert unreacted NASI to NIPAM, 4-amino-benzo-15-crown-5 was used to form the *N*-benzo-15-crown-5-acrylamide (B15C5AM). Silicon wafers were also used as substrates in this section for surface grafting. The same functionalization procedure for silicon wafer was followed as described in Chapter V. Also, the same 9:1 NIPAM/NASI PNIPAM-*c*-PNASI (M_w = 30 kDa) copolymer and aminated silica nanoparticles (10- and 100-nm diameter) used earlier for nanocomposite surface grafting were also used in this covalent assembly as electrophiles and nucleophiles respectively. The nanocomposite graft that we prepared for this study is denoted as SW/[PNIPAM-*c*-PB15C5AM/SiO_2]$_6$/PNIPAM-*c*-PB15C5AM. This nomenclature indicates that six polymer/SiO_2 bilayers are grafted and that the functional polymer in this graft is PNIPAM-*c*-PB15C5AM copolymer.

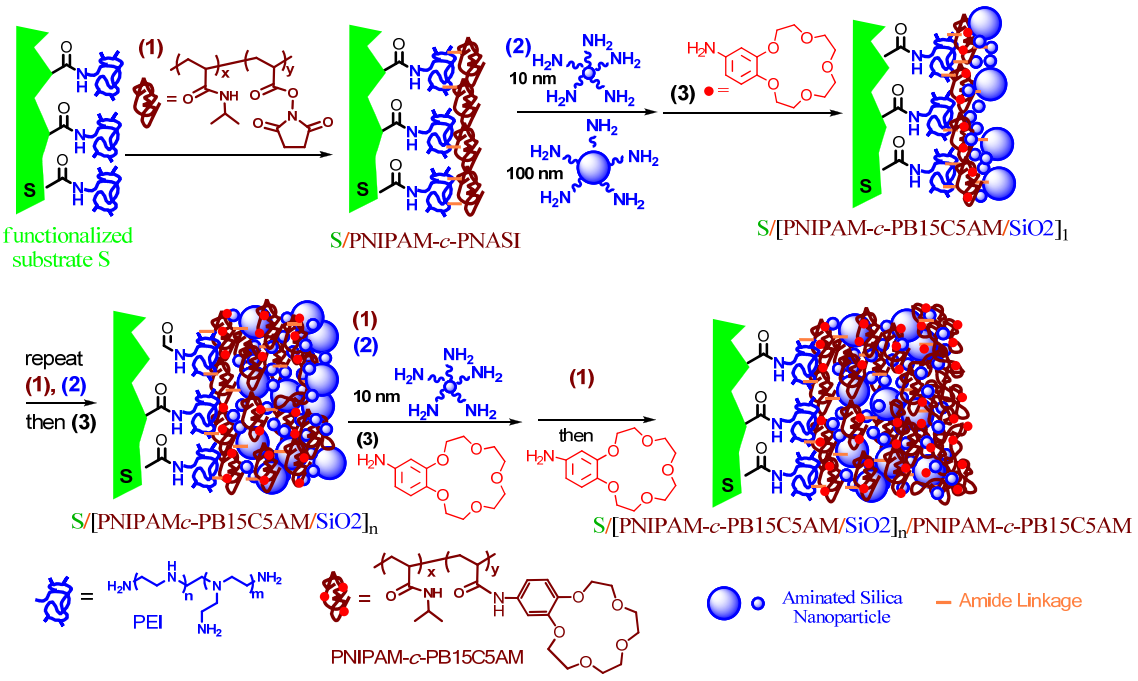

Scheme 15. Covalent layer-by-layer assembly of a SW/(PNIPAM-*c*-PB15C5AM/SiO_2)n/PNIPAM-*c*-PB15C5AM nanocomposite graft. The final structure is not drawn to scale.

I expected that the PNIPAM-*c*-PB15C5AM copolymer that have pendent crown ether groups that would serve as sensors binding differently to different cations and that the NIPAM groups will serve as actuators to provide visible macroscopic changes.[196] Prior work by Niu and coworkers had earlier shown that PNIPAM-*c*-PB15C5AM copolymer had cation-responsiveness in aqueous solution.[193] They found out that this copolymer's LCST decreased with the addition of alkali metal nitrate salts and the effects of the cations was correlated to strength of the metal/crown ether binding. The order of significance of the effect of alkali metal ions to decrease the PNIPAM-*c*-PB15C5AM LCST was $K^+ >> Cs^+ > Na^+ > Li^+$. The greater the binding is, the more significant the cation is in lowering the LCST. Other groups had also used crown ether-

containing PNIPAM copolymer to fabricate a molecular recognition ion gating membrane.[197,198] For example, poly(*N*-isopropylacrylamide)-*c*-poly(benzo-18-crown-6-acrylamide) functionalized porous polyethylene films responded selectively to K^+ or Ba^{2+}. To study how a PNIPAM-*c*-PB15C5AM/SiO_2 nanocomposite surface would respond to different alkali metal ions, we measured the advancing contact angles (Θ_α) of this surface with series solutions of alkali metal chloride salts. As discussed in previous chapters, the roughness enhanced PNIPAM/SiO_2 nanocomposite grafts prepared by our covalent layer-by-layer assembly method can change from hydrophilic to very hydrophobic by varying salt solution concentrations or salt identity. Since changes in crown ether/alkali metal cation binding can change the PNIPAM-*c*-PB15C5AM copolymer's LCST, I expected that the SW/[PNIPAM-*c*-PB15C5AM/SiO_2]$_6$/PNIPAM-*c*-PB15C5AM nanocomposite surface would also show different wetting behavior in response to the treatment of different alkali metal salt solutions. The results of alkali metal chlorides on the wettability of SW/[PNIPAM-*c*-PB15C5AM/SiO_2]$_6$/PNIPAM-*c*-PB15C5AM nanocomposite surface are shown in Figure 40. The advancing contact angles were measured three times for each concentration of the alkali chlorides on random spots of the same SW/[PNIPAM-*c*-PB15C5AM/SiO_2]$_6$/PNIPAM-*c*-PB15C5AM nanocomposite surface. The as prepared crown ether-containing nanocomposite surface had a advancing contact angles (Θ_a) of 68° with water which was about 8° smaller than the Θ_a of water (~ 76°) in a PNIPAM nanocomposite surface. This $\Delta\Theta_a$ indicate that incorporating the 15-crown-5 ether onto the PNIPAM graft make the PNIPAM/SiO_2 nanocomposite surface more hydrophilic. Figure 40 shows that all four alkali chloride

salts increased the advancing contact angles when increasing salt concentrations on this PNIPAM-*c*-PB15C5AM functionalized nanocomposite surface. However, no difference was seen between Na^+ and K^+ in their ability to change the wettability of a PNIPAM-*c*-PB15C5AM functionalized nanocomposite surface. But Li^+ and Cs^+ had noticeable smaller effects on changing the surface wettability than Na^+ and K^+.

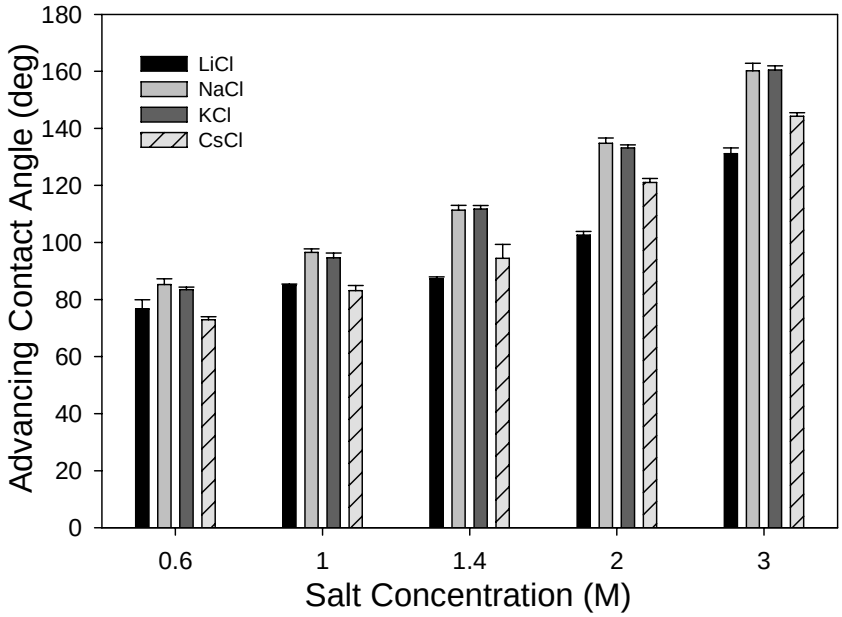

Figure 40. Advancing contact angles of SW/[PNIPAM-*c*-PB15C5AM/SiO_2]$_6$/PNIPAM-*c*-PB15C5AM nanocomposite surface measured with different alkali metal chlorides at varied concentrations.

Control experiments using a PNIPAM functionalized nanocomposite graft – SW/[PNIPAM/SiO_2]$_6$/PNIPAM – were also carried out with the same alkali metal chlorides. The results (Figure 41) show that Na^+, K^+ and Cs^+ halid solutions are similar in their ability to change the wettability of the SW/[PNIPAM/SiO_2]$_6$/PNIPAM nanocomposite surface. Only Li^+ has a significantly different cation effect which is smaller than the effects of Na^+, K^+ and Cs^+ on the wettability of

SW/[PNIPAM/SiO_2]$_6$/PNIPAM nanocomposite surface. The cation effects of the alkali metal ions on wettability of this SW/[PNIPAM/SiO_2]$_6$/PNIPAM nanocomposite surface are like the alkali cation effects on the LCST of PNIPAM solution reported by Freitag *et al*. They investigated the effects of five alkali metal hydroxides and five alkali metal chlorides on the cloud point temperature of PNIPAM oligomers. These authors noted that variation of alkali cations, with the exception of Li^+, had little difference in depressing PNIPAM's LCST.

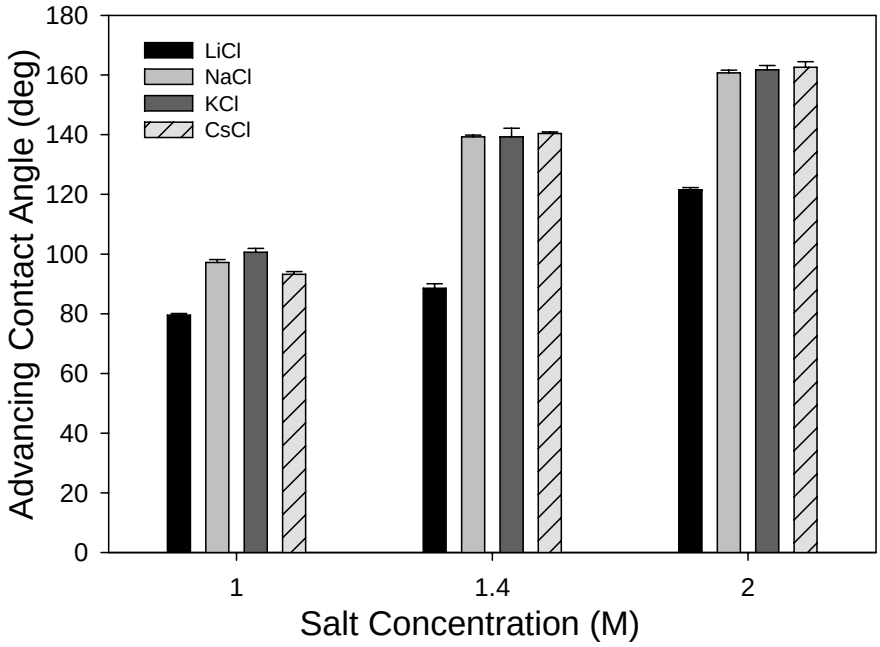

Figure 41. Advancing contact angles of SW/[PNIPAM/SiO_2]$_6$/PNIPAM nanocomposite surface measured with different alkali metal chlorides at varied concentrations.

However, CsCl shows measurable smaller cation effect on the wettability of the SW/[PNIPAM-*c*-PB15C5AM/SiO_2]$_6$/PNIPAM-*c*-PB15C5AM nanocomposite surface than NaCl and KCl do in Figure 40. The difference seen for CsCl on the wettability of the SW/[PNIPAM-*c*-PB15C5AM/SiO_2]$_6$/PNIPAM-*c*-PB15C5AM nanocomposite

surface (Figure 40) and the SW/[PNIPAM/SiO_2]$_6$/PNIPAM nanocomposite surface (Figure 41) might be due to the smaller binding of 15-crown-5 ether to Cs^+. This speculation was drawn based on the observation that in solution the formation of 15-crown-5 ether/metal ions complexes shifted the PNIPAM-*c*-PB15C5AM's LCST to lower temperature as mentioned earlier.[193] This is only preliminary result for using 15-crown-5 ether-containing PNIPAM to construct a cation-selective responsive surface. The numbers of incorporated 15-crown-5 ethers to the PNIPAM chains are difficult to quantify by using the assembly procedure shown in Scheme 14. An alternative assembly procedure can use polymer **20** shown below as the electrophile for the covalent layer-by-layer assembly procedure. Since polymer **20** can be characterized before using it for the grafting, we can make the SW/[PNIPAM-*c*-PB15C5AM/SiO_2]$_6$/PNIPAM-*c*-PB15C5AM nanocomposite surface with a controllable amount of 15-crown-5 ethers on the grafted surface. More researches need be carried out in the future.

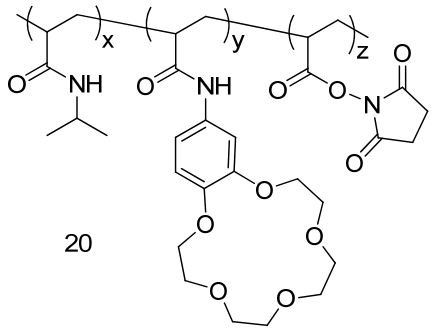

20

Conclusion

In this chapter, I have shown examples of PNIPAM copolymers with different functional groups and shown how incorporating functional groups into PNIPAM can be

used to advantage. By attaching an appropriate functional group to the PNIPAM chain, different applications based on PNIPAM's property can be realized. Specially, the poly(*N*-isopropylacrylamide)-*c*-poly(4-(*N*,*N*-diallylamino)pyridine) copolymer were shown to be useful as recyclable organocatalysts. I also showed that these catalysts are recyclable by solvent precipitation or by using a thermomorphic solvent system. The poly(*N*-isopropylacrylamide)-*c*-poly(2,2,6,6-tetramethylpiperidineoxylacrylamide) is a radical-containing redox sensitive copolymer. Its LCST can be tune higher or lower depending on its redox state. Finally, poly(*N*-isopropylacrylamide)-*c*-poly((*N*-benzo-15-crown-5)acrylamide) was used in an attempt to prepare cation-selective responsive nanocomposite surface. The advancing contact angle measurement showed that the Cs^+ had some sort of cation-selective responsiveness on the wettability of PNIPAM-*c*-PB15C5AM grafted nanocomposite surface but more studies are need to get a true conclusion.

CHAPTER VII

SUMMARY AND EXPERIMENTAL SECTION

Summary

In this dissertation, I described the development of a clouding point assay by using a simple digital melting point apparatus for analysis of phase separations that generate clouding curves. I had shown that in cases where the clouding simply shifts as a function of the heating rate of the analysis, it is possible to use the data from these analyses to generate 'corrected' clouding point curves that approximate the phase separation at an infinitely slow heating rate. The temperature range of the apparatus also allows for analyses at much higher temperatures and provides a simple way to examine irregular clouding behavior in more complex systems. This clouding point assay was further used in the studies of LCSTs of thermoresponsive polymers. The effects of various sodium anion salts on the LCST of the triblock copolymer Pluronic® 10R5 followed the Hofmeister series, which is in accordance with our previous results showing that the anion salt effects on PNIPAM solution is essential a Hofmeister effect. The less studied cation effects on the LCST of thermoresponsive polymers were also carried out by addition of sulfate cation salts to PNIPAM solutions. The results showed that cations also have distinct and comparable effects on the LCST of PNIPAM. When the salt activity was under consideration, the cation effects were determined by the cation charge density and the ability of cation in lowing the LCST followed the order of trivalent > divalent > monovalent.

A radical-containing PNIPAM copolymer, PNIPAM-*c*-PTEMPOAM was synthesized and the effects of redox state on the LCST of this copolymer were studied. The shifting of the clouding curves with the addition of oxidizing or reducing reagents was analyzed by using the automatic melting point apparatus. The results showed that incorporation of redox-active TEMPO moiety in the PNIPAM chain leaded to a material that had reversible redox-sensitive LCST behavior. The observed LCSTs of the TEMPO-containing PNIPAM copolymers at different oxidation states varied from 18 to 40 °C. This large temperature variation could be useful in design of redox-sensitive materials for drug delivery application *in vivo* and in synthesis of surfaces with redox-mediated wettability.

PNIPAM had also been grafted on surface by using covalent layer-by-layer assembly method. The nanocomposite surface prepared with PNIPAM and silica nanoparticles combined both the surface roughness and responsiveness. As mentioned before, PNIPAM's solubility can be affected by the addition of salts and the salt effects on its solubility followed the Hofmeister effect. The wettability of a PNIPAM grafted surface is expected to be affected by applying different salts on this surface. Our results discussed in Chapter III and IV showed that the wettability of the PNIPAM/SiO_2 nanocomposite surfaces responded to the salt identity and salt concentration. In general, the higher the concentration of the solution of a chosen salt applied to the nanocomposite surface, the more hydrophobic the surface became. The effectiveness of the salts in changing the surface wettability is depended on the identity of the salts. For anion salts with sodium as common cation, the anion effects followed the Hofmeister series. For

cation salts with sulfate as common anion in our studies, the results showed that effects of varying the cation were comparable with the anion effects. When the salt solution activity was under consideration, the cation effects were determined by the cation's charge number and the order of the effect of cations in increasing the surface wettability followed trivalent > divalent > monovalent. The parallel studies of the cation effects on the solubility of PNIPAM solutions were also carried out. The LCSTs of PNIPAM solution with different cation salts were analyzed by using the automatic digital melting point apparatus as described in Chapter II. The cation effects in PNIPAM solution parallel the cation effects on PNIPAM grafted nanocomposite surfaces.

Experimental Section

Synthesis and fractionation of PNIPAM. A solution of 10 g (89 mmol) of recrystalized *N*-isopropylacrylamide and 50 mg (0.3 mmol) of 2,2'-azobisisobutyronitrile (AIBN) in 200 mL of *tert*-butylalcohol was degassed three times and heated to70 °C under positive pressure of N_2. After 18 h the *tert*-butylalcohol was removed under reduced pressure and the crude polymer product was dried under vacuum. The crude product was reprecipitated from 100 mL THF into 1 L of hexanes to remove any unreacted monomers or oligomers and the yield of the pure polymer was > 95%. ^{1}H NMR ($CDCl_3$) δ 1.18 (bs, 6H), 1.40-2.25 (bm, 3H), 4.00 (bs, 1H).

The product polymer was fractionated into several samples with different molecular weights by selective solvent precipitation as described previously.[30] One of the fractions was used in the studies described in Chapter II and was characterized by GPC and laser light scattering. It had a M_w of 322 kDa by GPC analysis and a M_w of

395 kDa by laser light scattering analysis. The PDI of this fractionated PNIPAM sample was 1.06 calculated from GPC analysis.

Molecular weight measurement of PNIPAM by laser light scattering. Laser light scattering experiments were performed with a Brookhaven Instruments BI-200SM goniometer equipped with a Melles Griot HeNe laser. The samples were dissolved in HPLC grade THF one day before the light scattering measurements. Generally, five THF solutions with different concentrations were prepared for each polymer sample. Each sample solution was filtered by a 0.2 μm PTFE filter before adding it to the sample cell for the analysis. Data of laser light scattering intensity was collected at a series of scattering angles ranged from 30 to 150 deg with a 15 deg increment. The M_w was calculated from the Zimm plots using the instrument's software.

Gel permeation chromatography (GPC) analysis of polymer molecular weight. GPC analyses for all the polymers I made in this dissertation were carried out on a Viscotek GPC instrument with a Viscotek I-MBMMW-3078 mixed bed column in THF. In a typical analysis, 15.0 mg of the polymer was dissolved in 5.0 mL of degassed THF 24 h before the analysis. 100 μL of this sample solution was then injected into the sample loop after filtering through a PTFE filter (0.45 μm in pore size). Triple detectors included a viscometer, a refractometer and a low angle laser light scattering were used together to obtain data which was then used by the OmniSEC software to calculate the polymer molecular weight. The GPC was calibrated with a polystyrene standard periodically.

Melting point apparatus and LCST measurements. An OptiMelt automatic melting point apparatus from Stanford Research Systems was used for all the LCST analyses in this dissertation.[17] This apparatus uses a digital image processor to detect the light scattering that occurs as a sample changes from a scattering solid to a liquid. Since an aqueous solution of PNIPAM during an LCST process exhibits analogous changes in its optical characteristics, this same melting point apparatus can determine an LCST and produce a clouding curve. Other features of this apparatus include linear temperature ramping and accurate temperature readings with 0.1 °C resolution. In a typical experiment, 8 uL of a polymer solution was introduced to a regular capillary melting point tube (Kimble 1.5-1.8 x 90-mm) using a microsyringe and the tube was sealed before placing it into the sample holder. Three sealed sample tubes were placed into the sample holders for simultaneous measurements of their clouding curves at the desired heating rate. During the heating process, the thermoresponsive polymers underwent phase transitions that changed the optical characteristics of the samples. The digital image processing on board the melting point apparatus analyzed the intensity changes and produced a graph of the percent light scattering versus temperature. The resulting usually sigmoidal curve of the extent of clouding and the data for specific scattering percentages was then used in our LCST studies. The supplied MeltView software transferred and stored the real-time images of the samples to a computer during the analysis. The software bundles all sample images together as a single package file and the file can be recalled at anytime to play back the phase transition process, frame-by-frame or as continuous movies. Such movies can provide a visual record of the phase

changes and allow qualitative differentiation of the phase separation process in milieu as similar as H_2O, 50/50 (v/v) H_2O/D_2O, and in pure D_2O. The reproducibility of phase transition behavior was monitored either by removing the tube from the apparatus and letting the polymer redissolve or by preparing a fresh sample. Repetition of the LCST measurement the same day or after several days using the same heating rate gave curves that were identical to the original curves.

Synthesis of *N*-acryloxysuccinimide monomer. This monomer was prepared from acrolyl chloride and *N*-hydroxysuccinimide following a literature procedure.[1] At 0 °C, acryloyl chloride (7.5 mL) was added dropwise to a stirred solution of *N*-hydroxysuccinimide (10 g) and triethylamine (12 mL) in dichloromethane (125 mL) by an addition funnel under nitrogen. The reaction was carried out at 0 °C for about 20 min and then allowed to reach room temperature and stirred for another hour. The reaction mixture was filtrated and washed with cold water (5 mL) and dichloromethane (10 mL) mixture. The filtrate was then washed with cold water (80 mL x 2) and cold brine (80 mL x 2) in a separatory funnel. The organic layer was dried with magnesium sulfate and the solvent was removed by rotary evaporation until about 20 mL left. The resulting solution was cooled to 0˚C and precipitated by adding 25 mL hexane/ethyl acetate mix (6:1). The solids were filtrated, washed with more hexane and then dried in oven under vacuum overnight. The resulting product yield was > 95%.

Synthesis of poly(*N*-acryloxysuccinimide) (PNASI) via free radical polymerization. A solution of *N*-acryloxysuccinimide (8.0 g, 47 mmol) and 2,2'-azobisisobutyronitrile (40 mg, 0.24 mmol) in 200 mL of benzene was degassed three

times by flushing with nitrogen for 20 min and then putting under vacuum for ~15 sec. Then the solution was heated to 70° and stirred for 24 h under positive N_2 pressure. The resulting mixture was allowed to cool to room temperature. The white precipitate of polymer product formed was collected by filtration, washed with benzene and THF and then dried under vacuum to yield 7.8 g (99 %) of the desired polymer. ^{1}H NMR (*d*-DMSO): δ 2.05 (bs, 2H), 2.80 (bs, 4H), 3.13 (bs, 1H). ATR-IR (powder): 1813, 1782, 1734, 1204, 1068, 648 cm^{-1}.

Synthesis of poly(*N*-isopropylacrylamide)-*c*-poly(*N*-acryloxysuccinimide) from PNASI. A solution of isopropylamine (1.8 mL, 21.5 mmol) in 10 mL of DMF was added to a solution of poly(*N*-acryloxysuccinimide) (4.0 g, 24 meq of NASI) in 80 mL of DMF. The resulting solution was stirred at room temperature for 18 h during which time some precipitate formed. The mixture was filtered to remove the precipitate. Then the 90 mL of the supernatant solution was added dropwise to 2 L of ethyl ether at room temperature to precipitate the copolymer. The precipitate of the desired copolymer was then isolated by filtration and redissolved in 100 mL of THF and again reprecipitated in 2 L of hexanes. This process was repeated 2 times, yielding 2.6 g (92 %) of the copolymer. The mole fraction of NIPAM and NASI groups in the copolymer was analyzed by ^{1}H NMR spectroscopy. Based on the ratio of the integrals for the broad singlet at δ 4.02 ppm (1 H, NIPAM –NH<u>CH</u>–) groups) and the peak at δ 2.61 ppm (4 H, NASI –C(=O)<u>CH_2</u>–), this ratio of NIPAM/NASI was 9:1. The polymer had a M_w of 30 kDa as analyzed by GPC in THF.

Syntheses of aminated silica nanoparticles (10 nm or 100 nm in diameter). These materials were prepared following a literature procedure.[199] In a typical procedure, 5 g of silica nanoparticles (10 nm or 100 nm in diameter) were first cleaned by placing them in 100 mL of 5 % hydrochloric acid at room temperature overnight. The silica nanoparticles were then recovered by filtration, washed with water, and dried under vacuum. The dried silica nanoparticles were then added to a 10 % solution of 3-aminopropyltriethoxysilane in 100 mL toluene. This mixture was heated to reflux overnight. The product aminated silica nanoparticles were isolated by filtration, washed with THF and MeOH then dried under vacuum. Titrimetric analysis of the aminated silica nanoparticles was carried out by first suspending a weighed amount of aminated silica nanoparticles in a 0.01 M HCl solution and shaking the mixture for 1 h. An aliquot of the resulting HCl solution was titrated with a 0.01 M NaOH solution to a pH 9 endpoint. In this way, the amount of HCl consumed by basic groups on the aminated silica nanoparticles could then be determined. These aminated silica nanoparticles had amine loadings of 0.74 mmol (10 nm) and 0.19 mmol (100 nm) of base/g, respectively.

Covalent layer-by-layer self-assembly of PNIPAM-*c*-PNASI with aminated silica nanoparticles on PE films. Following a literature procedure,[170] an oxidized PE film was first activated by treatment with a mixture of ethyl chloroformate and *N*-methylmorpholine in DMF for 15 min. The activated PE film was removed from the solution of excess ethyl chloroformate and then rinsed with DMF. The activated PE film was then placed into a DMF solution of PEI (2.5 wt %) and this mixture was shaken for 30 min at room temperature. The product aminated PE film was removed from the PEI

solution and washed with DMF. This PEI-treated PE film was placed into a DMF solution of PNIPAM-*c*-PNASI (20 wt %) for 30 min, removed from the polymer solution and washed with DMF. The polymer treated PE film was placed in a 20 mL DMF suspension of aminated silica nanoparticles (10 and 100 nm particles, 0.5 wt % each and 0.5 vol % of triethylamine) and shaken for 30 min. The aminated silica treated PE film was again removed from the aminated silica nanoparticles suspension, washed with DMF, and placed into a DMF solution of isopropylamine (10 vol %) and shaken for 30 min. This step was designed to convert any unreacted NASI groups to NIPAM. This isopropylamine-treated PE film was again removed from the isopropylamine solution and then washed with DMF. This isopropylamine treated PE film could then be placed into the PNIPAM-*c*-PNASI solution again for a second run of the assembly process. This cycle of aminated silica nanoparticles treatment followed by PNIPAM-*c*-PNASI treatment was repeated 5 times to obtain the PE/(PNIPAM/SiO_2)$_5$. The resulting polymer treated PE films were treated with one more cycle of PNIPAM-*c*-PNASI and aminated silica nanoparticles (10 nm particles only, 1.0 wt % and 0.5 vol % of triethylamine), followed by isopropylamine treatment to yield the final PE/(PNIPAMP/SiO_2)$_6$/PNIPAM nanocomposite surface.

Contact angle measurements. Static contact angles (Θ) were measured on a KSV CAM 200 optical goniometer with an automatic single liquid dispenser at ambient temperature. A 10 μL aqueous solution droplet size was placed on a random spot on the surface. Photographs were taken until the droplet was no longer spreading (usually within 2-3 min), at which point the contact angles were measured by the CAM 200

software. Dynamic advancing contact angles (Θ_a) were recorded as aqueous solution was continuously added to a 10 μL droplet which was allowed to equilibrate with the surface for 2 minutes before the measurement. The aqueous solution was added at a rate of 1 μL/s and the images were taken at a rate of 400 ms/frame.

Atomic force microscopy studies. All the AFM measurements were done by Mr. Albert Wan or Dr. Xiaotong Hong from Batteas's group. The PNIPAM/SiO_2 nanocomposite surfaces grafted either on PE films or silicon wafers were characterized by atomic force microscopy in tapping mode using a commercial AFM (Alpha300 S, WITec, Germany). Images were collected using ultrasharp silicon AFM tips (VISTA probes, NanoScience Instruments, Phoenix, Arizona) with nominal tip radii of < 10 nm, a lever resonance frequency of ~ 300 kHz and a force constant of ~ 40 N/m. The tip was modified with octadecyltrichlorosilane (OTS) prior to the measurement to minimize the adhesion between the tip and the polymer surface. To coat the tips, they were immersed in a $NH_4OH/H_2O_2/H_2O$ solution (vol. ratio: 1:1:4) for 1 minute, rinsed with water, acetone and dried with N_2 flow. The tips were then immersed in a solution of 1 μm OTS/ 10 ml hexane for 30 seconds, rinsed with hexane, ethanol, water, acetone, and dried with N_2 flow. To follow changes in morphology under varying solute conditions, the samples were scanned in the following order: ambient air, high purity water, various salt solutions, and then again in high purity water. Between each solute condition the samples were rinsed with water, THF, and dried with N_2 flow. In each condition the representative root-mean-square (rms) roughness of the surface was determined from the average of a series of 2.5 μm x 2.5 μm regions at random positions.

Functionalization of silicon wafers (SW). A single-side polished silicon wafer (100) (1 x 1.5 cm) was sonicated for 2 minutes successively in hexane, tetrahydrofuran and ethanol to remove any contaminants. The washed silicon wafer was then blow-dried with nitrogen stream and then treated with 7:3 (vol/vol) concentrated sulfuric acid and 30% H_2O_2 for 1 h (*caution: the piranha solution is highly corrosive and extremely reactive with organic substances*). The cleaned silicon wafer was then rinsed with a copious amount of water and ethanol before being immersed into a 5 mM 3-aminopropyltriethoxysilane (APTES) ethanol solution. The wafer/APTES solution mixture was shaken by a shaker at moderate speed overnight. The APTES treated wafers were then removed from this solution and washed with ethanol and dried in a vacuum oven at 120 °C for 2 h. The resulting amine-functionalized wafer had a hydrophilic surface with an advancing water contact angle of less than 15°. The thickness of the APTES layer was 2 nm as determined by ellipsometry measurement. The ellipsometric data was measured by a Nanofilm EP^3 imaging ellipsometer at 660 nm wavelength with an incidence angle of 75 deg. The film thickness was calculated by fitting the ellipsometric data using the supplied EP^3View software. An AFM image of this ATPES-treated silicon wafer was obtained by Mr. Albert Wan in the Batteas group. This image shows a featureless surface with a measured rms roughness of 0.7 ± 0.3 nm. The smooth surface indicated that a monolayer of APTES was attached to the silicon wafer surface.

Covalent layer-by-layer self-assembly of PNIPAM/SiO_2 nanocomposite on silicon wafers. Prior to the PNIPAM/SiO_2 nanocomposite grafting, the APTES-functionalized silicon wafer was primed by covalently attaching two PNASI/PEI

bilayers to its surface to increase the numbers of surface amine groups. This was accomplished by allowing the APTES-treated silicon wafer to react first with the electrophilic poly(*N*-acryloxysuccinimide) (PNASI) for 30 minutes. The active ester of NASI was readily converted to an amide upon reacting with an amine. This condensation reaction coupled the polyvalent electrophilic polymers to the originally aminated wafer surface and the remaining unreacted NASI groups could react further with subsequently introduced nucleophilic polyethyleneimine (PEI) by the same condensation reaction. The surface was amine-rich after one PNASI/PEI bilayer treatment. While the surface could be used directly for a second PNASI/PEI bilayer treatment, we treated this surface with *i*-$PrNH_2$ to quantitatively convert any unreacted NASI groups into NIPAM groups. A second PNASI/PEI bilayer treatment was carried out after the *i*-$PrNH_2$ treatment and the wafer surface by now presumablely was covered with a sufficient amount of amine groups. The same covalent layer-by-layer assembly process that mentioned earlier to covalently assemble PNIPAM/SiO_2 nanocomposite surfaces on PE films was then carried out on this 'primed' silicon wafer to make the SW/(PNIPAM/SiO_2)$_6$/PNIPAM nanocomposite surfaces. The same 9:1 NIPAM/NASI PNIPAM-*c*-PNASI (M_w = 30 kDa) copolymer and aminated silica nanoparticles (10- and 100-nm diameter) used earlier for nanocomposite surface grafting were also used in this covalent assembly as electrophiles and nucleophiles respectively.

Synthesis of 4-*N*,*N*-diallylaminopyridine (DAAP).[200] 8.0 g 4-aminopyridine (0.083 mol) dissolved in 60 mL dry THF at ambient temperature followed by the addition of 4.45 g (0.185 mol) clean sodium hydride. The mixture was allowed to react

at ambient temperature until all H_2 was evolved and then cooled down to 0 °C. A solution of 13.5 g (0.176 mol) acryloyl chloride and 20 mL dry THF was then added dropwise to the reaction mixture. The reaction mixture was kept stirring at ambient temperature overnight and turned to a red color. The reaction mixture was filtrated and washed with CH_2Cl_2. All the filtrate was combined and concentrated by rotary evaporation to yield the crude product as a red-brown viscous liquid. The crude product was distilled at reduced pressure (0.4 mm Hg) to obtain 9.6 g (65%) yellow color product at 88-93 °C. ^{1}H NMR ($CDCl_3$, 300 MHz): δ 3.87 (d, 4H); 5.23 (q, 4H); 6.06 (m, 2H); 7.90 (m, 2H); 8.18 (m, 2H).

Synthesis of poly(*N*-isopropylacrylamide)-c-poly(4-(*N*,*N*-diallylamino)pyridine) (PNIPAM-*c*-PDAAP). A mixture of 0.32 g (1.8 mmol) of 4-(*N*,*N*-diallylamino)pyridine and 0.83 g (7.4 mmol) of NIPAM was dissolved in 2.5 mL of 15% HCl aqueous solution at 0 °C under positive N_2 pressure. The initiator, 5.0 mg (0.018 mmol) of 2,2'-azo-bis(2-methylpropionamidine) dihydrochloride (V-50) in 5 ml of DI-H_2O was added to the reaction mixture which was degassed three times. The reaction mixture was heated to 60 °C under nitrogen for 48 h until a highly viscous solution was obtained. The crude polymer product precipitated when saturated $NaHCO_3$ was added to the reaction mixture. This polymer precipitate was filtrated, washed with warm DI-H_2O and dried in vacuum oven. The polymer product was further purified by redissolving in 20 mL chloroform and precipitating into 200 mL hexane. The mole fraction of the comonomers was determined by ^{1}H NMR and in this example the NIPAM/DAAP was ~ 14:1. Two other PNIPAM-*c*-PDAAP copolymers with

NIPAM/DAAP mole fraction of 5:2 and 20:1were also prepared followed this procedure with varied NIPAM and DAAP feed ratio. GPC analyses (Viscotek multidetector GPC system) showed that the 5:2, 14:1 and 20:1 PNIPAM-*c*-PDAAP copolymers had a M_w of 43 kDa, 40 kDa and 42 kDa respectively.

Synthesis of poly(4-(*N*,*N*-diallylamino)pyridine) (PDAAP). PDAAP was synthesized followed a literature procedure.[200] DAAP (1.0 g, 5.74 mmol) was dissolved in 2.5 mL of 15% HCl at 0 °C under positive N_2 pressure and degassed three times. The initiator, 15.0 mg (0.018 mmol) of 2,2'-azo-bis(2-methylpropionamidine) dihydrochloride (V-50) in 5 ml of DI-H_2O was added to the reaction mixture. The polymerization was carried out at 60 °C for 48 h. The crude polymer product precipitated when saturated $NaHCO_3$ was added to the reaction mixture to make it basic. This polymer precipitate was filtrated, washed with warm DI-H_2O and dried in vacuum oven. The obtained crude polymer product was further purified by dissolving in 20 mL methanol and filtering through a 0.2 μm PTFE filter. The filtrate was concentrated by rotary evaporation to yield the PDAAP product which had a M_w of 35 kDa by GPC analysis.

Synthesis of poly(*N*-isopropylacrylamide)-*c*-poly(2,2,6,6-tetramethyl-piperidineoxyl-acrylamide) (PNIPAM-*c*-PTEMPOAM) from PNASI. A DMF solution of desired mole ratio of isopropylamine and 4-amino-2,2,6,6-tetramethyl-piperidinoxyl (4-amino-TEMPO) was added to a DMF solution of PNASI dropwise. Reaction was allowed to stir under positive N_2 pressure at ambient temperature overnight. Rotary evaporation was used to remove DMF. The remaining polymer was

re-dissolved in dichloromethane and the solution was precipitated in ethyl ether anhydrous. The precipitation process was repeated one more time and the polymer product was filtrated and dried in oven under vacuum overnight.

Synthesis of poly(*N*-isopropylacrylamide)-*c*-poly(2,2,6,6-tetramethyl piperidinyl-acrylamide) (PNIPAM-*c*-PTEMPAM) analogue from PNASI. A DMF solution of desired mole ratio of isopropylamine and 4-amino-2,2,6,6-tetramethylpiperidine (4-amino-TEMP) was added to a DMF solution of PNASI dropwise. Reaction was allowed to stir under positive N_2 pressure at ambient temperature overnight and then the solvent DMF was removed under reduced pressure. The remaining polymer was redissolved in dichloromethane and the solution was precipitated in ethyl ether anhydrous. The precipitation process was repeated one more time and the polymer product was filtrated and dried in oven under vacuum overnight.

Covalent layer-by-layer self-assembly of poly(*N*-isopropylacrylamide)-*c*-poly((*N*-benzo-15-crown-5)acrylamide) (PNIPAM-*c*-PB15C5AM) with aminated silica nanoparticles on silicon wafers. A silicon wafer was functionalized and primed with two PNASI/PEI bilayers according to the procedures mentioned earlier. The covalent layer-by-layer assembly procedure that used for grafting PNIPAM/SiO_2 nanocomposite surfaces on silicon wafers earlier was followed with some changes. In this synthesis, instead of using *i*-$PrNH_2$ after each PNIPAM-*c*-PNASI/SiO_2 bilayer treatment to convert unreacted NASI to NIPAM, 4-amino-benzo-15-crown-5 was used to form the benzo-15-crown-5-acrylamide (B15C5AM). In general, the primed silicon wafer was treated in DMF solution of PNIPAM-*c*-PNASI (9:1 mole ratio), DMF

suspension of 10- and 100- nm aminated silica nanoparticles, and DMF solution of 4-amino-benzo-15-crown-5 sequentially. In between each treatment, the silicon wafer was washed with DMF to remove any unreacted reagents. After five cycles of those treatments, the surface so formed was treated in DMF solution of PNIPAM-*c*-PNASI (9:1 mole ratio), DMF suspension of 10 nm aminated silica nanoparticles, and DMF solution of 4-amino-benzo-15-crown-5 one time. Finally, the surface was treated with DMF solution of PNIPAM-*c*-PNASI (9:1 mole ratio) followed by treatment in DMF solution of 4-amino-benzo-15-crown-5 to have the outmost surface covered with functional PNIPAM-*c*-PB15C5AM copolymer.

REFERENCES

(1) Filipcsei, G.; Fehér, J.; Zrínyi, M. *J. Mol. Struct.* **2000,** *554*, 109-117.

(2) ZrÃ-nyi, M. *Colloid. Polym. Sci.* **2000,** *278*, 98-103.

(3) Jiang, J.; Tong, X.; Zhao, Y. *J. Am. Chem. Soc.* **2005,** *127*, 8290-8291.

(4) Ghosh, S.; Irvin, K.; Thayumanavan, S. *Langmuir* **2007,** *23*, 7916-7919.

(5) Napoli, A.; Valentini, M.; Tirelli, N.; Muller, M.; Hubbell, J. A. *Nat. Mater.* **2004,** *3*, 183-189.

(6) Weder, C. *Nature* **2009,** *459*, 45-46.

(7) Lenhardt, J. M.; Black, A. L.; Craig, S. L. *J. Am. Chem. Soc.* **2009,** *131*, 10818-10819.

(8) Baltes, T.; Garret-Flaudy, F.; Freitag, R. *J. Polym. Sci., Part A: Polym. Chem.* **1999,** *37*, 2977-2989.

(9) Tiktopulo, E. I.; Uversky, V. N.; Lushchik, V. B.; Klenin, S. I.; Bychkova, V. E.; Ptitsyn, O. B. *Macromolecules* **1995,** *28*, 7519-7524.

(10) Graziano, G. *Int. J. Biol. Macromol.* **2000,** *27*, 89-97.

(11) Inomata, H.; Goto, S.; Saito, S. *Macromolecules* **2002,** *23*, 4887-4888.

(12) Barker, I. C.; Cowie, J. M. G.; Huckerby, T. N.; Shaw, D. A.; Soutar, I.; Swanson, L. *Macromolecules* **2003,** *36*, 7765-7770.

(13) Suwa, K.; Morishita, K.; Kishida, A.; Akashi, M. *J. Polym. Sci., Part A: Polym. Chem.* **1997,** *35*, 3087-3094.

(14) Winnik, F. M.; Tamai, N.; Yonezawa, J.; Nishimura, Y.; Yamazaki, I. *J. Phys. Chem.* **2002,** *96*, 1967-1972.

(15) Gao, J.; Haidar, G.; Lu, X. H.; Hu, Z. B. *Macromolecules* **2001,** *34*, 2242-2247.

(16) Vasheghani-Farahani, E.; Cooper, D. G.; Vera, J. H.; Weber, M. E. *Chem. Eng. Sci.* **1992,** *47*, 31-40.

(17) Zhu, Y.; Ni, C. H.; Shao, D.; Jiang, X. *Acta Polym Sin* **2007**, 765-769.

(18) Kanazawa, H.; Yamamoto, K.; Matsushima, Y.; Takai, N.; Kikuchi, A.; Sakurai, Y.; Okano, T. *Anal. Chem.* **1996,** *68*, 100-105.

(19) Kanazawa, H.; Sunamoto, T.; Matsushima, Y.; Kikuchi, A.; Okano, T. *Anal. Chem.* **2000,** *72*, 5961-5966.

(20) Liu, Y. Y.; Shao, Y. H.; Lu, J. *Biomaterials* **2006,** *27*, 4016-4024.

(21) Zha, L. S.; Li, L.; Bao, L. Y. *J. Appl. Polym. Sci.* **2007,** *103*, 3893-3898.

(22) Zhang, J.; Chu, L. Y.; Li, Y. K.; Lee, Y. M. *Polymer* **2007,** *48*, 1718-1728.

(23) Karg, M.; Pastoriza-Santos, I.; Rodriguez-Gonzalez, B.; von Klitzing, R.; Wellert, S.; Hellweg, T. *Langmuir* **2008,** *24*, 6300-6306.

(24) Zhang, S. B.; Chu, L. Y.; Xu, D.; Zhang, J.; Ju, X. J.; Xie, R. *Polym. Adv. Technol.* **2008,** *19*, 937-943.

(25) Nuopponen, M.; Tenhu, H. *Langmuir* **2007,** *23*, 5352-5357.

(26) Wu, C. *Polymer* **1998,** *39*, 4609-4619.

(27) Zhang, W. A.; Zhou, X. C.; Li, H.; Fang, Y.; Zhang, G. Z. *Macromolecules* **2005,** *38*, 909-914.

(28) Mao, H. B.; Li, C. M.; Zhang, Y. J.; Furyk, S.; Cremer, P. S.; Bergbreiter, D. E. *Macromolecules* **2004,** *37*, 1031-1036.

(29) Zhang, Y. J.; Furyk, S.; Bergbreiter, D. E.; Cremer, P. S. *J. Am. Chem. Soc.* **2005,** *127*, 14505-14510.

(30) Furyk, S.; Zhang, Y. J.; Ortiz-Acosta, D.; Cremer, P. S.; Bergbreiter, D. E. *J. Polym. Sci., Part A: Polym. Chem.* **2006,** *44*, 1492-1501.

(31) Zhang, Y.; Furyk, S.; Sagle, L. B.; Cho, Y.; Bergbreiter, D. E.; Cremer, P. S. *J. Phys. Chem. C* **2007,** *111*, 8916-8924.

(32) Cho, Y. H.; Zhang, Y. J.; Christensen, T.; Sagle, L. B.; Chilkoti, A.; Cremer, P. S. *J. Phys. Chem. B* **2008,** *112*, 13765-13771.

(33) Zhang, Y. J.; Trabbic-Carlson, K.; Albertorio, F.; Chilkoti, A.; Cremer, P. S. *Biomacromolecules* **2006,** *7*, 2192-2199.

(34) Freitag, R.; Baltes, T.; Eggert, M. *J. Polym. Sci., Part A: Polym. Chem.* **1994,** *32*, 3019-3030.

(35) Chee, C. K.; Rimmer, S.; Rutkaite, R.; Soutar, I.; Swanson, L. *J. Photochem. Photobiol., A* **2006,** *180*, 1-8.

(36) Burba, C. M.; Carter, S. M.; Meyer, K. J.; Rice, C. V. *J. Phys. Chem. B* **2008,** *112*, 10399-10404.

(37) Ahmed, Z.; Gooding, E. A.; Pimenov, K. V.; Wang, L. L.; Asher, S. A. *J. Phys. Chem. B* **2009,** *113*, 4248-4256.

(38) Andersson, M.; Maunu, S. L. *Colloid. Polym. Sci.* **2006,** *285*, 293-303.

(39) Maeda, H. *J. Polym. Sci., Part B: Polym. Phys.* **1994,** *32*, 91-97.

(40) Nishio, Y.; Chiba, R.; Miyashita, Y.; Oshima, K.; Miyajima, T.; Kimura, N.; Suzuki, H. *Polym. J.* **2002,** *34*, 149-157.

(41) Krasovitski, E.; Cohen, Y.; Bianco-Peled, H. *J. Polym. Sci., Part B: Polym. Phys.* **2004,** *42*, 3713-3720.

(42) Chiba, R.; Nishio, Y.; Miyashita, Y. *Macromolecules* **2003,** *36*, 1706-1712.

(43) Chen, J. H.; Chen, H. H.; Chang, Y. X.; Chuang, P. Y.; Hong, P. D. *J. Appl. Polym. Sci.* **2008,** *107*, 2732-2742.

(44) Zhu, P. W.; Napper, D. H. *Langmuir* **1996,** *12*, 5992-5998.

(45) Housni, A.; Narain, R. *Eur. Polym. J.* **2007,** *43*, 4344-4354.

(46) Collins, K. D.; Washabaugh, M. W. *Q. Rev. Biophys.* **1985,** *18*, 323-422.

(47) Freitag, R.; Garret-Flaudy, F. *Langmuir* **2002,** *18*, 3434-3440.

(48) Kunz, W.; Henle, J.; Ninham, B. W. *Curr. Opin. Colloid Interface Sci.* **2004,** *9*, 19-37.

(49) Hippel, P. H. V.; Wong, K. Y. *Biochemistry* **1962,** *1*, 664-&.

(50) Warren, J. C.; Cheatum, S. G. *Biochemistry* **1966,** *5*, 1702-&.

(51) Warren, J. C.; Peterson, D. M. *Science* **1966,** *152*, 1245-&.

(52) Ebel, C.; Faou, P.; Kernel, B.; Zaccai, G. *Biochemistry* **1999,** *38*, 9039-9047.

(53) Guo, F.; Friedman, J. M. *J. Am. Chem. Soc.* **2009,** *131*, 11010-11018.

(54) Kokufuta, E.; Zhang, Y. Q.; Tanaka, T.; Mamada, A. *Macromolecules* **2002,** *26*, 1053-1059.

(55) Schild, H. G.; Tirrell, D. A. *Langmuir* **2002,** *7*, 665-671.

(56) Winnik, F. M.; Ringsdorf, H.; Venzmer, J. *Langmuir* **1991,** *7*, 912-917.

(57) Wu, C.; Zhou, S. *J. Polym. Sci., Part B: Polym. Phys.* **1996,** *34*, 1597-1604.

(58) Tam, K. C.; Ragaram, S.; Pelton, R. H. *Langmuir* **2002,** *10*, 418-422.

(59) Kumar, A. C.; Bohidar, H. B.; Mishra, A. K. *Colloids Surf., B* **2009,** *70*, 60-67.

(60) Sjoeberg, A.; Karlstroem, G.; Tjerneld, F. *Macromolecules* **2002,** *22*, 4512-4516.

(61) Shpigelman, A.; Portnaya, I.; Ramon, O.; Livney, Y. D. *J. Polym. Sci., Part B: Polym. Phys.* **2008,** *46*, 2307-2318.

(62) Roux, E.; Francis, M.; Winnik, F. M.; Leroux, J. C. *Int. J. Pharm.* **2002,** *242*, 25-36.

(63) Kim, J. C.; Bae, S. K.; Kim, J. D. *J. Biochem. (Tokyo)* **1997,** *121*, 15-19.

(64) Liu, S. X.; Liu, X.; Li, F.; Fang, Y.; Wang, Y. J.; Yu, J. *J. Appl. Polym. Sci.* **2008,** *109*, 4036-4042.

(65) He, C. L.; Zhao, C. W.; Guo, X. H.; Guo, Z. J.; Chen, X. S.; Zhuang, X. L.; Liu, S. Y.; Jing, X. B. *J. Polym. Sci., Part A: Polym. Chem.* **2008,** *46*, 4140-4150.

(66) Chourdakis, N.; Bokias, G.; Staikos, G. *J. Appl. Polym. Sci.* **2004,** *92*, 3466-3470.

(67) Liu, L.; Wu, C. L.; Zhang, J. C.; Zhang, M. M.; Liu, Y. W.; Wang, X. J.; Fu, G. Q. *J. Polym. Sci., Part A: Polym. Chem.* **2008,** *46*, 3294-3305.

(68) Nykanen, A.; Nuopponen, M.; Laukkanen, A.; Hirvonen, S. P.; Rytela, M.; Turunen, O.; Tenhu, H.; Mezzenga, R.; Ikkala, O.; Ruokolainen, J. *Macromolecules* **2007,** *40*, 5827-5834.

(69) Chen, Y. G.; Sone, M.; Fuchise, K.; Sakai, R.; Kakuchi, R.; Duan, Q.; Sun, J. L.; Narumi, A.; Satoh, T.; Kakuchi, T. *React. Funct. Polym.* **2009,** *69*, 463-469.

(70) You, Y. Z.; Zhou, Q. H.; Manickam, D. S.; Wan, L.; Mao, G. Z.; Oupicky, D. *Macromolecules* **2007,** *40*, 8617-8624.

(71) Dufresne, M. H.; Le Garrec, D.; Sant, V.; Leroux, J. C.; Ranger, M. *Int. J. Pharm.* **2004,** *277*, 81-90.

(72) Li, G. Y.; Guo, L.; Ma, S. M.; Liu, J. S. *J. Polym. Sci., Part A: Polym. Chem.* **2009,** *47*, 1804-1810.

(73) Wang, H.; An, Y. L.; Huang, N.; Ma, R. J.; Li, J. B.; Shi, L. Q. *Macromol. Rapid Commun.* **2008,** *29*, 1410-1414.

(74) Zhang, Y. F.; Hao, L.; Hu, J. M.; Li, C. H.; Liu, S. Y. *Macromol. Rapid Commun.* **2009,** *30*, 941-947.

(75) Goodwin, A. P.; Mynar, J. L.; Ma, Y.; Fleming, G. R.; Frechet, J. M. J. *J. Am. Chem. Soc.* **2005,** *127*, 9952-9953.

(76) Anderson, V. C.; Thompson, D. H. *Biochim. Biophys. Acta* **1992,** *1109*, 33-42.

(77) Nishiyama, N.; Iriyama, A.; Jang, W. D.; Miyata, K.; Itaka, K.; Inoue, Y.; Takahashi, H.; Yanagi, Y.; Tamaki, Y.; Koyama, H.; Kataoka, K. *Nat. Mater.* **2005,** *4*, 934-941.

(78) Davis, D. A.; Hamilton, A.; Yang, J. L.; Cremar, L. D.; Van Gough, D.; Potisek, S. L.; Ong, M. T.; Braun, P. V.; Martinez, T. J.; White, S. R.; Moore, J. S.; Sottos, N. R. *Nature* **2009,** *459*, 68-72.

(79) Annaka, M.; Yahiro, C.; Nagase, K.; Kikuchi, A.; Okano, T. *Polymer* **2007,** *48*, 5713-5720.

(80) Bradley, C.; Jalili, N.; Nett, S. K.; Chu, L. Q.; Forch, R.; Gutmann, J. S.; Berger, R. *Macromol. Chem. Phys.* **2009,** *210*, 1339-1345.

(81) Ishida, N.; Biggs, S. *Langmuir* **2007,** *23*, 11083-11088.

(82) Balamurugan, S.; Mendez, S.; Balamurugan, S. S.; O'Brie, M. J.; Lopez, G. P. *Langmuir* **2003,** *19*, 2545-2549.

(83) Jhon, Y. K.; Bhat, R. R.; Jeong, C.; Rojas, O. J.; Szleifer, I.; Genzer, J. *Macromol. Rapid Commun.* **2006,** *27*, 697-701.

(84) Kizhakkedathu, J. N.; Norris-Jones, R.; Brooks, D. E. *Macromolecules* **2004,** *37*, 734-743.

(85) Binder, W. H.; Gloger, D.; Weinstabl, H.; Allmaier, G.; Pittenauer, E. *Macromolecules* **2007,** *40*, 3097-3107.

(86) Pan, Y. V.; Wesley, R. A.; Luginbuhl, R.; Denton, D. D.; Ratner, B. D. *Biomacromolecules* **2001,** *2*, 32-36.

(87) Yamada, N.; Okano, T.; Sakai, H.; Karikusa, F.; Sawasaki, Y.; Sakurai, Y. *Makromol. Chem. Rapid Commun.* **1990,** *11*, 571-576.

(88) Reuber, J.; Reinhardt, H.; Johannsmann, D. *Langmuir* **2006,** *22*, 3362-3367.

(89) Hirata, I.; Okazaki, M.; Iwata, H. *Polymer* **2004,** *45*, 5569-5578.

(90) Ye, J.; Hou, Y.; Zhang, G. Z.; Wu, C. *Langmuir* **2008,** *24*, 2727-2731.

(91) Shan, J.; Chen, J.; Nuopponen, M.; Tenhu, H. *Langmuir* **2004,** *20*, 4671-4676.

(92) Zhao, M. Q.; Liu, Y. L.; Crooks, R. M.; Bergbreiter, D. E. *J. Am. Chem. Soc.* **1999,** *121*, 923-930.

(93) Schild, H. G. *Progress in Polymer Science* **1992,** *17*, 163-249.

(94) Boutris, C.; Chatzi, E. G.; Kiparissides, C. *Polymer* **1997,** *38*, 2567-2570.

(95) Bae, Y. C.; Lambert, S. M.; Soane, D. S.; Prausnitz, J. M. *Macromolecules* **1991,** *24*, 4403-4407.

(96) Qiu, X. P.; Li, M.; Kwan, C. M. S.; Wu, C. *J. Polym. Sci., Part B: Polym. Phys.* **1998,** *36*, 1501-1506.

(97) Schonhoff, M.; Larsson, A.; Welzel, P. B.; Kuckling, D. *J. Phys. Chem. B* **2002,** *106*, 7800-7808.

(98) Larsson, A.; Kuckling, D.; Schonhoff, M. *Colloids Surf., A* **2001,** *190*, 185-192.

(99) Zeng, F.; Tong, Z.; Feng, H. Q. *Polymer* **1997,** *38*, 5539-5544.

(100) Yushmanov, P. V.; Furo, I.; Iliopoulos, I. *Macromol. Chem. Phys.* **2006,** *207*, 1972-1979.

(101) Lessard, D. G.; Ousalem, M.; Zhu, X. X.; Eisenberg, A.; Carreau, P. J. *J. Polym. Sci., Part B: Polym. Phys.* **2003,** *41*, 1627-1637.

(102) Wu, Y. Q.; Meersman, F.; Heremans, K.; Ozaki, Y. *J. Mol. Struct.* **2006,** *799*, 134-140.

(103) Koopmans, C.; Ritter, H. *J. Am. Chem. Soc.* **2007,** *129*, 3502-+.

(104) Kujawa, P.; Tanaka, F.; Winnik, F. M. *Macromolecules* **2006,** *39*, 3048-3055.

(105) Chee, C. K.; Rimmer, S.; Soutar, I.; Swanson, L. *Polymer* **1997,** *38*, 483-486.

(106) Cai, T.; Marquez, M.; Hu, Z. B. *Langmuir* **2007,** *23*, 8663-8666.

(107) Zhou, M.; Sivaramakrishnan, A.; Ponnamperuma, K.; Low, W. K.; Li, C. M.; Liu, J. O.; Bergbreiter, D. E.; Romo, D. *Org Lett* **2006,** *8*, 5247-5250.

(108) Duan, Q.; Narumi, A.; Miura, Y.; Shen, X. D.; Sato, S. I.; Satoh, T.; Kakuchi, T. *Polym. J.* **2006,** *38*, 306-310.

(109) Tsutsui, H.; Akashi, R. *J. Polym. Sci., Part A: Polym. Chem.* **2006,** *44*, 4644-4655.

(110) Kim, J.; Nayak, S.; Lyon, L. A. *J. Am. Chem. Soc.* **2005,** *127*, 9588-9592.

(111) Reese, C. E.; Mikhonin, A. V.; Kamenjicki, M.; Tikhonov, A.; Asher, S. A. *J. Am. Chem. Soc.* **2004,** *126*, 1493-1496.

(112) Kawaguchi, H.; Kisara, K.; Takahashi, T.; Achiha, K.; Yasui, M.; Fujimoto, K. *Macromol Symp* **2000,** *151*, 591-598.

(113) Mao, H. B.; Li, C. M.; Zhang, Y. J.; Bergbreiter, D. E.; Cremer, P. S. *J. Am. Chem. Soc.* **2003,** *125*, 2850-2851.

(114) The detailed information for the OptiMelt® automatic melting point apparatus can be found from the web site of Stanford Research Systems, InC. http://www.thinksrs.com/downloads/PDFs/Manuals/MPA100m.pdf (accessd on feburary 2, 2010).

(115) Kujawa, P.; Winnik, F. M. *Macromolecules* **2001,** *34*, 4130-4135.

(116) Kumar, A.; Srivastava, A.; Galaev, I. Y.; Mattiasson, B. *Progress in Polymer Science* **2007,** *32*, 1205-1237.

(117) Luzinov, I.; Minko, S.; Tsukruk, V. V. *Soft Matter* **2008,** *4*, 714-725.

(118) Peez, R. F.; Dermody, D. L.; Franchina, J. G.; Jones, S. J.; Bruening, M. L.; Bergbreiter, D. E.; Crooks, R. M. *Langmuir* **1998,** *14*, 4232-4237.

(119) Wang, Y.; Wei, G. W.; Zhang, W. Q.; Jiang, X. W.; Zheng, P. W.; Shi, L. Q.; Dong, A. J. *J Mol Catal a-Chem* **2007,** *266*, 233-238.

(120) Fulghum, T. M.; Estillore, N. C.; Vo, C. D.; Armes, S. P.; Advincula, R. C. *Macromolecules* **2008,** *41*, 429-435.

(121) Xia, F.; Feng, L.; Wang, S.; Sun, T.; Song, W.; Jiang, W.; Jiang, L. *Adv Mater* **2006,** *18*, 432-436.

(122) Sun, T.; Wang, G.; Feng, L.; Liu, B.; Ma, Y.; Jiang, L.; Zhu, D. *Angewandte Chemie International Edition* **2004,** *43*, 357-360.

(123) Van Durme, K.; Rahier, H.; Van Mele, B. *Macromolecules* **2005,** *38*, 10155-10163.

(124) Liu, Y. L.; Zhao, M. Q.; Bergbreiter, D. E.; Crooks, R. M. *J. Am. Chem. Soc.* **1997,** *119*, 8720-8721.

(125) Bruening, M. L.; Zhou, Y. F.; Aguilar, G.; Agee, R.; Bergbreiter, D. E.; Crooks, R. M. *Langmuir* **1997,** *13*, 770-778.

(126) Liao, K. S.; Wan, A.; Batteas, J. D.; Bergbreiter, D. E. *Langmuir* **2008,** *24*, 4245-4253.

(127) Cole, M. A.; Voelcker, N. H.; Thissen, H.; Griesser, H. J. *Biomaterials* **2009,** *30*, 1827-1850.

(128) Luzinov, I.; Minko, S.; Tsukruk, V. V. *Prog. Polym. Sci.* **2004,** *29*, 635-698.

(129) Sun, A.; Lahann, J. *Soft Matter* **2009,** *5*, 1555-1561.

(130) Gras, S. L.; Mahmud, T.; Rosengarten, G.; Mitchell, A.; Kalantar-Zadeh, K. *Chemphyschem* **2007,** *8*, 2036-2050.

(131) Mendes, P. M. *Chem. Soc. Rev.* **2008,** *37*, 2512-2529.

(132) Zhang, T.; Zheng, Z. H.; Ding, X. B.; Peng, Y. X. *Macromol. Rapid Commun.* **2008,** *29*, 1716-1720.

(133) Plunkett, K. N.; Zhu, X.; Moore, J. S.; Leckband, D. E. *Langmuir* **2006,** *22*, 4259-4266.

(134) Lindqvist, J.; Nystrom, D.; Ostmark, E.; Antoni, P.; Carlmark, A.; Johansson, M.; Hult, A.; Malmstrom, E. *Biomacromolecules* **2008,** *9*, 2139-2145.

(135) Yim, H.; Kent, M. S.; Mendez, S.; Lopez, G. P.; Satija, S.; Seo, Y. *Macromolecules* **2006,** *39*, 3420-3426.

(136) Meyer, D. E.; Chilkoti, A. *Nat. Biotechnol.* **1999,** *17*, 1112-1115.

(137) Uchida, K.; Sakai, K.; Ito, E.; Kwon, O. H.; Kikuchi, A.; Yamato, M.; Okano, T. *Biomaterials* **2000,** *21*, 923-929.

(138) Canavan, H. E.; Cheng, X. H.; Graham, D. J.; Ratner, B. D.; Castner, D. G. *Langmuir* **2005,** *21*, 1949-1955.

(139) Winnik, F. M.; Ottaviani, M. F.; Bossman, S. H.; Pan, W. S.; Garciagaribay, M.; Turro, N. J. *J. Phys. Chem.* **1993,** *97*, 12998-13005.

(140) Wu, C.; Zhou, S. Q. *Macromolecules* **1997,** *30*, 574-576.

(141) Collins, K. D. *Biophys. J.* **1997,** *72*, 65-76.

(142) von Hippel, P. H.; Schleich, T. The effects of neutral salts on the structure and conformational stability of macromolecules in solution. In *Structure and stability of biological macromolecules*, Timasheff, S. N.; Fasman, G. D. Dekker: New York, **1969**.

(143) Hyun, J.; Lee, W. K.; Nath, N.; Chilkoti, A.; Zauscher, S. *J. Am. Chem. Soc.* **2004,** *126*, 7330-7335.

(144) Liao, K. S.; Fu, H.; Wan, A.; Batteas, J. D.; Bergbreiter, D. E. *Langmuir* **2009,** *25*, 26-28.

(145) Bergbreiter, D. E.; Liao, K. S. *Soft Matter* **2009,** *5*, 23-28.

(146) Troll, K.; Kulkarni, A.; Wang, W.; Darko, C.; Koumba, A. M. B.; Laschewsky, A.; Muller-Buschbaum, P.; Papadakis, C. M. *Colloid Polym. Sci.* **2008,** *286*, 1079-1092.

(147) Ishida, N. *Advanced Powder Technology* **2007,** *18*, 631-642.

(148) Marcus, Y. *Chem. Rev.* **2009,** *109*, 1346-1370.

(149) Fennell, C. J.; Bizjak, A.; Vlachy, V.; Dill, K. A. *J. Phys. Chem. B* **2009,** *113*, 6782-6791.

(150) Rudolph, W.; Schonherr, S. *Z. Phys. Chem.* **1991,** *172*, 31-48.

(151) Petrou, A. L. *Coord. Chem. Rev.* **2002,** *228*, 153-162.

(152) Cotton, F. A.; Wilkinson, G.; Murillo, C. A.; Bochmann, M. *Advanced inorganic chemistry*, 6th ed.; Wiley: New York, **1999**.

(153) Atkinson, G.; Petrucci, S. *J. Phys. Chem.* **1966,** *70*, 3122-&.

(154) Pitzer, K. S.; Mayorga, G. *J. Solution Chem.* **1974,** *3*, 539-546.

(155) Pye, C. C.; Rudolph, W. W. *J. Phys. Chem. A* **1998,** *102*, 9933-9943.

(156) Akitt, J. W.; Farnsworth, J. A.; Letellier, P. *J. Chem. Soc. Farad. T. 1* **1985,** *81*, 193-205.

(157) Maciel, G. E.; Simeral, L.; Ackerman, J. J. H. *J. Phys. Chem.* **1977,** *81*, 263-267.

(158) Simeral, L.; Maciel, G. E. *J. Phys. Chem.* **1976,** *80*, 552-557.

(159) Mibe, K.; Chou, I. M.; Anderson, A. J.; Mayanovic, R. A.; Bassett, W. A. *Chem. Geol.* **2009,** *259*, 48-53.

(160) Robinson, R. A.; Stokes, R. H. *Electrolyte solutions*, 2nd ed.; Butterworths Scientific Publications: London, **1959**.

(161) Goldberg, R. N. *J. Phys. Chem. Ref. Data* **1981,** *10*, 671-764.

(162) Lide, D. R. *CRC handbook of chemistry and physics*, 89th ed.; CRC Press, **2008**.

(163) Pitzer, K. S. *Activity coefficients in electrolyte solutions*, 2nd ed.; CRC Press: Boca Raton, **1991**.

(164) Reardon, E. J. *J. Phys. Chem.* **1988,** *92*, 6426-6431.

(165) Montagne, F.; Polesel-Maris, J.; Pugin, R.; Heinzelmann, H. *Langmuir* **2009,** *25*, 983-991.

(166) Zhu, D. M.; Wu, K.; Wu, B.; Wang, P.; Fang, J. J.; Hou, Y.; Zhang, G. Z. *J. Phys. Chem. C* **2007,** *111*, 18679-18686.

(167) Li, X. M.; Reinhoudt, D.; Crego-Calama, M. *Chem. Soc. Rev.* **2007,** *36*, 1529-1529.

(168) Bergbreiter, D. E.; Fu, H. *J. Polym. Sci., Part A: Polym. Chem.* **2008,** *46*, 186-193.

(169) Sedlak, E.; Stagg, L.; Wittung-Stafshede, P. *Arch. Biochem. Biophys.* **2008,** *474*, 128-135.

(170) Kim, Y. S.; Liao, K. S.; Jan, C. J.; Bergbreiter, D. E.; Grunlan, J. C. *Chem. Mater.* **2006,** *18*, 2997-3004.

(171) Dejeu, J.; Buisson, L.; Guth, M. C.; Roidor, C.; Membrey, F.; Charraut, D.; Foissy, A. *Colloids Surf., A* **2006,** *288*, 26-35.

(172) Haller, I. *J. Am. Chem. Soc.* **1978,** *100*, 8050-8055.

(173) Moon, J. H.; Shin, J. W.; Park, J. W. *Mol. Cryst. Liq. Cryst. Sci. Technol., Sect. A* **1997,** *294*, 483-486.

(174) Bravo, J.; Zhai, L.; Wu, Z. Z.; Cohen, R. E.; Rubner, M. F. *Langmuir* **2007,** *23*, 7293-7298.

(175) Rouse, J. H.; Ferguson, G. S. *J. Am. Chem. Soc.* **2003,** *125*, 15529-15536.

(176) Winnik, F. M.; Ottaviani, M. F.; Bossmann, S. H.; Garciagaribay, M.; Turro, N. J. *Macromolecules* **1992,** *25*, 6007-6017.

(177) Bergbreiter, D. E.; Case, B. L.; Liu, Y. S.; Caraway, J. W. *Macromolecules* **1998,** *31*, 6053-6062.

(178) Scriven, E. F. V. *Chem. Soc. Rev.* **1983,** *12*, 129-161.

(179) Deratani, A.; Darling, G. D.; Horak, D.; Frechet, J. M. J. *Macromolecules* **1987,** *20*, 767-772.

(180) Rubinsztajn, S.; Zeldin, M.; Fife, W. K. *Macromolecules* **1991,** *24*, 2682-2688.

(181) Helms, B.; Liang, C. O.; Hawker, C. J.; Frechet, J. M. J. *Macromolecules* **2005,** *38*, 5411-5415.

(182) Bergbreiter, D. E.; Li, C. M. *Org Lett* **2003,** *5*, 2445-2447.

(183) Helms, B.; Guillaudeu, S. J.; Xie, Y.; McMurdo, M.; Hawker, C. J.; Fréchet, J. M. J. *Angewandte Chemie International Edition* **2005,** *44*, 6384-6387.

(184) Huang, J. T.; Sun, J. W.; Liu, Z. H. *J. Appl. Polym. Sci.* **1995,** *56*, 1805-1806.

(185) Vaidya, R. A.; Mathias, L. J. *J. Am. Chem. Soc.* **1986,** *108*, 5514-5520.

(186) Sheldon, R. A.; Arends, I. W. C. E. *Adv. Synth. Catal.* **2004,** *346*, 1051-1071.

(187) Nishide, H.; Oyaizu, K. *Science* **2008,** *319*, 737-738.

(188) Bergbreiter, D. E.; Hughes, R.; Besinaiz, J.; Li, C. M.; Osburn, P. L. *J. Am. Chem. Soc.* **2003,** *125*, 8244-8249.

(189) Nishide, H.; Iwasa, S.; Pu, Y. J.; Suga, T.; Nakahara, K.; Satoh, M. *Electrochim. Acta* **2004,** *50*, 827-831.

(190) Nakahara, K.; Iwasa, S.; Satoh, M.; Morioka, Y.; Iriyama, J.; Suguro, M.; Hasegawa, E. *Chemical Physics Letters* **2002,** *359*, 351-354.

(191) Zhang, Z.; Chen, P.; Murakami, T. N.; Zakeeruddin, S. M.; Grätzel, M. *Adv. Funct. Mater.* **2008,** *18*, 341-346.

(192) Winnik, F. M.; Ottaviani, M. F.; Bossmann, S. H.; Garciagaribay, M.; Turro, N. J. *Macromolecules* **1992,** *25*, 6007-6017.

(193) Mi, P.; Chu, L. Y.; Ju, X. J.; Niu, C. H. *Macromol. Rapid Commun.* **2008,** *29*, 27-32.

(194) Yagi, K.; Ruiz, J. A.; Sanchez, M. C. *Makromol. Chem-Rapid.* **1980,** *1*, 263-268.

(195) Kopolow, S.; Esch, T. E. H.; Smid, J. *Macromolecules* **1973,** *6*, 133-142.

(196) Huh, D. S.; Park, S. H.; Kim, Y. J.; Park, D. Y.; Zhao, Y. S.; Ahn, S. H.; Yoshida, R.; Yamaguchi, T. *J. Phys. Chem. B* **2006,** *110*, 13405-13409.

(197) Ito, T.; Hioki, T.; Yamaguchi, T.; Shinbo, T.; Nakao, S.; Kimura, S. *J. Am. Chem. Soc.* **2002,** *124*, 7840-7846.

(198) Yamaguchi, T.; Ito, T.; Sato, T.; Shinbo, T.; Nakao, S.-i. *J. Am. Chem. Soc.* **1999,** *121*, 4078-4079.

(199) Bergbreiter, D. E.; Simanek, E. E.; Owsik, I. *J. Polym. Sci., Part A: Polym. Chem.* **2005,** *43*, 4654-4665.

(200) Huang, J.-T.; Wang, Q.; Sun, J.-W. *J. Appl. Polym. Sci.* **2000,** *77*, 363-367.

VITA

Name: Hui Fu

Address: Department of Chemistry, Texas A&M University
P.O. Box 30012, College Station, TX 77842-3012

Email Address: hfu@mail.chem.tamu.edu

Education: B.A., Chemistry, Sichuang University, China, 1993

M.S., Chemistry, Tsinghua University, China, 1996

M.S., Chemistry, University of Southern California, U.S.A. 2002

Ph.D., Chemistry, Texas A&M University, U.S.A. 2010